Analysis of Structural Characteristics and Extremal Behaviour of Transformed Spatiotemporal Processes

University of Granada
Doctoral Program in Mathematical and Applied Statistics

José Luis Romero Béjar

Thesis supervised by:
Prof. José Miguel Angulo Ibáñez

Granada 2020

Editor: Universidad de Granada. Tesis Doctorales
Autor: José Luis Romero Béjar
ISBN: 978-84-1306-562-5
URI: http://hdl.handle.net/10481/63328

Acknowledgements

First, I am sincerely grateful and indebted to my supervisor Prof. José Miguel Angulo Ibáñez. He assumed the responsibility and the challenge of making his own ideas my own. He is still working on it but, it is enough at this stage.

I am grateful to Prof. Illya Molchanov and Prof. Georges Christakos for having invited me to work with them, first in the Institute of Mathematics and Actuarial Sciences at the University of Bern (Switzerland) and, second in the Department of Geography of the San Diego State University at California (USA), affording me the opportunity to obtain an international doctorate and live a great experience.

I must also acknowledge the department of Statistics and Operational Research of the University of Granada. From the beginning of my studies it has supplied me wonderful teachers, later colleagues, and now friends.

I would like to show my gratitude to all the people who have shared my life during the development of this thesis and who have helped me in the hard times, in particular to my family. To my parents and brothers, for always helping me.

Finally, I dedicate this thesis to Susana, Cayetano and Jimena, not only for their patience, support and help during its performance, but also for their protagonist role in my life.

Agradecimientos

En primer lugar, estoy sinceramente agradecido y en deuda con mi director de tesis, el Prof. José Miguel Angulo Ibáñez. Asumió la responsabilidad y desafío de hacer que sus propias ideas fueran las mías. Aún sigue trabajando en ello, pero es suficiente en esta etapa.

Agradezco al Prof. Illya Molchanov y al Prof. Georges Christakos por haberme invitado a trabajar con ellos, primero en el Instituto de Matemáticas y Ciencias Actuariales de la Universidad de Berna (Suiza) y, segundo, en el Departamento de Geografía de San Diego State University en California (USA).

También debo reconocer al departamento de Estadística e Investigación Operativa de la Universidad de Granada. Desde el comienzo de mis estudios me ha proporcionado maravillosos maestros, más tarde colegas y ahora amigos.

Me gustaría mostrar mi gratitud a todas las personas que han compartido mi vida durante el desarrollo de esta tesis y que me han ayudado en los momentos difíciles, en particular a mi familia. A mis padres y hermanos, por ayudarme siempre.

Finalmente, dedico esta tesis a Susana, Cayetano y Jimena, no solo por su paciencia, apoyo y ayuda durante su actuación, sino también por su papel protagonista en mi vida.

Contents

List of Figures

List of Tables

Summary

With the reference goal of bringing together the theory of risk measures and the analysis of structural characteristics of random field excursion sets, this thesis work addresses two general objectives: (i) to develop methodologies for risk assessment in spatial and spatiotemporal scenarios in relation to threshold exceedances; (ii) to analyze the effect of transformations, with reference to the spatial domain and the state space, on structural characteristics of threshold exceedance sets, as well as the consideration of related generalizations.

Regarding the first objective, a general and flexible methodology for spatial and spatiotemporal risk assessment is proposed based on a conditional approach. More specifically, for a given random field model and available observations, empirical distributions of different threshold exceedance indicators are obtained from conditional simulation, as a basis for evaluation of measures of risk. In particular, the study is focused on the global and local assessment of exceedance area and excess volume indicators, from which different risk maps are derived. For these first-order indicators, the compound cumulative distribution function plays a key role, both formally and regarding the practical threshold specification. Illustrations based on simulation and applications to real data (Hydrology and Environmental Health) of this methodology are performed in spatial and spatiotemporal scenarios.

Relationships between widely used risk measures such as Value-at-Risk and Average Value-at-Risk, and structural characteristics of excursion sets of the underlying random field such as exceedance area and excess volume, for varying thresholds, are established. The asymptotics of these relationships are interpreted in relation to the shape parameter of the Generalized Pareto Distribution. Formal extensions are developed in scenarios of special interest ('level' and 'flow' type deformation effects and population covariate effect), and finally, a generalized formulation in terms of non-constant thresholds and non-Lebesgue measures is also established.

In addition with respect to the second objective, in this thesis work two approaches are proposed to address the asymptotic behaviour for threshold exceedance probabilities for random fields without some restrictive conditions of regularity, stationarity or isotropy. A first approach is based on regularizing sequences and a second approach on adequate spatial deformation and blurring transformations.

Resumen

Con el objetivo de referencia de hacer interactuar la teoría de medidas de riesgo con el análisis de características estructurales de conjuntos de excursión de campos aleatorios, este trabajo de tesis aborda dos objetivos generales: (i) desarrollo de metodologías para la valoración de riesgos en entornos espaciales y espacio-temporales relativos a excedencias de umbrales; (ii) análisis del efecto de transformaciones, con referencia al dominio espacial y al espacio de estados, sobre características estructurales de conjuntos de excedencia de umbrales así como la consideración de formas generalizadas.

Con respecto al primer objetivo, se propone una metodología general y flexible para la valoración de riesgos en entornos espaciales y espacio-temporales basada en un enfoque condicional. De forma específica, para un modelo de campo aleatorio dado y para un conjunto de observaciones disponibles, se obtienen distribuciones empíricas de distintos indicadores de excedencia de umbral por medio de simulación condicionada, como base para la evaluación de medidas de riesgo. En concreto, el estudio se centra en la valoración global y local de indicadores relacionados con el área de excedencia y con el volumen en exceso, a partir de los cuales se derivan diferentes mapas de riesgo. Para éstos, también llamados indicadores de primer orden, la función de distribución acumulativa compuesta juega un papel clave, tanto desde un punto de vista formal como práctico, en este último caso relacionada con la especificación práctica del umbral. Se realizan ilustraciones basadas en simulaciones y aplicaciones con datos reales (Hidrología y Medio Ambiente) con esa metodología en entornos espaciales y espacio-temporales.

Se formalizan relaciones analíticas entre los indicadores área de excedencia y volumen de exceso con las medidas de riesgo VaR y AVaR, para umbrales variables. Estas relaciones proporcionan interpretaciones asintóticas interesantes en términos del parámetro de forma de la distribución de Pareto generalizada. Se realizan extensiones formales de los resultados anteriores en escenarios generalizados (efectos de deformaciones tipo 'nivel' y 'flujo' y el efecto de la covariable población) y, finalmente, se establece una formulación generalizada que involucra umbrales no constantes y medidas no Lebesgue.

Adicionalmente con respecto al segundo objetivo, en este trabajo de tesis se proponen dos enfoques para abordar el comportamiento asintótico de las probabilidades de excedencia de umbrales para campos aleatorios sin algunas condiciones restrictivas de regularidad, estacionariedad o isotropía. Un primer enfoque está basado en sucesiones regularizantes y un segundo enfoque en

deformaciones espaciales y trasformaciones de borrosidad adecuadas.

Introduction

This thesis work is carried out within the framework of the research line *Structural complexity and extreme values in spatio-temporal processes*, included in the doctoral program in Mathematical and Applied Statistics of the University of Granada with RD99/2011 regulations. The projects of Spanish MINECO/FEDER, EU entitled "*Spatio-temporal analysis: structural complexity, extreme behaviour and generalized information measures*" (ref. MTM2012-32666) and "*Risk analysis in complex systems. Theoretical and methodological advances*" (ref. MTM2015-70840-P), and the project "*Space-time random fields, point processes and multifractal measures: information, complexity and risk analysis approaches*" of MCIU/AEI/FEDER, EU, of which Prof. José Miguel Angulo is the Chief Investigator, support this research line.

The dynamics of a wide variety of physical phenomena (e.g. in Geophysics, Environmental Sciences, etc.) can be appropriately represented in terms of random field models. There is a vast literature related to modelling of these phenomena, in particular under the hypotheses of stationarity and isotropy in the covariance structure. In this sense, depending on the phenomenon of interest and the relevant characteristics analyzed in the spatial or spatio-temporal scenario, different families of covariance models are used: Gaussian, exponential, Cauchy, spherical models (see, for example, Stein 1999; Gneiting and Schlather 2004; Gelfand et al. 2010; Strokorb et al. 2015), fractal Brownian motion, Matern, stable (powered exponential) (see Handcock and Wallis 1994; Diggle et al. 1998; Chiles and Delfiner 1999; Stein 2002; Guttorp and Gneiting 2006); Cauchy or Dagum families are suitable for modeling the fractal dimension and the Hurst effect (see Gneiting and Schlather 2004; Berg et al. 2008), etc. Different probabilistic aspects of random fields are addressed, for example, in Adler (1981, 2008), Yaglom (1987a,b), Christakos (1992, 2000, 2017), Piterbarg (1996), Vanmarcke (2010). Extreme behaviour analysis is associated with the study of threshold exceedance probabilities, intrinsically related to geometric characteristics of excursion sets defined by threshold exceedances, and constitutes one of the main objectives of many applications. Deriving formal asymptotic results to assess threshold exceedance probabilities implies a certain degree of complexity depending on the assumptions of the model under consideration. In this context, Adler and Taylor (2007) and Azaïs and Wschebor (2009) prove that, for a Gaussian random field, under rather restrictive appropriate conditions, an explicit error-bound for the order of approximation between the threshold exceedance probabilities and the expected Euler-Poincaré characteristic of the associated excursion set, can be established. This approach has been

followed by some extensions to certain classes of random fields (see, for instance, Adler et al. 2010, 2013). The literature in this context is usually related to Gaussian fields under stationarity hypotheses, but with an increasing interest in more general scenarios. Spatial deformation has been used in different application areas, such as image analysis or environmental studies, to represent certain forms of heterogeneity which can be explained by transformation of a reference stationary random field (see, for instance, Amit et al. 1991; Christensen et al. 1996; Glasbey and Mardia 1998, 2001; Goitía et al. 2004; Mardia et al. 2006; Angulo and Madrid 2014). Fitting homogeneous/isotropic random field models to spatially non-homogeneous data is also of interest (see, for example, Sampson and Guttorp 1992; Perrin and Senoussi 2000; Clerc and Mallat 2003; Anderes and Stein 2008; Anderes and Chatterjee 2009; Fouedjio et al. 2015; Vera et al. 2017). In this context, Angulo and Madrid (2010) study the asymptotic behaviour of the Euler-Poincaré characteristic, under the effect of spatial deformation and blurring transformation. Derivation of results in relation to threshold exceedance probabilities constitutes an open field in terms of the development of extensions with respect to the conditions required of the reference model, regarding the consideration of generalized forms of thresholds, etc. On the other hand, analysis of extremal behaviour also constitutes one of the main objectives in many applications oriented to risk assessment. In fact, different functionals related to geometrical characteristics of excursion sets, such as the exceedance area, the excess volume or the number of connected components, among others, provide suitable random indicators useful for quantification of risk (see, for example, Christakos and Hristopulos 1996, 1997; Adler and Taylor 2007; Angulo and Madrid 2010, 2014; Madrid et al. 2012, 2016; Chiu et al. 2013; Yang and Christakos 2015). If closed random sets defined from a random field are considered in terms of threshold exceedances, getting their probability distribution would be desirable. In this sense, approaches based on the theory of random closed sets (see Matheron 1975, as the origin of the mathematical basis), address this problem. The concept of *capacity functional* (see, for instance, Molchanov 2005, 2017; Schneider and Weil 2008; Chiu et al. 2013; Vila 2014) is a first approximation to the distribution of these sets, without actually being a probability distribution. From this concept, distributional properties such as independence, stationarity, isotropy and ergodicity, as well as expectation or covariance structure has been studied (see Castaing et al. 1997; Bohm and Schmidt 2003; Teran 2008), among other aspects.

Concerning risk analysis, in the last two decades, the development of a well-founded theory of measures of risk has arisen as a new scientific discipline, mainly motivated and also impulsed by areas of applications such as Finance and Insurance (see, for instance Artzner 1998; Wang and Dhaene 1998; Artzner et al. 1999; Wang 2000; Szego 2002; Goovaerts et al. 2004), although with an increasing interest in many other areas of knowledge due to its potential applicability (see, for example, Haimes 2004; Klüppelberg et al. 2014; Föllmer and Schied 2016). Among the variety of risk measure families introduced in this framework, quantile-based risk measures such as Value-at-Risk (VaR) and Average Value-at-Risk (AVaR) have received special attention because of their direct interpretation and easy computational implementation, besides the compliance of

certain axioms. There is a very vast literature on applications of risk measures under this approach in diverse fields; in the geostatistical context, see, for example, Bernardi et al. (2018), Li et al. (2018). This theory quickly advances in different challenging directions from the complexity perspective, including entropic risk measures (e.g. Fölmer and Knispel 2011; Ahmadi-Javid 2012) and systemic risk measures (e.g. Souza et al. 2016; Kleinow et al. 2017), risk transfer optimization (e.g. Filipović and Kupper 2008; Haier et al. 2016), generalized risk measures (e.g. Bellini et al. 2014), new properties/axioms such as elicitability (Wang and Ziegel 2015), etc. Because of the financial origin, this theory, has been mainly focused on risks analysis for random variables that represent monetary gains or losses. In particular, there is an increasing interest to formalize a theory of spatial risk measures (see, for example Koch 2017, 2019; Ahmed et al. 2019).

With the reference goal of bringing together the theory of risk measures and the analysis of structural characteristics of random field excursion sets, this thesis work addresses two general objectives:

(i) To develop methodologies for risk assessment in spatial and spatiotemporal scenarios in relation to threshold exceedances.

(ii) To analyze the effect of transformations, with reference to the spatial domain and the state space, on structural characteristics of threshold exceedance sets, as well as the consideration of related generalizations.

Regarding the first objective, a general and flexible methodology for spatial and spatiotemporal risk assessment is proposed based on a conditional approach. More specifically, for a given random field model and available observations, empirical distributions of different threshold exceedance indicators are obtained from conditional simulation, as a basis for evaluation of measures of risk. In particular, the study is focused on the global and local assessment of exceedance area and excess volume indicators, from which different risk maps are derived. For these first-order indicators, the compound cumulative distribution function (e.g. Lahiri et al. 1999; Wright et al. 2003; Craigmile et al. 2005; Zhang et al. 2008; French and Sain 2013) plays a key role, both formally and regarding the practical threshold specification (a formal definition is given in Chapter 3). Illustrations based on simulation are also performed for different spatial and spatiotemporal scenarios. Applications of this methodology, in spatial and spatio-temporal frameworks, are illustrated in fields such as Hydrology and Environmental Health. Relationships between widely used risk measures such as Value-at-Risk and Average Value-at-Risk, and structural characteristics of excursion sets of the underlying random field such as exceedance area or excess volume, for varying thresholds, are established. The asymptotics of these relationships are interpreted in relation to the shape parameter of the Generalized Pareto Distribution. Formal extensions are developed in scenarios of special interest ('level' and 'flow' type deformation effects and population covariate effect), and finally, a generalized formulation in terms of non-constant thresholds and non-Lebesgue measures is also established. In addition with respect to the second objective, in

this thesis work two approaches are proposed to address the asymptotic behaviour for threshold exceedance probabilities for random fields without some restrictive conditions of regularity, stationarity or isotropy. A first approach is based on regularizing sequences and a second approach on adequate spatial deformation and blurring transformations. For both approaches, the behaviour of the error bounds proposed by Adler and Taylor (2007) and Azaïs and Wschebor (2009) is discussed. This thesis report is structured as follows:

Part I provides a basic introduction to preliminary concepts and results used in the investigation. This part is divided in two chapters. In Chapter 1 aspects related to quantile-based risk measures are introduced. Chapter 2 refers to some aspects related to notation and definition of random field threshold exceedance indicators, with, a brief review of the asymptotics for threshold exceedance probabilities.

Part II is focused on spatial and spatiotemporal risk assessment of exceedances. This part is structured in tree chapters. In Chapter 3 a conditionally quantile-based risk assessment methodology is proposed for general scenarios. Random indicators based on structural characteristics of the underlying random field are considered in terms of exceedance areas and excess volumes. Some preliminary results concerning these indicators an their expected values are formalized in terms of the compound cumulative distribution function and its corresponding compound random variable. A detailed analysis of the methodology is described, first formally and then from a computational point of view. Finally, an illustration based on simulations under different spatial (Cauchy, Student and Fisher-Snedecor random fields) and spatiotemporal (blur-generated autoregressive model) scenarios is performed, emphasizing different aspects of particular relevance. Chapter 4 consists of three applications of the methodology proposed in the previous chapter in real scenarios: first, a comparative spatial rainfall risk analysis in Andalusia (Spain) for the same rainfall period but in different years; second, a predictive spatiotemporal rainfall risk analysis, in Cádiz province (Andalusia); third, the pollution issue of the *Carboneras* industrial area in the province of Almería is illustrated with this methodology as an example of spatiotemporal risk analysis. Analytical aspects and formal extension to generalized scenarios are addressed in Chapter 5. This chapter is structured in four sections. Section 5.1 establishes a reciprocal VaR-related interpretation of the expected excess volume vs. expected excedance area ratio in terms of the compound CDF AVaR-VaR increment. The asymptotics of this relationship is analyzed in relation to the shape parameter of the Generalized Pareto Distribution (GPD). In Section 5.2, 'level' and 'flow' type deformation are considered as generalized scenarios and previous results are developed under these effects. In Section 5.3 the population covariate effect is formalized. Here random indicators based on population density are considered. These indicators are analyzed in a real data application of ambient PM10 pollution population exposure, as before, in the *Carboneras* industrial area. Finally Section 5.4 establishes a generalized formulation in terms of non-constant thresholds an non-Lebesgue measures.

Part III is related to extensions of threshold exceedance asymptotic error bounds in generalized scenarios. This part consists of only one chapter with two sections. Section 6.1 analyses

this issue for non-suitable regular random fields by means of regularizing sequences (*mollifers*). Under appropriate assumptions, regularizing sequences provide sample-path convergence to the reference model. In this section, the smoothing effect and order of approximation are studied in relation to exceedance probabilities for increasing thresholds, considering different regularizing sequences, within different scenarios regarding the underlying random field. In Section 6.2 the asymptotic approaches introduced in Chapter 2 are discussed in the context of spatially deformed random fields.

Part IV also consists of one chapter. A summary, including references of contributions related to this thesis work (see Romero and Angulo 2014; Romero et al. 2015a,b; Angulo et al. 2016a,b; Romero et al. 2018), is given with further details on some directions of continuing research.

Source code developed was written with the R Statistical Computing software and the MATLAB environment. In particular, the R-package `RandomFields` was used for conditional simulation and model fitting, and for the generation of realizations of the different random field scenarios considered. The MATLAB environment was used for the remaining computational and graphical aspects (*mollifier* kernels, sliding windows, random indicators, etc.). A selection of source codes is included in the Appendix.

Introducción

Esta tesis doctoral se desarrolla en el marco de la línea de investigación "*Complejidad estructural y valores extremos en procesos espacio-temporales*", incluida en el programa de doctorado en Estadística Matemática y Aplicada de la Universidad de Granada con normativa RD99/2011. Los proyectos nacionales a través de MINECO/FEDER, EU denominados "*Análisis espacio-temporal: complejidad estructural, comportamiento extremal y medidas de información generalizadas*" (ref. MTM2012-32666) y "*Análisis de riesgos en sistemas complejos. avances teóricos y metodológicos*" (ref. MTM2015-70840-P), y el proyecto "*Campos aleatorios, procesos puntuales y medidas multifractales en espacio-tiempo: enfoques de análisis de información, complejidad y riesgo*" de MCIU/AEI/FEDER, EU, de los que es investigador principal el Prof. José Miguel Angulo, sustentan esta línea de trabajo.

La dinámica de una amplia variedad de fenómenos físicos (e.g. en Ciencias Medioambientales, Geofísica, etc.) se puede representar de forma apropiada según modelos de campos aleatorios. Existe una amplia literatura relacionada con la modelización de estos fenómenos, en particular bajo hipótesis de estacionariedad e isotropía en la estructura de covarianzas. En este sentido, dependiendo del fenómeno bajo estudio y de las características que se deseen analizar en el escenario espacial o espaciotemporal, se utilizan distintas familias de modelos de covarianzas: gausianas, exponenciales, Cauchy, modelos esféricos (ver, por ejemplo, Stein 1999; Gneiting and Schlather 2004; Gelfand et al. 2010; Strokorb et al. 2015), movimiento Browniano fraccionario, Matern, estables (ver, por ejemplo, Handcock and Wallis 1994; Diggle et al. 1998; Chiles and Delfiner 1999; Stein 2002; Guttorp and Gneiting 2006); familias como la de Cauchy o Dagum son apropiadas para modelar la dimensión fractal y el efecto de Hurst (ver Gneiting and Schlather 2004; Berg et al. 2008), etc. Diferentes aspectos probabilísticos de campos aleatorios son tratados, por ejemplo, en Adler (1981, 2008), Yaglom (1987a,b), Christakos (1992, 2000, 2017), Piterbarg (1996), Vanmarcke (2010). El análisis de comportamientos extremos está asociado al estudio de probabilidades de excedencia de umbrales, intrínsecamente relacionadas con características geométricas de conjuntos de excursión definidos por excedencias de umbrales, y constituye uno de los principales objetivos de muchas aplicaciones. La derivación de resultados asintóticos formales para evaluar probabilidades de excedencia de umbrales implica cierto grado de complejidad dependiendo de los supuestos del modelo bajo consideración. En este contexto, Adler and Taylor (2007) y Azaïs and Wschebor (2009) prueban que para un campo aleatorio gaussiano, bajo condiciones adecuadas

bastante restrictivas, se puede establecer una cota explícita para el orden de aproximación entre las probabilidades de excedencia de umbrales y la esperanza de la característica de Euler-Poincaré del conjunto de excursión asociado. A este enfoque le han seguido algunas extensiones a ciertas clases de campos aleatorios (ver, por ejemplo, Adler et al. 2010; Adler et al. 2013). La literatura en este contexto suele estar relacionada con campos gaussianos bajo hipótesis de estacionariedad, pero con un creciente interés en escenarios más generales. La deformación espacial se ha utilizado en diferentes áreas de aplicación, como el análisis de imágenes o estudios ambientales, para representar ciertas formas de heterogeneidad que pueden explicarse mediante la transformación de un campo aleatorio estacionario de referencia (ver, por ejemplo, Amit et al. 1991; Christensen et al. 1996; Glasbey and Mardia 1998, 2001; Goitía et al. 2004; Mardia et al. 2006; Angulo and Madrid 2014). El ajuste de modelos de campos aleatorios isotrópicos/homogéneos a datos espacialmente no homogéneos es otro área donde se ha trabajado mediante deformación espacial (ver, por ejemplo, Sampson and Guttorp 1992; Perrin and Senoussi 2000; Clerc and Mallat 2003; Anderes and Stein 2008; Anderes and Chatterjee 2009; Fouedjio et al. 2015; Vera et al. 2017). En este contexto, Angulo and Madrid (2010) estudian el comportamiento asintótico de la característica de Euler-Poincaré bajo el efecto de transformaciones de borrosidad y deformación espacial. La derivación de resultados relativos a probabilidades de excedencia de umbrales constituye un campo abierto en cuanto al desarrollo de extensiones, con respecto a las condiciones exigibles al modelo de referencia, sobre la consideración de formas generalizadas de los umbrales, etc. Por otro lado, el análisis de comportamientos extremos también constituye uno de los principales objetivos en muchas aplicaciones centradas en el análisis de riesgos. De hecho, distintos funcionales referidos a características geométricas de conjuntos de excedencias de umbrales proporcionan indicadores aleatorios útiles para la cuantificación del riesgo (ver, por ejemplo, Christakos and Hristopulos 1996, 1997; Adler and Taylor 2007; Angulo and Madrid 2010, 2014; Madrid et al. 2012, 2016; Chiu et al. 2013; Yang and Christakos 2015). Si se consideran conjuntos aleatorios cerrados definidos a partir de un campo aleatorio en términos de excedencia de umbrales, sería útil conocer su distribución de probabilidad. En este sentido, enfoques basados en la teoría de conjuntos aleatorios cerrados (ver Matheron 1975, como origen de su base matemática) abordan este problema. La introducción del conocido como funcional de capacidad (ver, por ejemplo, Molchanov 2005, 2017; Schneider and Weil 2008; Chiu et al. 2013; Vila 2014) es una primera aproximación a la distribución de estos conjuntos, sin ser realmente una distribución de probabilidad. A partir de este concepto, se han estudiado propiedades distribucionales como la independencia, estacionariedad, isotropía y ergocididad, la esperanza o la estructura de covarianzas (ver Castaing et al. 1997; Bohm and Schmidt 2003; Teran 2008), entre otros aspectos.

En el contexto del análisis de riesgos, a lo largo de las últimas dos décadas se ha llevado a cabo el desarrollo de toda una teoría de medidas de riesgo, que de hecho se ha convertido en una nueva disciplina científica, principalmente motivada e impulsada por áreas de aplicación tales como Finanzas y Seguros (ver, por ejemplo Artzner 1998; Wang and Dhaene 1998; Artzner et al. 1999; Wang 2000; Szego 2002; Goovaerts et al. 2004), aunque con un creciente interés en otras

muchas áreas del conocimiento debido a su potencial aplicabilidad (ver, por ejemplo, Haimes 2004; Klüppelberg et al. 2014; Föllmer and Schied 2016). Entre la diversidad de familias de medidas de riesgo introducidas en estos ámbitos, las medidas de riesgo basadas en cuantiles tales como el Valor en Riesgo o Value-at-Risk (VaR) y el Déficit Esperado o Average Value-at-Risk (AVaR) han recibido especial atención dado lo directo de su interpretación y fácil implementación computacional, además del cumplimiento de ciertos axiomas con interpretaciones significativas. Existe una amplia literatura sobre aplicaciones de medidas de riesgo bajo este enfoque en diversas áreas; en el contexto geoestadístico, ver, por ejemplo, Bernardi et al. (2018), Li et al. (2018). Esta teoría avanza rápido en diferentes direcciones que abordan importantes desafíos desde la perspectiva de la complejidad, medidas de riesgo entrópicas (e.g. Fölmer and Knispel 2011; Ahmadi-Javid 2012), medidas de riesgo sistémicas (e.g. Souza et al. 2016; Kleinow et al. 2017), optimización de las transferencias de riesgos (e.g. Filipović and Kupper 2008; Haier et al. 2016), medidas de riesgo generalizadas (e.g. Bellini et al. 2014), nuevas propiedades como la elicitabilidad (Wang and Ziegel 2015), etc. Dado su origen, eminentemente financiero, esta teoría ha estado centrada principalmente en al análisis de riesgos de variables aleatorias que representan perdidas o ganancias monetarias. En particular, hay un creciente interés en el desarrollo de una teoría fundamentada de medidas de riesgo espaciales (ver Koch 2017, 2019; Ahmed et al. 2019).

Con el objetivo de referencia de hacer interactuar la teoría de medidas de riesgo con el análisis de características estructurales de conjuntos de excursión de campos aleatorios, este trabajo de tesis aborda dos objetivos generales:

(i) Desarrollo de metodologías para la valoración de riesgos en entornos espaciales y espacio-temporales relativos a excedencias de umbrales.

(ii) Análisis del efecto de transformaciones, con referencia al dominio espacial y al espacio de estados, sobre características estructurales de conjuntos de excedencia de umbrales así como la consideración de formas generalizadas.

Con respecto al primer objetivo, se propone una metodología general y flexible para la valoración de riesgos en entornos espaciales y espacio-temporales basada en un enfoque condicional. De forma específica, para un modelo de campo aleatorio dado y para un conjunto de observaciones disponibles, se obtienen distribuciones empíricas de distintos indicadores de excedencia de umbral por medio de simulación condicionada, como base para la evaluación de medidas de riesgo. En concreto, el estudio se centra en la valoración global y local de indicadores relacionados con el área de excedencia y con el volumen en exceso, a partir de los cuales se derivan diferentes mapas de riesgo. Para éstos, también llamados indicadores de primer orden, la función de distribución acumulativa compuesta (e.g. Lahiri et al. 1999; Wright et al. 2003; Craigmile et al. 2005; Zhang et al. 2008; French and Sain 2013) juega un papel clave, tanto desde un punto de vista formal como práctico, en este último caso relacionada con la especificación práctica del umbral. Se realiza una ilustración basada en simulación en diferentes escenarios espaciales y espacio-temporales.

Se aplica esta metodología en entornos espaciales y espacio-temporales en campos tales como la Hidrología y Medio Ambiente. Se formalizan relaciones analíticas entre los indicadores área de excedencia y volumen de exceso con las medidas de riesgo VaR y AVaR, para umbrales variables. Estas relaciones proporcionan interpretaciones asintóticas interesantes en términos del parámetro de forma de la distribución de Pareto generalizada. Se realizan extensiones formales en escenarios generalizados (efectos de deformaciones tipo 'nivel' y 'flujo' y el efecto de la covariable población) y, finalmente, se establece una formulación generalizada que involucra umbrales no constantes y medidas no Lebesgue. Adicionalmente con respecto al segundo objetivo, en este trabajo de tesis se proponen dos enfoques para abordar el comportamiento asintótico de las probabilidades de excedencia de umbrales para campos aleatorios sin algunas condiciones restrictivas de regularidad, estacionariedad o isotropía. Un primer enfoque está basado en sucesiones regularizantes y un segundo enfoque en deformaciones espaciales y trasformaciones de borrosidad adecuadas. Para ambos enfoques se discute el comportamiento de las cotas del error propuestas por Adler and Taylor (2007) y Azaïs and Wschebor (2009). Se realizan extensiones formales de los resultados anteriores en escenarios generalizados (efectos de deformaciones tipo 'nivel' y 'flujo' y el efecto de la covariable población) y, finalmente, se establece una formulación generalizada que involucra umbrales no constantes y medidas no Lebesgue.

Esta memoria de tesis se estructura como sigue:

En la Parte I se proporciona una introducción básica de conceptos y resultados que son utilizados a lo largo del texto. Esta parte está dividida en dos capítulos. En el Cap. 1 se introducen aspectos relacionados con medidas de riesgo basadas en cuantiles. El Cap. 2 se refiere a notación y definición de indicadores de excedencia de umbrales de campos aleatorios, con una revisión breve de algunos enfoques asintóticos para la cota del error de probabilidades de excedencia de umbrales.

La Parte II se centra en la valoración de riesgos de excedencia de umbrales en entornos espaciales y espacio-temporales. Esta parte está estructurada en tres capítulos. En el Cap. 3 se propone una metodología condicional de valoración de riesgos basada en cuantiles para escenarios generales. Se consideran indicadores aleatorios basados en características estructurales del campo aleatorio subyacente en términos de áreas de excedencia y volúmenes de exceso. Algunos resultados preliminares referidos a estos indicadores y a sus valores esperados son formalizados en términos de la función de distribución compuesta y su variable aleatoria asociada. Se realiza un análisis detallado de la metodología de un modo formal y desde un punto de vista computacional. Para terminar, se ilustran por simulación diferentes aspectos de especial relevancia en varios escenarios espaciales (modelos de Cauchy, Student y Fisher-Snedecor) y espacio-temporales (modelo autorregresivo generado por borrosidad). En el Cap. 4 se consideran tres aplicaciones de la metodología utilizando datos asociados a problemas reales: en primer lugar, se realiza un análisis espacial comparativo del riesgo de precipitación para el mismo periodo pluviométrico pero en distintos años; en segundo lugar se realiza, en un entorno espacio-temporal, un análisis predictivo del riesgo de precipitación en la provincia de Cádiz; en tercer lugar, esta metodología

es utilizada para abordar el problema de la contaminación del aire por partículas pesadas en la zona industrial de *Carboneras* en la provincia de Almería, como un ejemplo de análisis espacio-temporal del riesgo. En el último capítulo de esta parte, Cap. 5, realiza un estudio detallado de aspectos analíticos y extensiones formales en escenarios generalizados. Este capítulo se estructura en cuatro secciones. En la Sección 5.1 se establece una interpretación recíproca (en relación al VaR) de la tasa de volumen de exceso esperado frente al área de excedencia esperada en términos del incremento AVaR-VaR para la variable aleratoria asociada a la distribución compuesta. El comportamiento asintótico de esta relación es analizado en relación al parámetro de forma de la distribución de Pareto generalizada (GPD). En la Sección 5.2 se desarrollan los resultados anteriores bajo el efecto de escenarios generalizados inducidos por deformaciones espaciales tipo 'nivel' y 'flujo'. En la Sección 5.3 se formaliza el efecto de la covariable población sobre estas relaciones. El problema real de la exposición de la población a contaminación del aire por partículas pesadas es analizado por medio de indicadores de población, como antes, en la zona industrial de *Carboneras*. Finalmente, en la Sección 5.4 se establece una formulación generalizada en términos de umbrales no constantes y medidas no Lebesgue.

En la Parte III se aborda el comportamiento asintótico de las cotas del error de aproximación de probabilidades de excedencia de umbrales en escenarios generalizados. Esta parte tiene un solo capítulo con dos secciones. En la sección 6.1 se analiza este problema para campos aleatorios sin condiciones de regularidad suficientes por medio de sucesiones regularizantes (*mollifers*). Bajo supuestos apropiados, las sucesiones regularizantes proporcionan convergencia al modelo de referencia. En esta sección, se estudian el efecto de suavizado y el orden de aproximación en relación con probabilidades de excedencia para umbrales crecientes considerando diferentes sucesiones regularizantes, para diferentes escenarios. Por último, en la Sección 6.2 se hace un análisis de los enfoques asintóticos introducidos en el Cap. 2 para campos aleatorios obtenidos por deformación espacial.

La Parte IV también contiene un solo capítulo. Se presenta un resumen, incluyendo referencias de contribuciones relacionadas con el trabajo de esta tesis (see Romero and Angulo 2014; Romero et al. 2015a,b; Angulo et al. 2016a,b; Romero et al. 2018), además de algunas direcciones a seguir y líneas abiertas para la continuación de la investigación.

El código fuente desarrollado ha sido escrito con el software R Statistical Computing y el entorno MATLAB. En particular, el paquete R `RandomFields` se ha usado para la simulación condicionada y el ajuste de modelos, y para la generación de realizaciones de los diferentes escenarios de campos aleatorios considerados. El entorno MATLAB se ha utilizado para los restantes aspectos computacionales y gráficos (núcleos *mollifier*, ventanas deslizantes, indicadores aleatorios, etc.). Una selección de códigos fuente se incluye en el Apéndice.

Part I

PRELIMINARIES

Chapter 1

Risk Measure Theory

In this chapter technical notation, definitions and some preliminary relations related to risk measures are introduced.

1.1 Coherent and Convex Risk Measures

Risk measure theory is a developing scientific discipline motivated by areas of application such as Finance, Insurance, Environmental and Health Sciences, etc., with increasing interest in risk measures that take into account spatial features of the environment to detect areas at risk (see, for example, Christakos 1992, 2000; Christakos and Hristopulos 1996, 1997; Föllmer and Schied 2002; Koch 2017, 2019). Mainly motivated by financial and actuarial problems and applications, different sets of properties are considered as reference for definition of classes of some risk measures.

Definition 1. *Given a probability space* $(\Omega, \mathscr{F}, P)$*, and* $\mathscr{M}_{\mathscr{B}}(\Omega, \mathscr{F}, P)$ *being the space of real-valued Borel-measurable functions defined on* $(\Omega, \mathscr{F}, P)$*, a risk measure is a functional*

$$\rho : \mathscr{M}(\Omega, \mathscr{F}, P) \to \bar{\mathbb{R}}$$

satisfying certain suitable conditions, where $\mathscr{M}(\Omega, \mathscr{F}, P)$ *is a linear subspace of* $\mathscr{M}_{\mathscr{B}}(\Omega, \mathscr{F}, P)$*, and* $\bar{\mathbb{R}}$ *denotes the compactification of* $\mathbb{R}$ *given by* $\mathbb{R} \cup \{-\infty, +\infty\}$. □

Often, $\mathscr{M}(\Omega, \mathscr{F}, P)$ is taken to be an $L^p(\Omega, \mathscr{F}, P)$ space, with $p \in [1, \infty]$. Hereafter, we assume that the argument random variables represent loss in some sense.

As mentioned above, mainly based on financial and actuarial problems, some fundamental classes such as *coherent* and *convex* risk measures (see, for example, Föllmer and Schied 2016) are attributed special significance, each one with some of the properties or axioms listed below:

(i) *Translation invariance*: $\rho(X + a) = \rho(X) + a$, for $a \in \mathbb{R}$.

(ii) *Monotonicity*: $X \leq Y \;\; P-\text{a.s.} \Rightarrow \rho(X) \leq \rho(Y)$.

(iii) *Positive homogeneity*: $\rho(aX) = a\rho(X)$, for $a > 0$.

(iv) *Sub-additivity*: $\rho(X+Y) \leq \rho(X) + \rho(Y)$.

(v) *Convexity*: $\rho(aX + (1-a)Y) \leq a\rho(X) + (1-a)\rho(Y)$, for $a \in [0,1]$.

A detailed analysis of axioms (i)-(v) is developed, for instance, in Föllmer and Schied (2016).

Definition 2. *A risk measure ρ is said to be coherent if it satisfies (i), (ii), (iii) and (iv).* □

Definition 3. *A risk measure ρ is said to be convex if it satisfies (i), (ii) and (v).* □

Every coherent risk measure is a convex risk measure, but not conversely. Coherent and convex risk measures are important, in particular, because they can be expressed in terms of mathematical expectations by means of dual representation theorems. (From a conceptual point of view, and in the context of financial risk assessment, coherency was formally introduced and justified as a desirable set of properties in the seminal paper by Artzner et al. (1999), while convexity was proposed by Föllmer and Schied (2002), and parallelly by Frittelli and Gianin (2002), for a less restrictive instrument regarding risk diversification.)

1.2 Quantile-Based Risk Measures

Risk measures formulated in terms of distribution moments and/or quantiles are usually considered because of their easy interpretation in terms of the probability distribution. Here, in particular, the definitions of the well-known quantile-based risk measures Value-at-Risk (VaR) and Average Value-at-Risk (AVaR) are introduced.

Definition 4. *Let X be a loss random variable, with cumulative distribution function (CDF) F_X. Let $\alpha \in (0,1]$. The Value-at-Risk at confidence level $1-\alpha$ of X, $VaR_{1-\alpha}(X)$, is defined as the lower $(1-\alpha)-$quantile of the distribution of X:*

$$VaR_{1-\alpha}(X) = \inf\{x \in \mathbb{R} : F_X(x) \geq 1-\alpha\}.$$

□

It follows that if X is a continuous random variable, then

$$VaR_{1-\alpha}(X) = F_X^{-1}(1-\alpha)^-,$$

where '$^-$' stands for the 'lim inf' of the set.

Definition 5. *Under the previous assumptions on X and α, the Average Value-at-Risk at confidence level $1-\alpha$ of X, $AVaR_{1-\alpha}(X)$, is defined as*

$$AVaR_{1-\alpha}(X) = \frac{1}{\alpha}\int_{1-\alpha}^{1} VaR_p(X)dp.$$

□

In the case where X has a continuous probability distribution, $AVaR_{1-\alpha}(X)$ is a conditional expectation:

$$AVaR_{1-\alpha}(X) = E[X|X > VaR_{1-\alpha}(X)].$$

Hence, in this case, while $VaR_{1-\alpha}(X)$ represents the minimal loss that will occur in the $100\alpha\%$ worst scenarios, $AVaR_{1-\alpha}(X)$ represents the average loss that will occur in the $100\alpha\%$ worst scenarios. In general, $VaR_{1-\alpha}(\cdot)$ is not a coherent risk measure, because of lack of sub-additivity, except for special cases, whereas $AVaR_{1-\alpha}(\cdot)$ is always a coherent risk measure. In fact, VaR does not take into account the tail behaviour above the specified confidence level quantile, whilst AVaR does it.

A generalized formulation of quantile-based risk measures is given by the so-called *spectral risk measures*, defined as follows

Definition 6. *Under the previous assumptions on X, the Spectral Risk Measure with weight function ϕ, $M_\phi(X)$, is defined as*

$$M_\phi(X) = \int_0^1 VaR_p(X)\phi(p)dp,$$

where ϕ satisfies the conditions $\phi(\cdot) \geq 0$ and $\int_0^1 \phi(p)dp = 1$.

$M_\phi(\cdot)$ is a coherent risk measure for monotonically non-decreasing weight functions (e.g. $AVaR_{1-\alpha}(\cdot)$). □

1.3 Analytical Examples

Quantile-based risk measures have, as mentioned above, the advantage of their easy interpretation in terms of the distribution function, but the disadvantage that they can not be always calculated analytically. Some examples of VaR and AVaR for different probability functions are illustrated below.

Example 1. *Let X be a Standard Gaussian random variable, $X \rightsquigarrow N(0,1)$. Then*

$$VaR_{1-\alpha}(X) = \sqrt{2}erf^{-1}(1-2\alpha)$$

$$AVaR_{1-\alpha}(X) = \frac{\sqrt{2}}{\alpha}\int_{1-\alpha}^{1} erf^{-1}(2p-1)dp$$

where erf denotes the Gauss error function, $erf(x) = \frac{2}{\sqrt{\pi}}\int_0^x \exp(-t^2)dt$*, whose inverse exists for* $\alpha \in [0,1]$ *and can be approximated numerically.* □

Example 2. *Let X be a Gaussian random variable,* $X \rightsquigarrow N(\mu,\sigma)$*. Then*

$$VaR_{1-\alpha}(X) = \mu + \sigma VaR_{1-\alpha}(Y)$$
$$AVaR_{1-\alpha}(X) = \mu + \sigma AVaR_{1-\alpha}(Y)$$

where $Y \rightsquigarrow N(0,1)$*.* □

Example 3. *Let X be a Exponential random variable,* $X \rightsquigarrow \exp(\lambda)$*. Then*

$$VaR_{1-\alpha}(X) = \frac{-\log\alpha}{\lambda}$$
$$AVaR_{1-\alpha}(X) = \frac{1-\log\alpha}{\lambda}$$

□

Example 4. *Let X be a Log-normal random variable,* $X \rightsquigarrow lognorm(\lambda,\sigma)$*, i.e.* $X = \exp(\lambda+\sigma Y)$ *with Y a standard Gaussian r.v.. Then*

$$VaR_{1-\alpha}(X) = \exp(\lambda + \sigma VaR_{1-\alpha}(Y))$$
$$AVaR_{1-\alpha}(X) = \frac{1}{\alpha}\exp\left(\lambda+\frac{\sigma^2}{2}\right)\Phi\left(\alpha - VaR_{1-\alpha}(Y)\right)$$

where Φ *represents the Standard Gaussian cumulative distribution function.* □

Unfortunately, for almost all of distributions it is only possible to obtain an implicit expression of these risk measures, providing a numerical approximation, as in the examples below.

Example 5. *Let X be a Gamma random variable,* $X \rightsquigarrow Gamma(\lambda,k)$*, with* $k \in \mathbb{N}$*. Then,* $VaR_{1-\alpha}(X)$ *is the only solution z of the equation*

$$\alpha - \exp(-\lambda z)\sum_{i=0}^{k-1}\frac{(\lambda z)^i}{i!} = 0,$$

and

$$AVaR_{1-\alpha}(X) = \frac{1}{\alpha}\left(\frac{k\alpha^k}{\lambda} + \frac{\lambda^{k-1}}{(k-1)!}z^k\exp(-\lambda z)\right),$$

where $z = VaR_{1-\alpha}(X)$*.*
In fact, if $k=1$ *this is the exponential distribution and both equations provide the same expressions for Value-at-Risk and Average Value-at-Risk obtained in Example 3.* □

The previous examples based on continuous r.v. highlight complexities related to obtaining analytical expressions or computational approximations of these risk measures in some cases. These problems even increase when discrete random variables are considered.

Example 6. *Let X be a Poisson random variable, $X \rightsquigarrow P(\lambda)$. Then, $VaR_{1-\alpha}(X)$ is the only integer solution of*

$$\inf_{z\in\mathbb{Z}}\left\{\sum_{k=0}^{z}\exp(-\lambda)\frac{\lambda^k}{k!}\geq 1-\alpha\right\}$$

Once the infimun above is solved, then

$$AVaR_{1-\alpha}(X)=\lambda+\frac{\lambda^{z+1}}{\alpha z!}\exp(-\lambda)+\frac{\lambda^{z}}{\alpha(z-1)!}\exp(-\lambda),$$

where $z=VaR_{1-\alpha}(X)$. □

These examples point out the need to develop methodologies that allow computing these measures for random elements arising from the phenomena under analysis.

Chapter 2

Random Field Threshold Exceedances

Random field models are involved in the representation and study of a wide range of real phenomena in Geophysics, Hydrology and Environmental Sciences, among other areas. There is a vast literature devoted to theoretical aspects and related statistical methodology, with particular emphasis in developments for the case of Gaussian and/or stationary random fields (see, for example, Adler and Taylor 2007; Piterbarg 1996; Yaglom 1987a), although with increasing interest in more general scenarios (see, for example, Adler et al. 2010, 2013; Christakos 1992; Vanmarcke 2010; Yakir 2013). In real applications concerning the assessment on extremal behaviour, one of the most significant problems refers to the evaluation of different forms of excursion probabilities; in particular,

$$P\left[\sup_{s\in D} X(s) \geq u\right], \tag{2.1}$$

where, formally, X is a centered random field on the set $D \subseteq \mathbb{R}^d$, which is assumed to be compact under the usual metric, and u represents a given threshold. Probabilistic and statistical aspects of random field excursion sets and extrema are addressed in key references such as Adler and Taylor (2007) and Azaïs and Wschebor (2009). Geometrical characteristics of excursion sets defined by threshold exceedances are intrinsically related to excursion probabilities (see, for example, Angulo and Madrid 2010; Azaïs and Wschebor 2009; Chiu et al. 2013), and can be used in practice in the formulation of indicators for risk assessment.

In this chapter, some aspects related to notation and definition of random field threshold exceedance indicators are introduced. A brief review of the asymptotic error bound approximation for threshold exceedance probabilities is also performed.

2.1 Preliminary Elements

Hereafter, X denotes a spatial random field (RF), i.e. $X = \{X(s) \in \mathscr{M}_{\mathscr{B}}(\Omega, \mathscr{F}, P) : s \in S \subseteq \mathbb{R}^d\}$, and $D \subseteq S$ is a bounded subdomain with non-null Lebesgue measure, $\lambda(D) > 0$. For simplicity, all the random variables $X(s)$ are assumed to have a continuous distribution. Let $u \in \mathbb{R}$ be a pre-fixed threshold level.

Definition 7. *$A_u(X,D) = \{s \in D : X(s) \geq u\}$ is the excursion set of X in D over level $u \in \mathbb{R}$.* □

While for $d = 1$ this is the disjoint union of closed sets some of which may be degenerate, for $d > 1$ the excursion set involves a higher geometrical complexity. In particular, aspects related to the fragmented structure of the set can be analyzed in terms of its connected components. A general treatment of the geometry of random field excursion sets based on intrinsic volumes is approached, for instance, by Adler and Taylor (2007).

Definition 8. *$\left\{I_u^X(s) = 1_{\{X(s) \geq u\}} : s \in S\right\}$ is the u-exceedance indicator RF.* □

Definition 9. *$\{X_u(s) = \max\{0, X(s) - u\} : s \in S\}$ is the u-excess RF.* □

Let $M = \sup_{s \in D} X(s)$, the random variable of the supremum, with $p_M(x)$ as the density of its distribution. As mentioned before, the interest is focused on the evaluation of $P[M \geq u]$. Since the distribution of the supremum is usually infeasible, a main goal consists of finding appropriate upper bounds for $p_M(x)$ or providing asymptotic error bound approximations for $P[M \geq u]$ with respect to structural characteristics of the excursion set of X in D above the level u.

2.2 Asymptotic Error Bound for Threshold Exceedance Probabilities

Derivation of formal asymptotic results involves a certain degree of complexity depending on model assumptions and probability specifications. Under Gaussianity and/or stationarity assumptions, jointly with *suitable regularity conditions* introduced bellow, different approaches succeed with this issue. In Azaïs and Wschebor (2009), sc. 7.1. a set of axioms, concerning the spatial domain and the random field, is introduced. Adler and Taylor (2007) also provide a set of suitable regularity conditions that is equivalent to this set of axioms. The definition bellow comprise these conditions according to Azaïs and Wschebor (2009).

Definition 10. *A random field X defined on a spatial domain D is said to satisfy suitable regularity conditions if:*

(i) D is a compact set.

(ii) $D = \bigcup_{j=1}^{m} S_j$ *is a disjoint union of a finite number of orientable* C^3 *manifolds of dimension* j *without boundary.*

(iii) Every S_j *has an atlas with 2nd derivatives of the inverse function all bounded by a fixed constant.*

(iv) X *is defined on an open set containing* D *and has* C^2 *paths.*

(v) $\forall s \in D$ *the distribution of* $(X(s), X'(s))$ *does not degenerate.*

(vi) $\forall t, s \in D, t \neq s$*, the distribution of* $(X(t), X(s))$ *does not degenerate.*

(vii) Almost surely the maximun of $X(s)$ *on* D *is attained at a single point.*

(viii) Almost surely $\forall j = 1, \ldots, m$ *there is no point* t *in* S_j *with* $X'_j(t) = 0$ *and* $det(X''_j(t)) = 0$*, where* X', X'' *denote the first and second order derivatives of* X *along* S_j*.*

□

It is important to highlight how restrictive are these conditions, particularly for the random field.

In this context, according to Azaïs and Wschebor (2009), p. 207, under appropriate conditions one attempts to write

$$P\left[\sup_{s\in D} X(s) \geq u\right] \simeq A(u)\exp\left(\frac{-u^2}{2\sigma^2}\right) + B(u), \tag{2.2}$$

where,

1. $A(u)$ is a known function having polynomially bounded growth as $u \longrightarrow +\infty$
2. $\sigma^2 = \sup_{s\in D} Var(X(s))$
3. $B(u)$ is the error of approximation, bounded by a centered Gaussian density with variance $\sigma_1^2 < \sigma^2$.

Adler and Taylor (2007) prove that, for a Gaussian random field and under appropriate regularity conditions,

$$\left| P\left[\sup_{s\in D} X(s) \geq u\right] - E\left[\varphi(A_u(X, D))\right] \right| < O\left(e^{\frac{-\alpha u^2}{2\sigma^2}}\right), \tag{2.3}$$

where φ represents the Euler-Poincaré characteristic (EPC), $A_u(X, D)$ is the excursion set of X over D at u-level, σ^2 is the variance of X (which is assumed to be constant) and $\alpha > 1$ is an

identifiable constant. Some extensions of this important result for certain classes of non-Gaussian random fields are also developed in several subsequent papers (e.g. Adler et al. 2010, 2013). The main goal of this approach is to find a suitable explicit error-bound for the approximation.

Azaïs and Wschebor (2009) establish, under appropriate conditions, an upper bound for the tail of the distribution of the supremum in the form

$$P\left[\sup_{s\in D} X(s) \geq u\right] \leq \int_{u}^{+\infty} \bar{p}(x)dx, \tag{2.4}$$

where $\bar{p}(x)$ (see Azaïs and Wschebor 2009, p. 217) is a certain upper bound of the real density. In contrast to Adler and Taylor, this approach is not focused on the error-bound of $B(u)$ in (2.2) but on the size of the variance of the Gaussian bound for this error $B(u)$. Furthermore, these authors also provide the explicit error-bound based on the EPC as in Adler and Taylor's approach. Indeed, according to Azaïs and Wschebor (2009) results (see Th. 12, Cor. 13 and Cor. 14),

$$\liminf_{u\longrightarrow+\infty} -2u^{-2}\log\left|E\left[\varphi(A_u(X,D))\right] - P[M\geq u]\right| \geq 1 + \inf_{s\in D}\frac{1}{\sigma_s^2+k_s^2}, \tag{2.5}$$

where,

1. $\sigma_s^2 = \sup_{t\neq s\in D}\frac{Var(X(t)|X(s),X^{'}(s))}{(1-r(t,s))^2}$
2. $r(t,s)$ is the covariance.
3. $k_s = \sup_{t\neq s\in D}\frac{dist(-r_{01}(t,s),C_{s,j})}{1-r(t,s)}$ (see Azaïs and Wschebor 2009 for definition of the first term of Taylor expansion, $-r_{01}(t,s)$, and the convex cone $C_{s,j}$.)

Other approaches, such us the double-sum method of Piterbarg (see Piterbarg 1996) as an important precursor to all of these results (although without realizing that the expected Euler-Poincaré characteristic of an excursion set was involved), methods concerning the distribution of the area in the cross-section threshold (see Vanmarcke 2010), and others based on the theory of random closed sets (see, Chiu et al. 2013; Molchanov 2005), have been applied in the study of exceedance probabilities for the Gaussian and/or stationary framework.

Extensions of this error-bound, for deformation and blurring transformations of stationary random fields and respect to a regularizing sequences based approach, are addressed in Chapter 6.

Part II

SPATIAL AND SPATIOTEMPORAL RISK ASSESSMENT OF EXCEEDANCES

Chapter 3

Methodological Aspects

In this chapter, a methodology for risk assessment in spatial and spatiotemporal scenarios is proposed. It is general in the sense that the only restriction for its applicability is related to the ability of generating data under conditional simulation. This methodology is based on classical quantile-based risk measures evaluated on random indicators related to structural characteristics of the underlying random field. A simulation study of this methodology for both, spatial and spatiotemporal frameworks, is performed.

3.1 Structural Random Indicators of Random Fields

As mentioned in Chapter 1, risk measures are evaluated on random variables representing loss in some sense. In this thesis work, indicators related to exceedance areas and excess volumes are considered (see Table 3.1 for notation), under the assumption that suitable regularity and measurability conditions (see Chapter 2, Definition 10) hold for their existence, as well as for the existence of their expectations (see, for instance, Adler 1981; Adler and Taylor 2007; Azaïs and Wschebor 2009, etc.)

Indicator of exceedance area	**Notation**	**Definition**
Absolute	$\lambda(A_u(X,D))$	$\int_{A_u(X,D)} ds$
Relative (w.r.t. D)	$\lambda^D(A_u(X,D))$	$\frac{\lambda(A_u(X,D))}{\lambda(D)}$
Indicator of excess volume	**Notation**	**Definition**
Absolute	$V(A_u(X,D))$	$\int_{\cup_{u'\geq u} A_{u'}(X,D)} ds du'$
Relative w.r.t. D	$V^D(A_u(X,D))$	$\frac{V(A_u(X,D))}{\lambda(D)}$
Relative w.r.t. A_u	$V^{A_u}(A_u(X,D))$	$\frac{V(A_u(X,D))}{\lambda(A_u(X,D))}$
Relative per connected component C_i (average, for $i = 1,\ldots,N_{cc}^D$)	$\bar{V}^{cc}(A_u(X,D))$	$\frac{1}{N_{cc}^D}\sum_{i=1}^{N_{cc}^D}\left\{\frac{V(A_u(X,C_i))}{\lambda(A_u(X,C_i))}\right\}$

Table 3.1: Some first-order random indicators of RF threshold exceedances.

For a given threshold u and a subdomain D, $\lambda(A_u(X,D))$ expresses the total area with the values of the random magnitude represented by the RF lying above the threshold u; $\lambda^D(A_u(X,D))$ represents the exceedance area ratio with respect to the subdomain D; hereafter $E[\lambda(A_u(X,D))]$ and $E[\lambda^D(A_u(X,D))]$ denote their respective expected values. Further, $V(A_u(X,D))$ expresses the total excess volume of the RF above the threshold u; $V^D(A_u(X,D))$ represents the excess volume ratio with respect to the subdomain D; as before, $E[V(A_u(X,D))]$ and $E[V^D(A_u(X,D))]$ denote their corresponding expected values. In Section 3.4, some other indicators of practical interest are analyzed, such as the volume ratio with respect to the area of the excursion set, $V^{A_u}(A_u(X,D))$, and the average volume ratio per (non-degenerate) connected component of the excursion set, $\bar{V}^{cc}(A_u(X,D))$ (this indicator is only considered when the number of non-degenerate connected components, N_{cc}^D, is finite or, otherwise, for connected components with a certain minimum area size). It should be noted that the specific indicators here considered are invariant with respect to changes in the values of the random field variables corresponding to subsets of locations with zero Lebesgue measure. In particular, the possibility of degenerate excursion sets consisting of only isolated points is not excluded; however, in such cases the exceedance area, as well as the excess volume, will be 0. This can be interpreted in the sense that, under such indicators, risk is evaluated on the basis of non-degenerate occurrences of exceedances with respect to the dimension of the domain. (Nevertheless, as an aspect of interest, for regularity conditions under which the probability of having degenerate tangence points to a given threshold becomes null, see multiparameter versions of Bulinskaya's theorem in Adler and Taylor 2007; Azaïs and Wschebor 2009, among other sources.)

In general, the distributions of these indicators are unknown, and analytical expressions or numerical approximations for the considered risk measures are unfeasible. This supports, as mentioned before, the importance of developing suitable methodologies that allow to compute these measures under general conditions.

3.2 Some Preliminary Results

In this section, some preliminary formalizations and results concerning the indicators defined in Section 3.1 and their expected values are introduced.

Let $F_X^D(x)$ be the *compound* cumulative distribution function (CDF) defined as

$$F_X^D(x) = \int_D F_{X(s)}(x)\lambda^D(ds), \tag{3.1}$$

where $F_{X(s)}$ denotes the CDF of $X(s)$, and $\lambda^D(ds) := \frac{ds}{\lambda(D)}$ represents the normalized Lebesgue measure on D. Let X^D be the corresponding *compound* r.v., whose values are obtained by first randomly (i.e. according to the normalized Lebesgue measure) selecting a location s within the domain D and then assigning the corresponding $X(s)$ realization. Let $S_X^D(\cdot) = 1 - F_X^D(\cdot)$, i.e. the *decumulative* distribution function (DDF) of X^D. In what follows, suitable regularity and measurability conditions will be referred to hold for random field X in order to guarantee that the indicators considered are well defined, as well as for the existence of their expectations (see, for instance, Adler 1981, Sec. 3.2; Adler and Taylor 2007, Sec. 6.2; Azaïs and Wschebor 2009, Sec. 7.1; Vanmarcke 2010, Sec. 3.6).

Proposition 3.2.1. *Given a spatial RF X on $S \in \mathbb{R}^d$ satisfying suitable regularity and measurability conditions, a bounded subdomain $D \subseteq S$, and a fixed threshold $u \in \mathbb{R}$, the following relations hold:*

(i) $\lambda(A_u(X,D)) = \int_D I_u^X(s)ds$

(ii) $E[\lambda(A_u(X,D))] = \lambda(D)S_X^D(u)$

(iii) $E[\lambda^D(A_u(X,D))] = S_X^D(u)$

(iv) $V(A_u(X,D)) = \int_u^{+\infty} \lambda(A_{u'}(X,D))du' = \int_D X_u(s)ds$

(v) $E[V(A_u(X,D))] = \lambda(D)\int_u^{+\infty} S_X^D(u')du' = \lambda(D)E[X_u^D]$

(vi) $E[V^D(A_u(X,D))] = \int_u^{+\infty} S_X^D(u')du' = E[X_u^D]$

where $X_u^D = \max\{0, X^D - u\}$.

Proof

(i) Since $I_u^X(s) = 1$ if $s \in A_u(X,D)$, and $I_u^X(s) = 0$ if $s \notin A_u(X,D)$, it follows that $\lambda(A_u(X,D)) = \int_{A_u(X,D)} ds = \int_D I_u^X(s)ds$.

(ii) By Fubini's theorem, $E[\lambda(A_u(X,D))] = \int_D P[X(s) \geq u]ds = \int_D S_{X(s)}ds = \int_D \left(1 - F_{X(s)}(u)\right) ds = \lambda(D) - \int_D F_{X(s)}(u)ds$, with $S_{X(s)}$ being the DDF of $X(s)$. Hence, by Eq. (3.1), $E[\lambda(A_u(X,D))] = \lambda(D)(1 - F_X^D(u)) = \lambda(D)S_X^D(u)$.

(iii) $E[\lambda^D(A_u(X,D))] = E\left[\dfrac{\lambda(A_u(X,D))}{\lambda(D)}\right] = \dfrac{1}{\lambda(D)}E[\lambda(A_u(X,D))] = S_X^D(u)$.

(iv) $V(A_u(X,D)) = \int_{D\times[u,+\infty)} I_{u'}^X(s)dsdu'$. Hence, by Fubini's theorem, $V(A_u(X,D)) = \int_u^{+\infty} \lambda(A_{u'}(X,D))du' = \int_D X_u(s)ds$.

(v) From the proof of (iv), $E[V(A_u(X,D))] = \int_{D\times[u,+\infty)} P[X(s) \geq u']dsdu'$. Hence, correspondingly, $E[V(A_u(X,D))] = \lambda(D)\int_u^{+\infty} S_X^D(u')du'$ and $E[V(A_u(X,D))] = \lambda(D)\int_u^{+\infty}(u'-u)F_X^D(u')du' = \lambda(D)E[X_u^D]$.

(vi) $E[V^D(A_u(X,D))] = E\left[\dfrac{V(A_u(X,D))}{\lambda(D)}\right] = \dfrac{1}{\lambda(D)}E[V(A_u(X,D))] = \int_u^{+\infty} S_X^D(u')du' = E[X_u^D]$.

□

This proposition shows the relevance of the *compound* CDF for the first-order indicators considered, playing a key role in the methodology proposed in the following section.

3.3 Methodology

In this section, formal and computational aspects of the proposed methodology are described. The approach is based on a conditional risk assessment, performed at global and local (subregional) scales, with the latter being used, in particular, for risk mapping. Specifically, risk measures are evaluated based on the empirical distributions of selected indicators, derived from simulation of the underlying random field conditional to the available spatial (or spatiotemporal) observations. As mentioned, two special cases of quantile-based risk measures, VaR and AVaR, are considered here for illustration.

Formally, let X be the random field representing the phenomenon under study, and let u be the reference threshold level considered for risk assessment. As mentioned before, commonly u may be prescribed as a certain critical level of a direct meaning regarding the physical magnitude and contextual aspects. However, in many cases risk assessment is performed under specification of different scenarios for threshold levels corresponding to percentage (or probabilistic) global exceedance considerations. A natural approach, then, consists in considering the compound CDF F_X^D for reference.

More precisely, as given in Prop. 3.2.1 (iii), for a given threshold level u, the value

$$F_X^D(u) = 1 - E[\lambda^D(A_u(X,D))]$$

represents the expected area proportion within D with no exceedance over u (i.e, $X(s) < u$). In particular, for any $\alpha \in (0,1)$, the threshold defined by the corresponding $(1-\alpha)-$quantile of the compound CDF F_X^D, i.e. $u_{1-\alpha} := F_{X^D}^{-1}(1-\alpha)^-$, satisfies

$$E[\lambda^D(A_{u_{1-\alpha}}(X,D))] = \alpha.$$

(Conversely, for a given threshold u, the corresponding exceedance area proportion is given by $\alpha_u = 1 - F_X^D(u)$, with an analogous interpretation.) In this approach, this form of threshold level specification is applied to the conditional random field derived from X with respect to the available observed data $\mathbf{X} = \{X(s_1), \ldots, X(s_n)\}$, denoted as $X|\mathbf{X}$. The corresponding excursion set is, in this case, $A_{u_{1-\alpha}}(X|\mathbf{X},D)$. In practice, the threshold $u_{1-\alpha}$ for a given α value is estimated from the empirical compound CDF obtained by aggregation of the conditional simulation samples (see Section 3.3.2, step 3).

For simplicity, let us denote by $\mathscr{I}_{1-\alpha}^{X|\mathbf{X},D}$ any first-order indicator (such as the exceedance area or the excess volume) which is defined as a function of the realizations on D of the joint random field $(I_{u_{1-\alpha}}^{X|\mathbf{X}}, (X|\mathbf{X})_{u_{1-\alpha}})$ (equivalently, as a function of the random excursion set family $\left\{A_{u_{1-\alpha'}}(X|\mathbf{X},D) : \alpha' \geq \alpha\right\}$.) Now, for a conveniently large number M of simulated realizations of $X|\mathbf{X}$, denoted here as $(X|\mathbf{X})^{[m]}$ $(m = 1, \ldots, M)$, the corresponding excursion sets and indicator values, $\left\{A_{u_{1-\alpha'}}((X|\mathbf{X})^{[m]},D)\right\}_{m=1,\ldots,M}$ and $\left\{\mathscr{I}_{1-\alpha}^{(X|\mathbf{X})^{[m]},D}\right\}_{m=1,\ldots,M}$, can be identified. Evaluation of different risk measures is then performed based on the empirical CDF, $\hat{F}_{\mathscr{I}}$, obtained from the latter. For instance, assume that a threshold level specification is given as $u_{1-\alpha_1}$, for a certain prescribed exceedance area proportion α_1. Then, the corresponding 'empirical' VaR and AVaR values of the $\mathscr{I}_{1-\alpha_1}^{X|\mathbf{X},D}$ indicator can be derived, for any confidence level $1-\alpha_2$, as $VaR_{1-\alpha_2}(\mathscr{I}_{1-\alpha_1}^{X|\mathbf{X},D})$ and $AVaR_{1-\alpha_2}(\mathscr{I}_{1-\alpha_1}^{X|\mathbf{X},D})$.

In a spatiotemporal scenario, this approach can be applied to the spatial cross-sections, thus allowing, by conditional simulation, the derivation of dynamic predictive risk assessment according to different temporal horizons.

3.3.1 Local Analysis and Risk Mapping

For a fixed threshold level u, possibly determined as $u_{1-\alpha_1}$ for a certain specified global exceedance area proportion α_1, a local analysis can be performed regarding the spatial distribution of the exceedances, by applying the above described procedure restricted to subregions, D', of the domain. For simplicity, among different approaches for implementation, here we assume that D

is a rectangular domain and D' is defined by the restrictions of D based on a rectangular sliding window of a certain size, which is moved in the directions of the coordinate axes at regular steps with a certain degree of overlapping. The evaluation of the selected indicators and risk measures is then performed on each particular D' subdomain, allowing the construction of 'local risk' maps on D at different resolution scales. The spatiotemporal extension can be similarly carried out.

3.3.2 Further Computational Aspects

In practice, simulation of the underlying random field, conditional on a set of observations at given locations, is performed based on a regular grid. The nodes are identified as the centroids of cells covering the spatial domain.

Computation of the empirical compound CDF based on the simulated realizations is obtained by discretization of the integral (3.1), as follows:

1. Based on a grid of $N_1 \times N_2$ cells for a (rectangular) domain D, generate M independent replicates of the considered random field $X|\mathbf{X}$ (hereafter denoted as X):

$$\{X[(i,j);m] : i = 1,\ldots,N_1; j = 1,\ldots,N_2\}, m = 1,\ldots,M,$$

where $X[(i,j);m]$ represents the value obtained for the conditional random field $(X|\mathbf{X})$ in the $m-$th simulated realization at the location corresponding to the grid node (i,j).

Let $m_{(i,j)}(x)$ be the number of values $X[(i,j);m] \leq x$ at the node (i,j), and consequently $m(x) := \sum_{i=1}^{N_1}\sum_{j=1}^{N_2} m_{(i,j)}(x)$, i.e. the accumulated number of values $X[(i,j);m] \leq x$ in the aggregated sample

$$\{X[(i,j);m] : m = 1,\ldots,M; i = 1\ldots,N_1; j = 1,\ldots,N_2\},$$

which can be seen as

$$\bigcup_{i=1}^{N_1}\bigcup_{j=1}^{N_2}\{X[(i,j);m] : m = 1,\ldots,M\},$$

i.e. the union of the set of replicates at each point (i,j), or as

$$\bigcup_{m=1}^{M}\{X[(i,j);m] : i = 1\ldots,N_1; j = 1,\ldots,N_2\},$$

i.e. the union of the m sample realization replicates.

2. Empirical CDF at each node (i,j): assign, for each $x \in \mathbb{R}$,

$$\hat{F}_{(i,j)}(x) = \begin{cases} 0 & \text{if } x < X[(i,j);(1)] \\ \dfrac{m}{M} & \text{if } X[(i,j);(m)] \leq x < X[(i,j);(m+1)]; m = 1,\ldots,M-1 \\ 1 & \text{if } x \geq X[(i,j);(m)] \end{cases}$$

where $\{X[(i,j);(m)] : m = 1,\ldots,M\}$ is the ordered sample at (i,j).

3. Empirical compound CDF: assign, for each $x \in \mathbb{R}$,

$$\begin{aligned} \hat{F}_X^D(x) &= \sum_{i=1}^{N_1}\sum_{j=1}^{N_2} \hat{F}_{(i,j)}(x)\frac{1}{N_1N_2} \\ &= \sum_{i=1}^{N_1}\sum_{j=1}^{N_2} \frac{m_{(i,j)}(x)}{M}\frac{1}{N_1N_2} \\ &= \frac{m(x)}{MN_1N_2}. \end{aligned}$$

Excursion sets, and corresponding evaluation of indicators, are approximated on a cell aggregation basis.

3.4 Illustration Based on Simulation

In this section, significant aspects of the quantile-based risk measures VaR and AVaR applied to some indicators of interest, as mentioned in sections 3.1 and 3.3, are analyzed under different scenarios in the purely spatial and spatiotemporal frameworks by means of a simulation study. For simplicity, hereafter X implicitly stands, when appropriate, for the conditional RF $X|\mathbf{X}$ on given observations. A percentile level $1-\alpha_1$ for the empirical compound CDF F_X^D, defining an excursion set over threshold $u_{1-\alpha_1}$, and a confidence level $1-\alpha_2$ for the empirical CDF of each specific indicator, are considered. Global and local measurements of these risk measures are illustrated and compared.

Moreover, in all the cases considered, and for illustration purposes, it must be understood that the random field of interest is the discrete version of the underlying continuous-domain random field consisting of the variables corresponding to a regular grid of a pre-fixed resolution. In this sense, we must emphasize that aspects related to regularity conditions are not involved, except for the fact that the results obtained are intrinsically related to the size of the grid cells (see Adler 1981, Ch. 8, for a discussion in reference to this issue).

Here, the package `RandomFields` of the R Statistical Computing software is used for conditional simulation. The MATLAB environment is used for the remaining computational and graphical aspects.

3.4.1 Spatial Analysis

Three classes of well-known random field models are considered: generalized Cauchy, Student and Fisher-Snedecor. From the global and local measurements, significant interpretations and comparisons, depending on the structural characteristics of the underlying model, are derived from the analysis performed.

The *Cauchy* class model (see Gneiting and Schlather 2004) is defined by the homogeneous and isotropic covariance function

$$C(h) = \sigma^2(1+|h|^{\alpha})^{-\beta/\alpha}, \quad \alpha \in (0,2] \text{ and } \beta > 0.$$

This class allows a separately characterization of local variability and dependence ranges. For a random field on $\mathbb{R}^d$ the parameter α determines the *fractal dimension* of realizations, $D = d+1-\alpha/2$. If $\beta \in (0,1)$, the process has *long memory*, with Hurst coefficient $H = 1-\beta/2$.

The *Student* and *Fisher-Snedecor* class models (see Leonenko and Olenko 2014) are defined as

$$T_n(x) = \frac{\eta_1(x)}{\sqrt{\frac{1}{n}\left(\eta_2^2(x)+\cdots\eta_{n+1}^2(x)\right)}} \quad \textit{(Student)}$$

$$F_{m,n}(x) = \frac{\frac{1}{m}\left(\eta_1^2(x)+\cdots\eta_m^2(x)\right)}{\frac{1}{n}\left(\eta_{m+1}^2(x)+\cdots\eta_{m+n}^2(x)\right)} \quad \textit{(Fisher-Snedecor)}$$

where $\eta_1,\ldots,\eta_{m+n}$ are independent copies of a mean-square continuous homogeneous isotropic zero-mean Gaussian random field.

For this illustration, the Gaussian Cauchy class model with variance $\sigma^2 = 0.1$ under four scenarios $(\alpha,\beta) = (0.5,0.1)$, $(2,0.1)$, $(0.5,0.9)$, $(2,0.9)$, and the Student and Fisher-Snedecor classes based on the Cauchy class model under these four scenarios, are considered. For each case, 200 realizations are simulated on the square $[-100,100]^2$, both unconditionally and conditionally. More specifically, for the conditional approach, the parameter values are fixed and an unconditional simulated realization of the random field X is generated at 50 pre-fixed locations randomly chosen within the domain. Then, adopting these values as the observed data, realizations are generated by conditional simulation using the same parameter values.

Results for various indicators including areas, volumes, and volumes relative to areas (total and per connected component), are derived and compared between the different scenarios, at global and local scales.

Fig. 3.1 displays, as an example, simulated realizations based on the four scenarios considered for the Cauchy class, allowing the visualization of the dependence structure and fractality features according to the parameter values. For instance, both aspects jointly depict a particularly contrastive behaviour for the cases $(\alpha,\beta) = (0.5,0.9)$ and $(2,0.1)$. The effect of conditioning can be seen comparing to the corresponding plot, for each case, in Fig. 3.2. Furthermore, as illustrated

in Figs. 3.3 and 3.4, long-range dependence determined by smaller β provides lower variability in the neighborhood of the conditioning points. The heavy-tailed behaviour of Student and Fisher-Snedecor models is clearly observed in Figs. 3.5 and 3.6, respectively, where the different scales of variation can be also noticed; to help visualization, nonlinearly rescaled representations of the generated values are also displayed, using the transformations $g(x) = \mathrm{sgn}(x)\ln(1+|x|)$ for Student case, and $h(x) = \ln(x)$ for Fisher-Snedecor case.

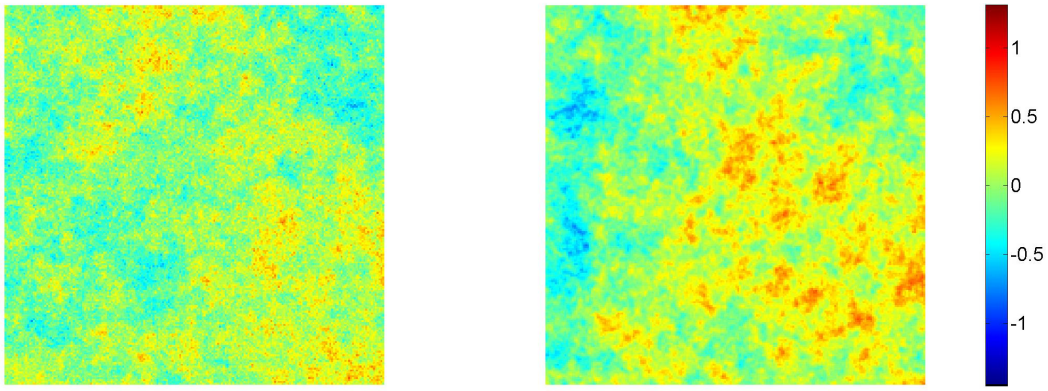

(a) $(\alpha,\beta) = (0.5, 0.1)$.

(b) $(\alpha,\beta) = (2, 0.1)$.

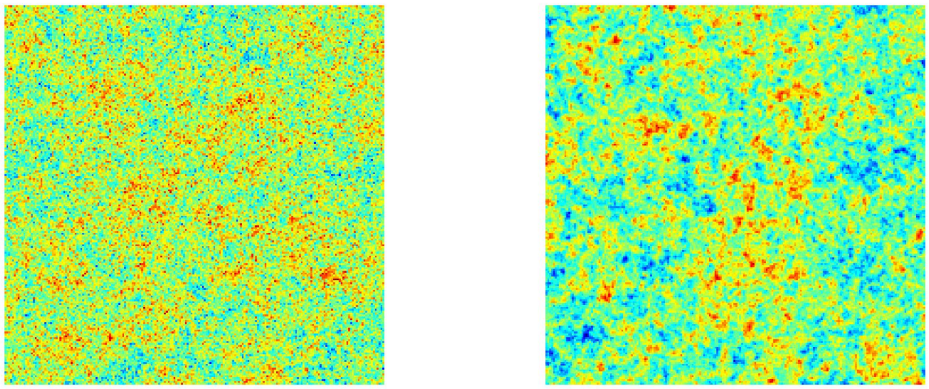

(c) $(\alpha,\beta) = (0.5, 0.9)$.

(d) $(\alpha,\beta) = (2, 0.9)$.

Figure 3.1: Simulated realizations on the square $[-100, 100]^2$ from Cauchy model with $\sigma^2 = 0.1$.

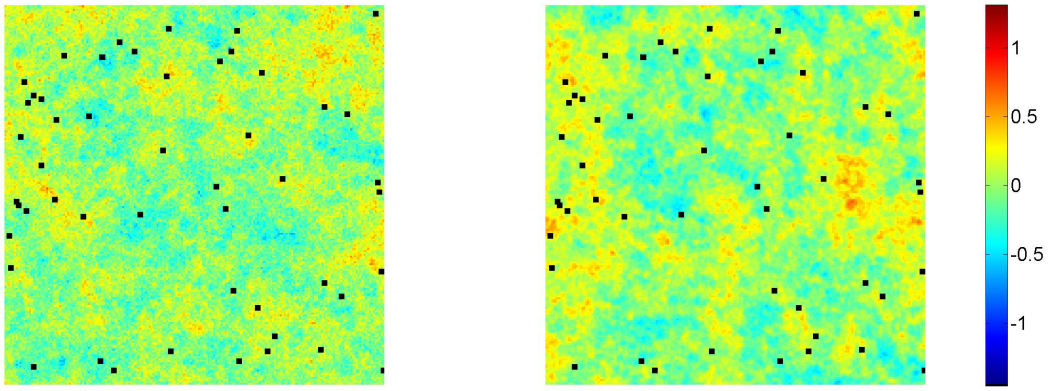

(a) $(\alpha,\beta) = (0.5, 0.1)$.

(b) $(\alpha,\beta) = (2, 0.1)$.

(c) $(\alpha,\beta) = (0.5, 0.9)$.

(d) $(\alpha,\beta) = (2, 0.9)$.

Figure 3.2: Simulated realizations on the square $[-100, 100]^2$ from Cauchy model with $\sigma^2 = 0.1$, conditional to given values at 50 pre-fixed points for each model.

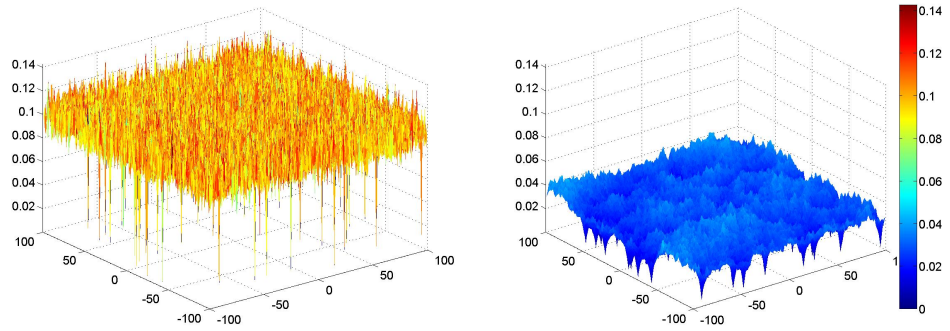

(a) $(\alpha, \beta) = (0.5, 0.9)$. (b) $(\alpha, \beta) = (2, 0.1)$.

Figure 3.3: Surface plots for the map of variances from Cauchy model.

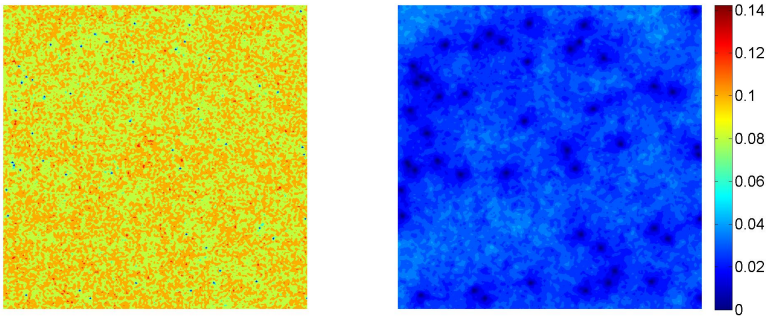

(a) $(\alpha, \beta) = (0.5, 0.9)$. (b) $(\alpha, \beta) = (2, 0.1)$.

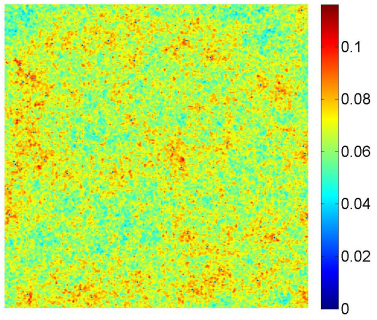

(c) Differences between (a) and (b)

Figure 3.4: Level plots for the map of variances (top plots) and corresponding level plot of differences of variances between scenarios (bottom plot) from Cauchy model.

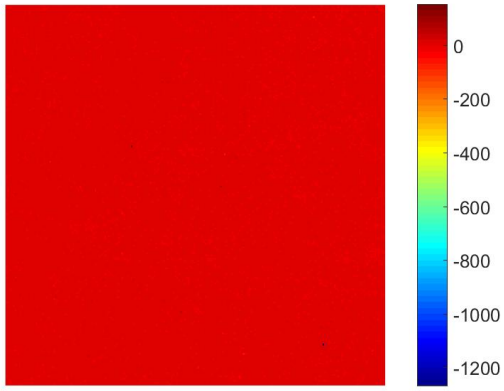

(a) $(\alpha,\beta) = (0.5, 0.9)$.

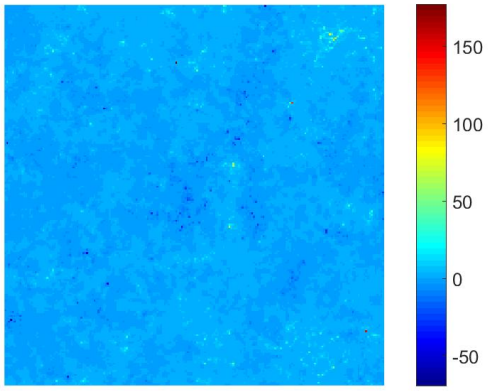

(b) $(\alpha,\beta) = (2, 0.1)$.

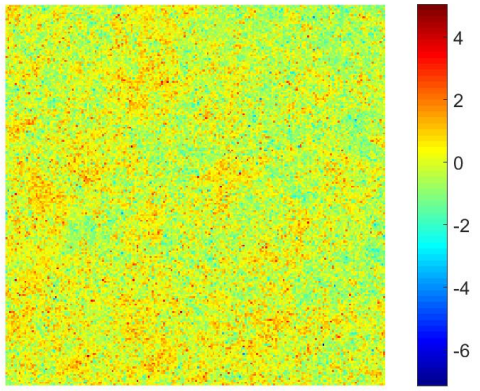

(c) $(\alpha,\beta) = (0.5, 0.9)$.

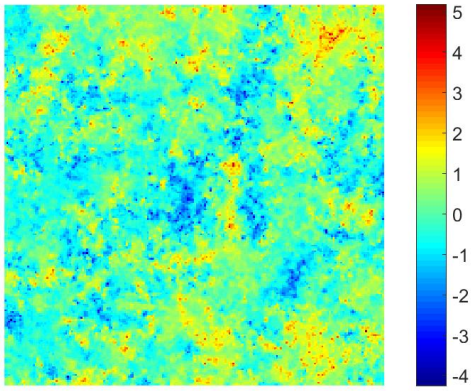

(d) $(\alpha,\beta) = (2, 0.1)$.

Figure 3.5: Simulated realizations on the square $[-100, 100]^2$ from Student model, (top plots) at original scale and (bottom plots) using the scale transformation $g(x) = \text{sgn}(x)\ln(1+|x|)$, for (left to right) $(\alpha,\beta) = (0.5, 0.9)$ and $(2, 0.1)$, with $\sigma^2 = 0.1$.

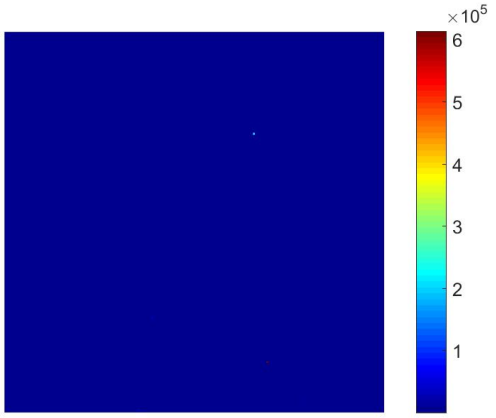

(a) $(\alpha,\beta) = (0.5, 0.9)$.

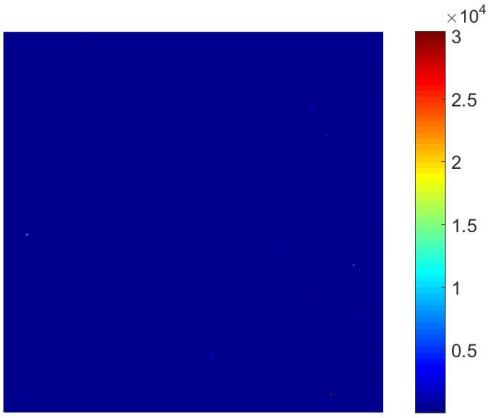

(b) $(\alpha,\beta) = (2, 0.1)$.

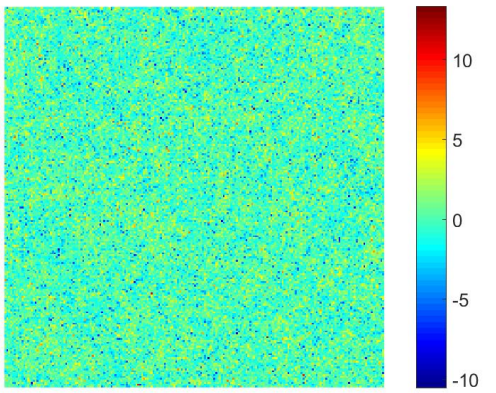

(c) $(\alpha,\beta) = (0.5, 0.9)$.

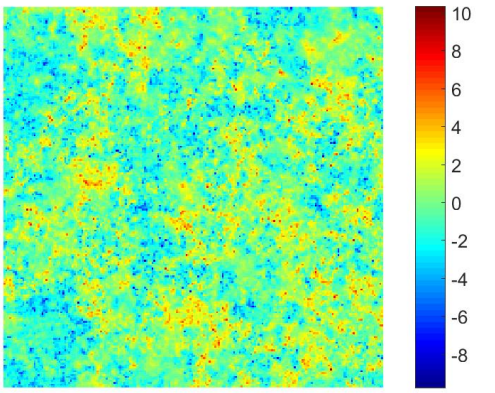

(d) $(\alpha,\beta) = (2, 0.1)$.

Figure 3.6: Simulated realizations on the square $[-100, 100]^2$ from Fisher-Snedecor model, (top plots) at original scale and (bottom plots) using the scale transformation $h(x) = \ln(x)$, for (left to right) $(\alpha,\beta) = (0.5, 0.9)$ and $(2, 0.1)$, with $\sigma^2 = 0.1$.

Global measures

Based on the empirical compound CDF F_X^D, obtained from the 200 simulated realizations, for the three models and under the different parameter values, the empirical distributions of various characteristics of excursion sets are analyzed in terms of related VaR and AVaR measures. Specifically, the aim is to assess the sensitivity of these risk measures for varying thresholds, $u_{1-\alpha_1}$, and varying confidence levels, $1-\alpha_2$, under different scenarios.

In Fig. 3.7 three indicators are analyzed for the Cauchy model with $(\alpha,\beta)=(2,0.1)$, $\sigma^2=0.1$, namely the absolute excess volume (V), the excess volume relative to the exceedance area (V^{Au}), and the average relative excess volume per connected component $\bar{V}^{cc}$. Plot (a) shows the rate of decay of V for increasing threshold $u_{1-\alpha_1}$, for different confidence levels $1-\alpha_2$. As expected, for fixed $u_{1-\alpha_1}$, $AVaR_{1-\alpha_2}(V(A_{u_{1-\alpha_1}}(X,D)))$ increases as α_2 tends to 0. For this particular model, a similar behaviour occurs for V^{A_u}, as displayed in plot (b), which indicates that the excess volume decreases faster than the exceedance area for increasing threshold. However, as seen in plot (c), due to the effect of fragmentation, the indicator $\bar{V}^{cc}$ changes to increase for higher threshold $u_{1-\alpha_1}$ values. Regarding indicator V^{A_u}, it is important to emphasize that, in the case of heavy-tailed scenarios, the excess volume may decrease slower than the exceedance area for increasing threshold, as shown in Fig. 3.8.

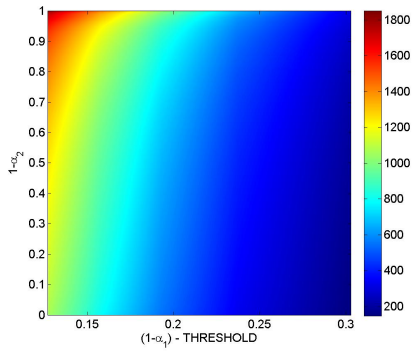

(a)

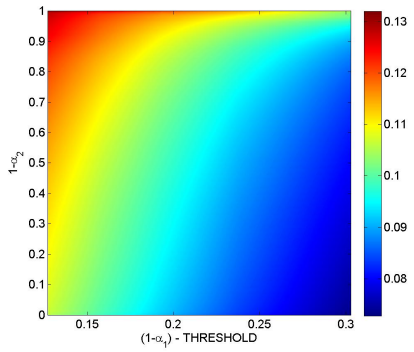

(b)

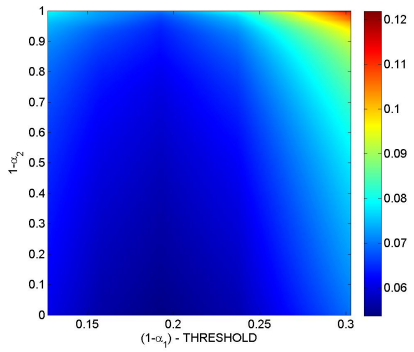

(c)

Figure 3.7: Level plots of $AVaR_{1-\alpha_2}(\mathscr{I}(A_{u_{1-\alpha_1}}(X,D)))$ for (a) $\mathscr{I}=V$, (b) $\mathscr{I}=V^{A_u}$ and (c) $\mathscr{I}=\bar{V}^{cc}$ based on varying $(u_{1-\alpha_1}, 1-\alpha_2)$ values, from Cauchy model with $(\alpha,\beta)=(2,0.1)$, $\sigma^2=0.1$.

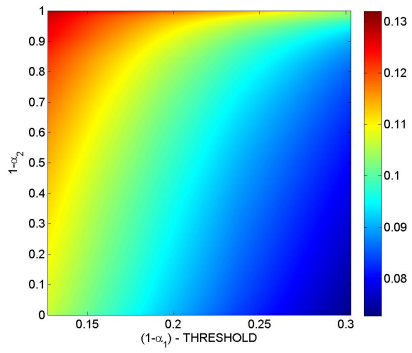

(a)

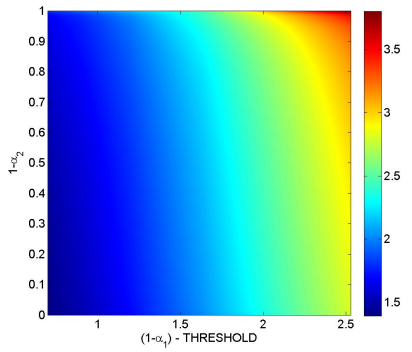

(b)

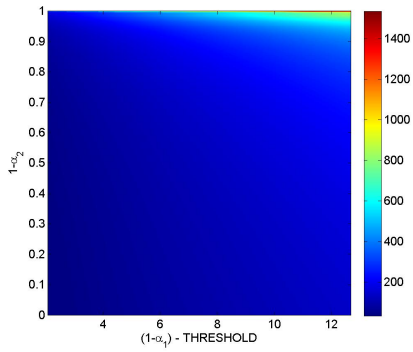

(c)

Figure 3.8: Level plots of $AVaR_{1-\alpha_2}(V^{A_u}(A_{1-\alpha_1}(X,D)))$ based on varying $(u_{1-\alpha_1}, 1-\alpha_2)$ values from (a) Cauchy, (b) Student and (c) Fisher-Snedecor models with $(\alpha,\beta) = (2,0.1)$, $\sigma^2 = 0.1$.

Local measures

A similar study is performed locally, based on sliding windows, for assessment of regional variations of risk. The scale of analysis and degree of interpolation are determined by the size of the window and the sliding step. Here a square window of size 33×33, and step equal to 11 cells are used. Risk surfaces and maps are drawn for different characteristics, models and parameter values. For illustration, in all the cases, an excursion set is determined for a fixed percentile $1-\alpha_1 = 0.90$, based on the compound CDF F_X^D. Then, the VaR and AVaR risk measures for a fixed confidence level $1-\alpha_2 = 0.95$ are calculated for the local indicators $\lambda^{D'}$ and $V^{A'_u}$ (with $A'_u = A_u(X,D) \cap D'$) at each subdomain D'.

Figs. 3.9 and 3.10 show the combined effect of conditioning and model structure for two contrastive Cauchy scenarios.

In Fig. 3.11, as expected, the AVaR surface is above the corresponding VaR surface, displayed in particular for indicator $V^{A'_u}$; however, the conditioning effect makes the relative differences between both measures to vary locally.

As noticed in Fig. 3.12, the heavy-tailed behaviour of the Student and Fisher-Snedecor random field models is reflected in a higher level of local heterogeneity in the relative excess volume compared to the corresponding exceedance area risk maps.

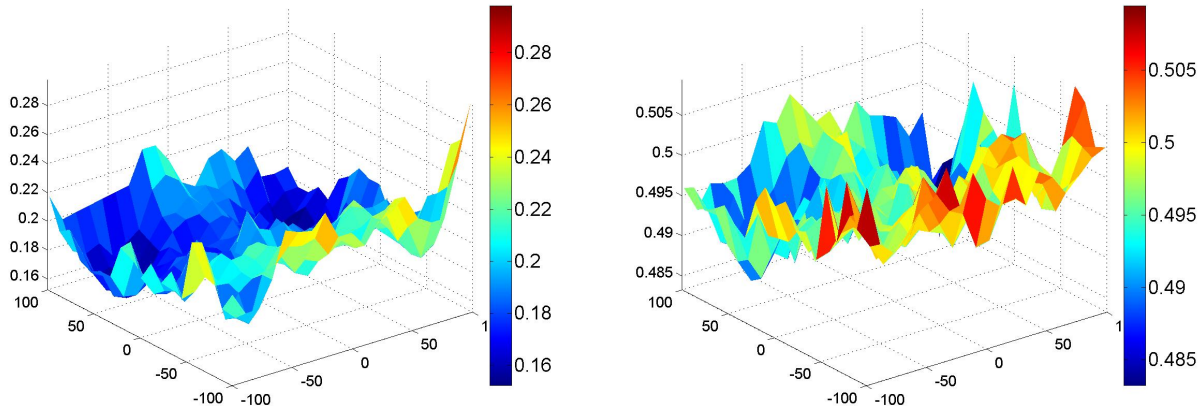

(a) $VaR_{0.95}(\lambda^{D'})$. (b) $VaR_{0.95}(V^{A'_u})$.

Figure 3.9: Local measurements of VaR for indicators (a) $\lambda^{D'}$ and (b) $V^{A'_u}$ from Cauchy class model with $(\alpha,\beta) = (0.5,0.9)$, $\sigma^2 = 0.1$.

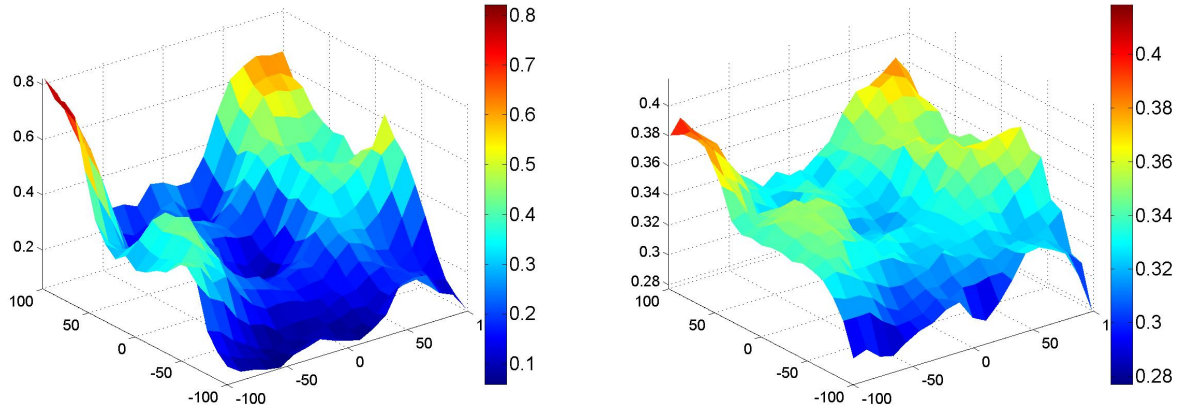

(a) $VaR_{0.95}(\lambda^{D'})$. (b) $VaR_{0.95}(V^{A'_u})$.

Figure 3.10: Local measurements of VaR for indicators (a) $\lambda^{D'}$ and (b) $V^{A'_u}$ from Cauchy class model with $(\alpha,\beta) = (2,0.1)$, $\sigma^2 = 0.1$.

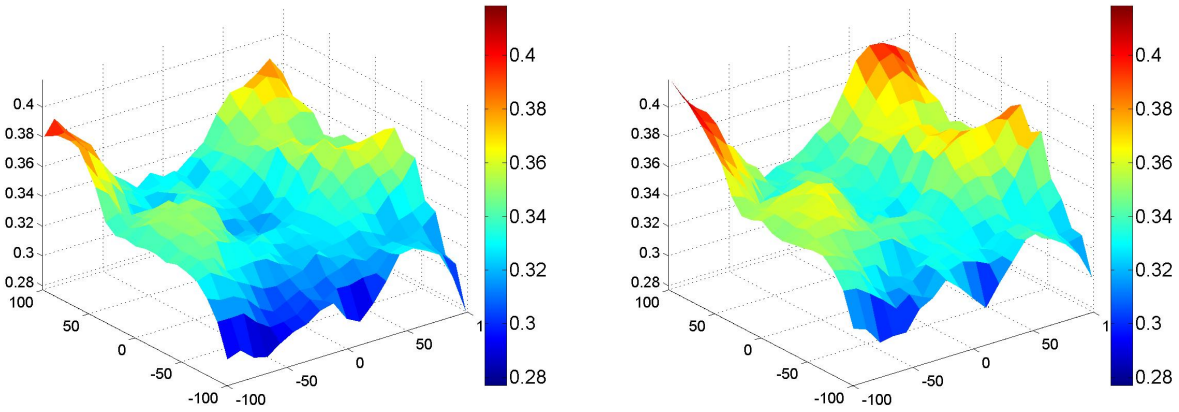

(a) $VaR_{0.95}(V^{A'_u})$. (b) $AVaR_{0.95}(V^{A'_u})$.

Figure 3.11: Local measurements of (a) VaR and (b) AVaR for indicator $V^{A'_u}$ from Cauchy class model with $(\alpha,\beta) = (2,0.1)$, $\sigma^2 = 0.1$.

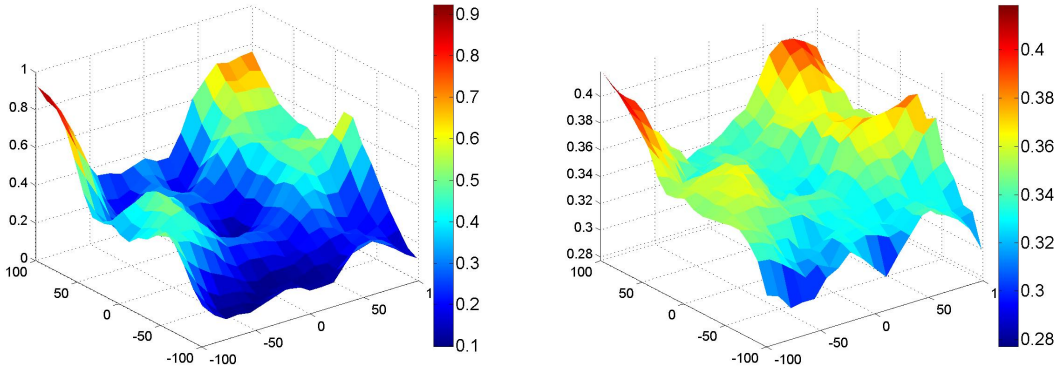

(a) Cauchy.

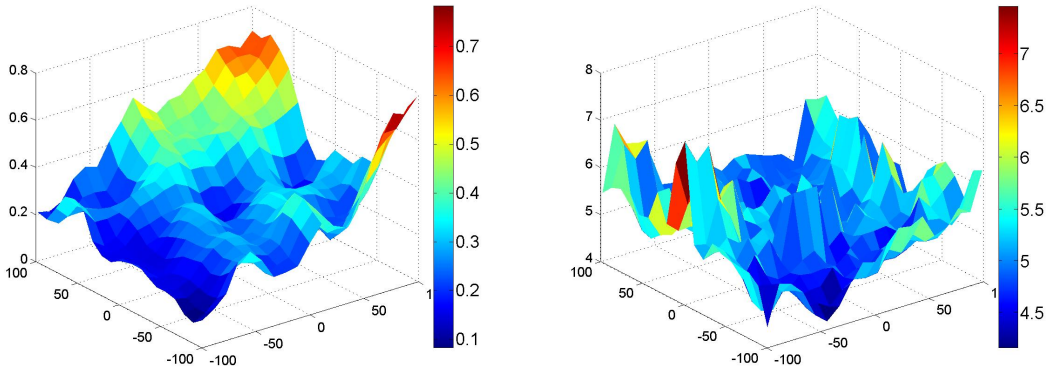

(b) Student.

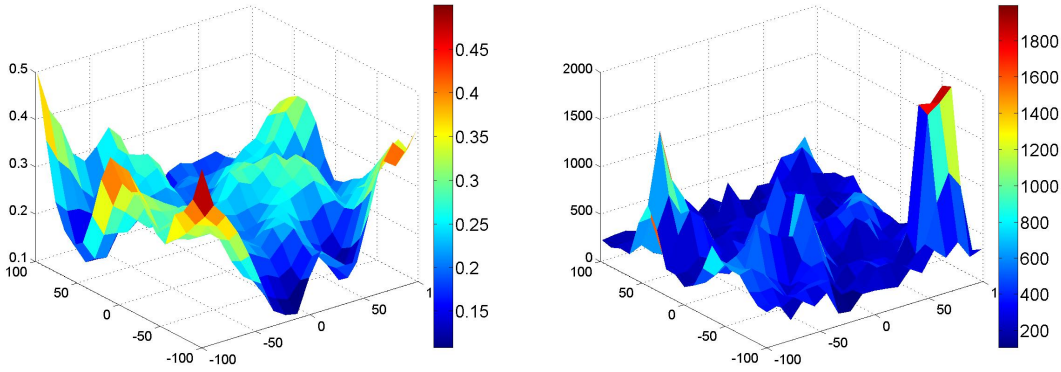

(c) Fisher-Snedecor.

Figure 3.12: Local measurements of $AVaR_{0.95}(\lambda^{D'})$ (left) and $AVaR_{0.95}(V^{A'_u})$ (right) from (a) Cauchy, (b) Student and (c) Fisher-Snedecor models with $(\alpha,\beta) = (2,0.1)$, $\sigma^2 = 0.1$.

3.4.2 Spatiotemporal Analysis

The methodology is also applied to conditional evaluation of risk in a spatiotemporal context. For illustration, the blur-generated non-separable space-time model introduced by Brown et al (2000) (see also Angulo and Madrid 2014, for an extended version with dynamic spatial deformation) is used:

$$Y(s,t) = aY[h](s,t-1) + Z(s,t), \tag{3.2}$$

where

$$Y[h](s,t-1) = h * Y(s,t-1) = \int_{\mathbb{R}^d} h(s,s')Y(s',t-1)ds', \tag{3.3}$$

with $Y(s,0) = Y_0$ being a spatial random field on $\mathbb{R}^d$, Z a spatiotemporal random field on $\mathbb{R}^d \times \mathbb{R}$ assumed to be white in time, h a blurring kernel, and a a constant such that $0 < a < 1$.

Here, a Cauchy class model for Z with $(\alpha,\beta) = (2,0.2)$ and $\sigma^2 = 0.1$, a homogeneous Gaussian blurring kernel with variance $\sigma_h^2 = 10$, and $a = 0.9$ are considered. Given a fixed complete realization at $t = 0$ obtained in stationary regime, 200 replicates are conditionally simulated for evolution at $t = 1,2,3$. In this case, a square window of size 21×21, and step equal to 6 cell units is used for local analysis. Predictive risk assessment is then peformed for different characteristics, at horizons 1, 2 and 3. Specifically, in Figs. 3.13, 3.14 and 3.15, corresponding risk maps obtained for the indicators $\lambda^{D'}$, $V^{D'}$ and $V^{A'_u}$ based on AVaR are displayed. As expected, the levels of risk increase for larger horizon, with this effect varying locally according to the spatiotemporal dependence structure of the underlying process. Also, these maps clearly reflect the dynamic behaviour in relation to the conditioning observation at $t = 0$.

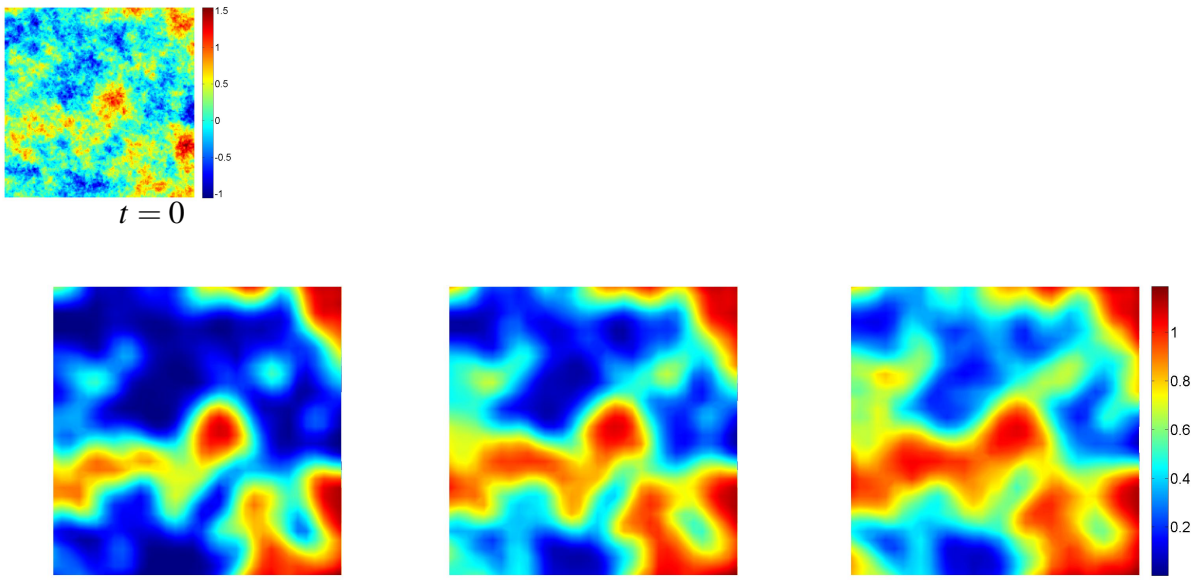

Figure 3.13: Local measurements of $AVaR_{0.95}(\lambda^{D'})$ from model (3.2)-(3.3) at horizons (left to right) $t = 1, 2, 3$. Top plot represents the observed realization at $t = 0$.

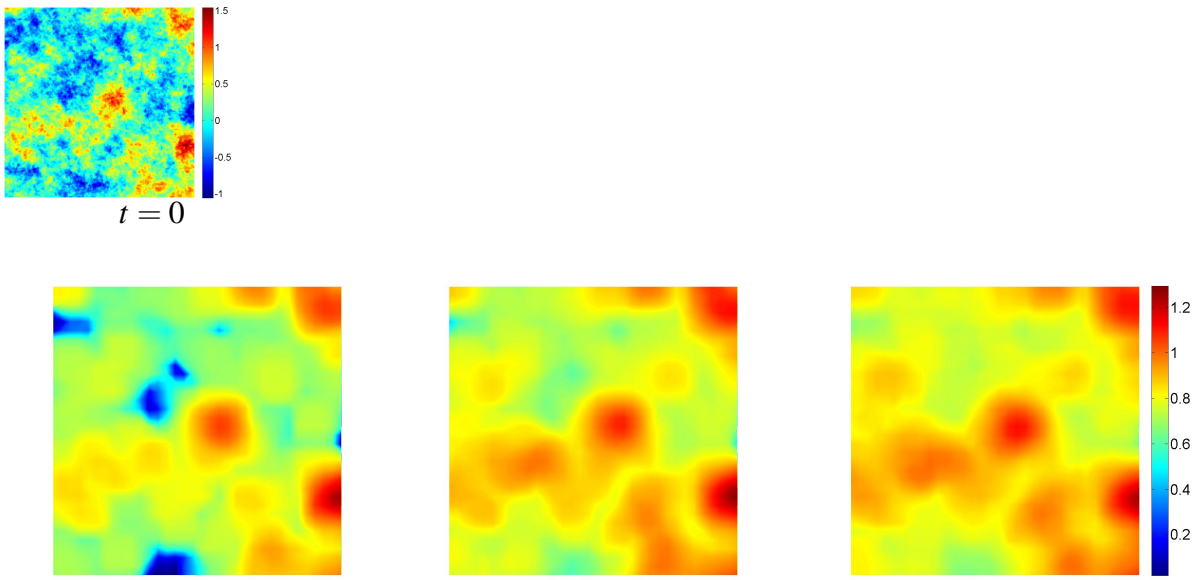

Figure 3.14: Local measurements of $AVaR_{0.95}(V^{D'})$ from model (3.2)-(3.3) at horizons (left to right) $t = 1, 2, 3$. Top plot represents the observed realization at $t = 0$.

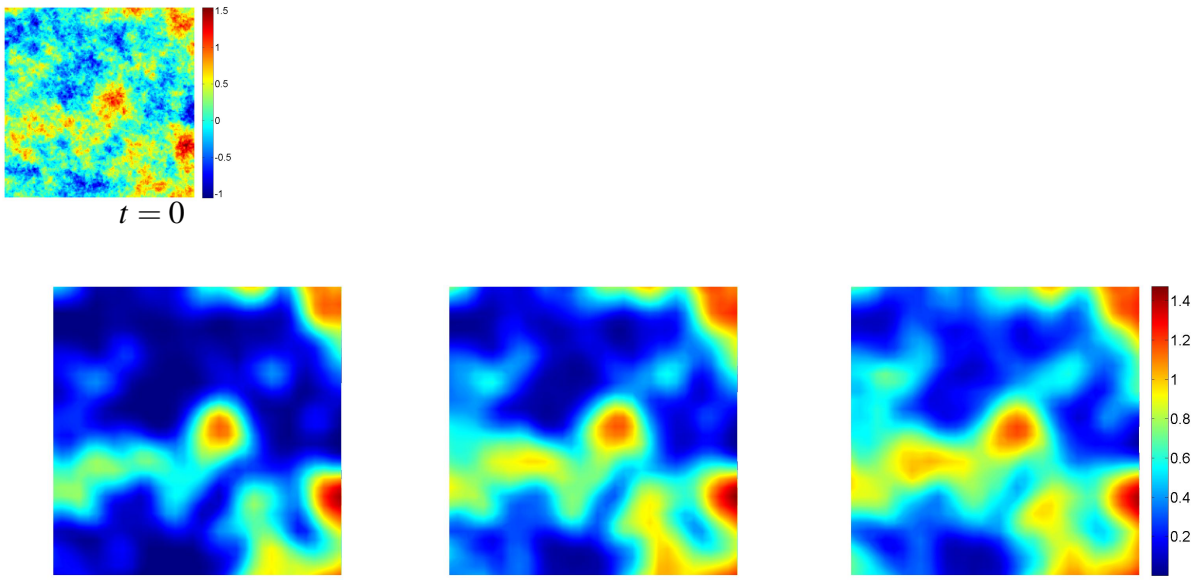

Figure 3.15: Local measurements of $AVaR_{0.95}(V^{A'_u})$ from model (3.2)-(3.3) at horizons (left to right) $t = 1, 2, 3$. Top plot represents the observed realization at $t = 0$.

Chapter 4

Real Data Applications

Random field models considered in Chapter 3, as well as their parameters, were chosen to illustrate the behaviour of risk measures on structural indicators of the random field for different scenarios. According to the degree of dependence and local variability, heavy tail behaviour, etc., they provided different interpretations. For the applications in this chapter, specific models that, according to the literature, are supposed to be adequate to model the phenomenon of interest, are considered and their parameters are estimated. The consideration of the most appropriate model for the data, as well as the optimal estimates of its parameters is not the main goal of this illustration, so that there is not a detailed validation. This chapter is aimed at illustrating the applicability of the proposed methodology in real scenarios under the assumption of quality for the conditionally simulated data. For this purpose, rainfall and ambient PM10 concentration data are considered due to the relevance of environmental scenarios in a stage of climate change nowadays.

Here, once again, the package `RandomFields` of the R Statistical Computing software is used for conditional simulation and models fitting. The MATLAB environment is used for the remaining computational and graphical aspects.

4.1 Rainfall Data

In this section, a risk analysis for real precipitation data is performed. First, a purely spatial scenario is considered, comparing risk maps in the same rainfall period but in different years. Second, in a spatiotemporal framework, the dynamics of rainfall amount above a prefixed threshold is addressed.

4.1.1 Spatial Analysis

For this application a comparative spatial risk analysis for the same rainfall period, April, in two consecutive years, 2014 and 2015, in the region of Andalusia, is developed. Precipitation

data measured at 93 stations of the AEMET network in Andalusia (http://www.datosclima.es) are considered. A conditional simulation, based on the observed data, of 200 realizations for each one of the two estimated models involved for the two periods, is performed. The empirical distributions of various characteristics of threshold exceedance sets in terms of the related VaR and AVaR measures are analyzed and compared based on the empirical compound CDF, F_X^D. The spatial domain of interest is defined by a rectangular grid $[0,175] \times [0,93]$ with 16.275 pixels at 3km scale, where each pixel is identified with its physical centroid. Logarithms of the mean-centered precipitation data are used for the estimation of the parameters of each model and for conditional simulation, whilst for the spatial risk analysis, the true values of the magnitude are used.

The Cauchy model class introduced in Chapter 3 (Section 3.4.1), with covariance $C(h) = \sigma^2(1+|h|^\alpha)^{-\beta/\alpha}$, is adopted for representation of the log-precipitation data, separately for each model. The scale of analysis and the degree of interpolation considered to assess local risk variations is given by a window size of 9 pixels and a sliding step of 3 units, so that 1.829 square windows are used. As in the simulation analysis performed in the previous chapter, risk surfaces and maps for different characteristics are drawn. The threshold exceedance set is determined by the percentile $1-\alpha_1 = 0.90$ of the compound CDF, F_X^D, and the confidence level to calculate the VaR and AVaR risk measures is $1-\alpha_2 = 0.95$, for the local indicators $\lambda^{A'_u}$ and $V^{A'_u}$ (with $A'_u = A_u(X,D) \cap D'$) at each window D'.

Table 4.1 below lists the Cauchy model parameter estimates for each rainfall period analyzed.

Parameter	April 2014	April 2015
α	0.83	1.93
β	0.11	0.10
σ^2	1.55	0.68

Table 4.1: Estimated parameter values of the Cauchy model for the two periods.

Fig. 4.1 shows the network of precipitation measurement stations in Andalusia, according to the AEMET data source. First, its physical UTM coordinates are shown on a map of Andalusia, (plot (a)) and then on the grid of pixels at 3 km scale (plot (b)). Fig. 4.2 displays, based on one generated realization, the effect of conditioning on the structure of dependence and fractality for each one of the estimated models. In addition, Fig. 4.3 illustrates how the degree of long-range dependence of these models provides a similar pattern of variability around the conditioning points, since both models have a small and practically the same β parameter. Furthermore, according to this figure, there was less global variability in precipitation data in April 2015 than in the same period of 2014. Figures 4.4 to 4.6 show, as expected, that the AVaR maps are slightly above those of the VaR for each random indicator and rainfall period considered. In addition, as is the simulation analysis of the previous chapter, if the combined effect of the conditioning and the structure of

the Cauchy models estimated in each period is compared, it is observed that, even being the same spring rainfall period, the spatial distribution of the relative area of exceedance with minimum precipitation values above the fixed threshold is very different from one year to the other, at the confidence level considered. Regarding the spatial distribution of the relative excess volume and the total excess volume, a similar behaviour is observed.

Finally, if the amount of rainfall above a given threshold is considered as a potential damage or hazard, according to the local risk mapping obtained it is clear that April 2014 was a more active period than April 2015. This is because for the first period there exist a wider area of exceedance exposed to risk as well as higher excess volume values than for the second period.

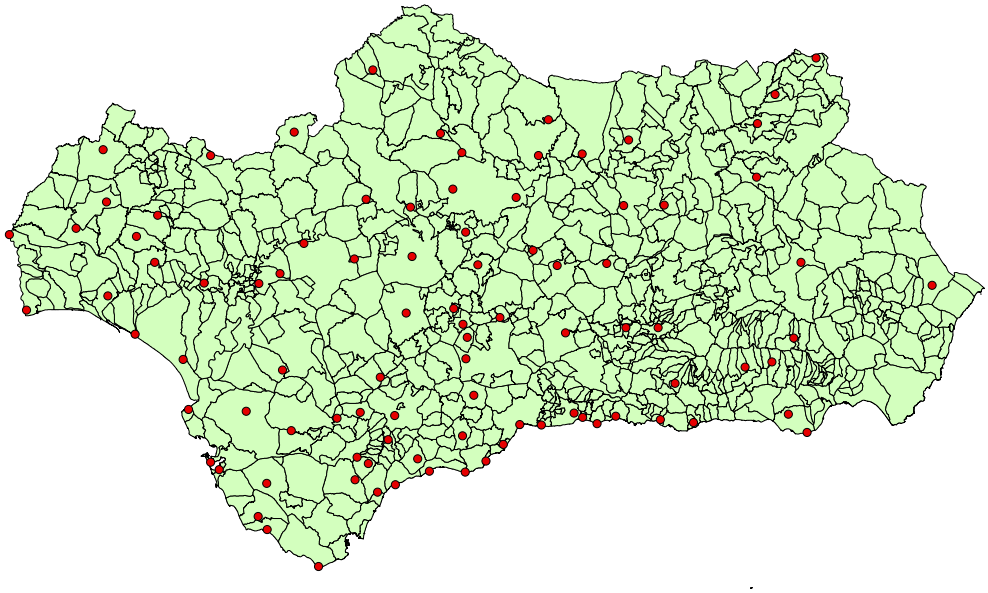

(a) UTM network.

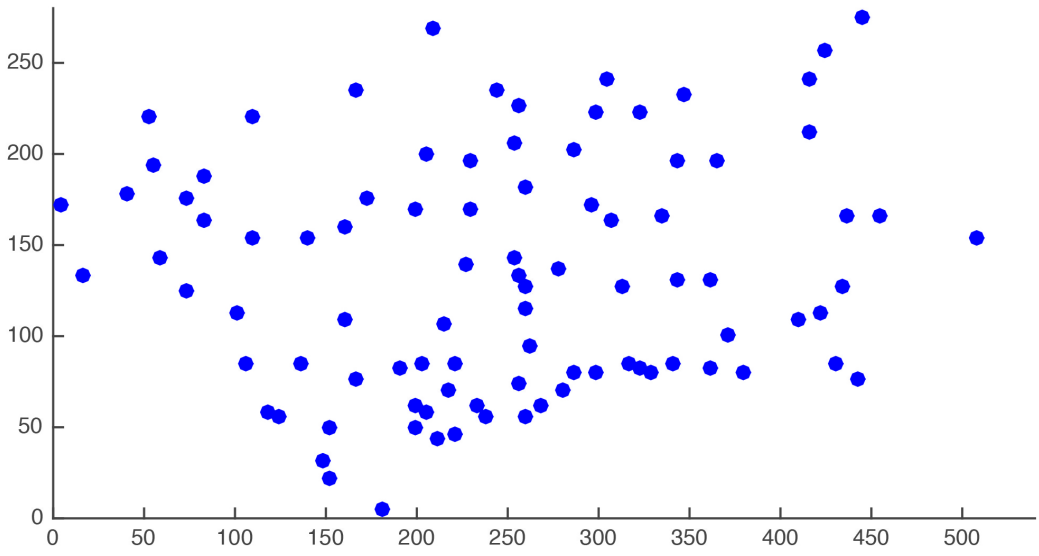

(b) Network within the grid of pixels.

Figure 4.1: Rainfall measurement network in Andalusia.

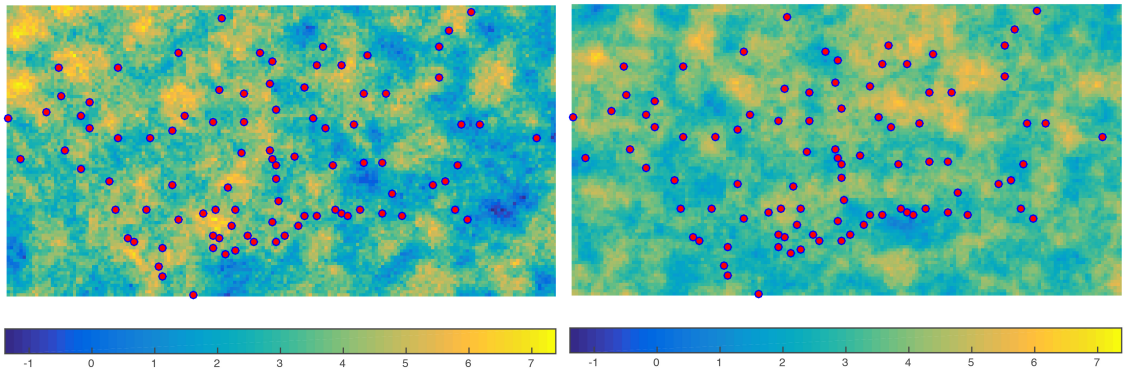

(a) April 2014. (b) April 2015.

Figure 4.2: Simulated realizations on the square $[0,175] \times [0,93]$ conditional to observed data.

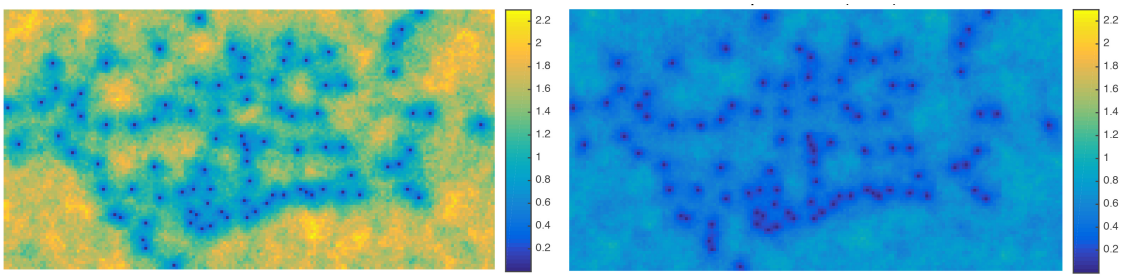

(a) April 2014. (b) April 2015.

Figure 4.3: Level plots for the map of variances for each period.

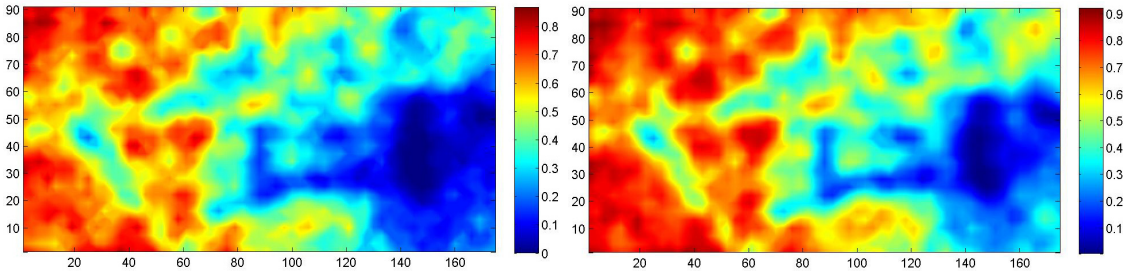

(a) April 2014.

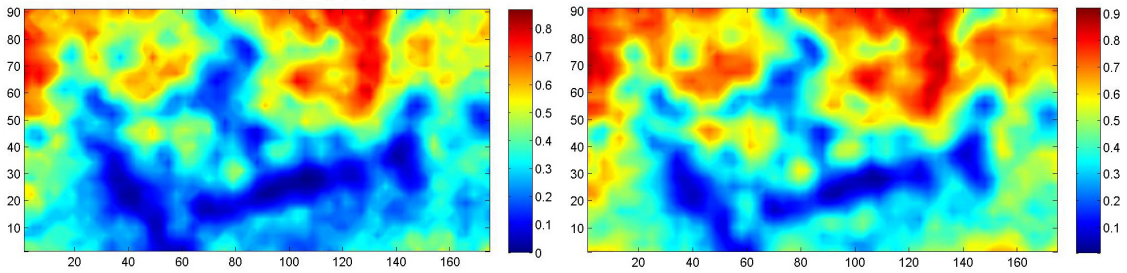

(b) April 2015.

Figure 4.4: Local measurements of VaR and AVaR for indicator $\lambda^{A'_u}$: $VaR_{0.95}(\lambda^{D'}(A_{0.9}(X,D')))$ (lelft) and $AVaR_{0.95}(\lambda^{D'}(A_{0.9}(X,D')))$ (right).

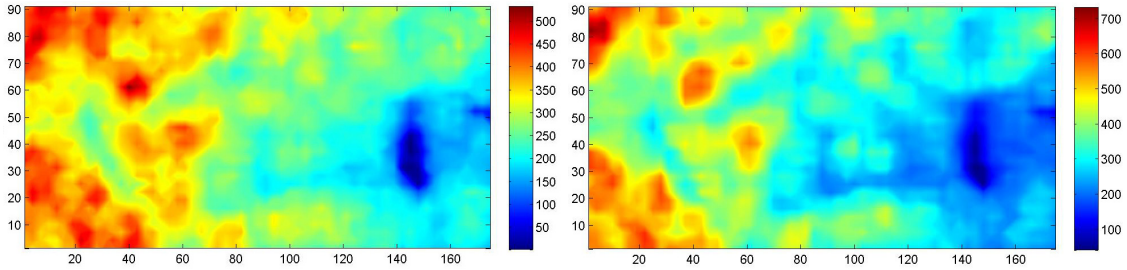

(a) April 2014.

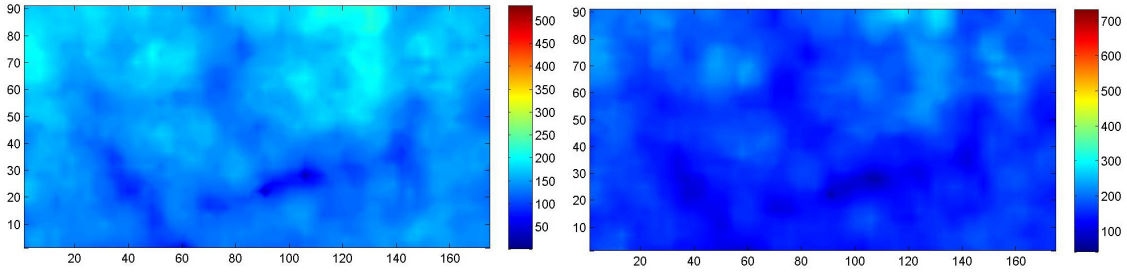

(b) April 2015.

Figure 4.5: Local measurements of VaR and AVaR for indicator $V^{A'_u}$: $VaR_{0.95}(V^{D'}(A_{0.9}(X,D')))$ (left) and $AVaR_{0.95}(V^{D'}(A_{0.9}(X,D')))$ (right).

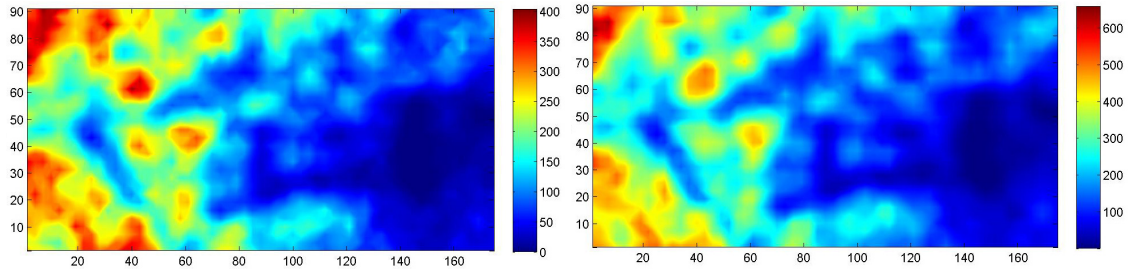

(a) April 2014.

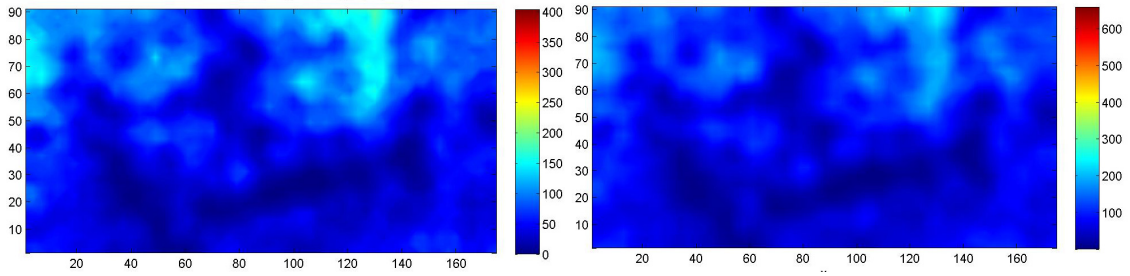

(b) April 2015.

Figure 4.6: Local measurements of VaR and AVaR for indicator $V^{D'}$: $VaR_{0.95}(V^{D'}(A_{0.9}(X,D')))$ (left) and $AVaR_{0.95}(V^{D'}(A_{0.9}(X,D')))$ (right).

4.1.2 Spatiotemporal Analysis

In the spatiotemporal framework, the main goal is to perform a dynamic-predictive risk assessment for future horizons. This study considers precipitation data measurements between October 2014 and April 2015 in the 13 stations of the AEMET network located in the province of Cádiz. One of the reasons for reducing the study area is to justify the versatility of this methodology from the regional point of view. However, in this particular case, the computational cost and the capacity of the parameter estimation methods for the spatiotemporal covariance model, are also taken into account. The Gneiting model (see Gneiting and Schlather 2004) is considered to be the one that best explains the spatiotemporal dynamics of this phenomenon. It is a space-time model where the spatial component is isotropic, defined by the covariance function

$$C(h,u) = (\psi(u)+1)^{\frac{-d}{2}} \phi\left(\frac{h}{\sqrt{(\psi(u)+1}}\right),$$

where ψ y ϕ are covariance models that control the spatial component and the spatiotemporal dependence, respectively. For this application it is considered that ψ is a covariance model of the generalized Cauchy class introduced in Chapter 3 (Section 3.4.1), and that ϕ is a stationary and isotropic covariance model of the stable process family $C(h) = e^{-h^\gamma}$ whose parameter γ determines the fractal dimension of the model. The Gneiting model obtained from the historical series of observed data has the form

$$C(h,u) = (\sigma^2(1+|u|^\alpha)^{-\beta/\alpha}+1)^{\frac{-d}{2}} exp\left(-\frac{h}{\sqrt{(\sigma^2(1+|u|^\alpha)^{-\beta/\alpha}+1}}\right)^\gamma.$$

The physical study area is defined to be the rectangular grid $[0,111]\times[0,104]$ of 11.544 pixels at 1km scale, where each pixel is identified, again, with its physical centroid. For model parameter estimation, the observations at the stations of the entire time series are considered (October 2014 to April 2015). The simulation of the field is performed, within the rectangular grid, conditioning to the observations of the last three months (February, March and April 2015), in those three months and in the two next future months (May and June 2015). As before, based on the empirical compound CDF, F_X^D, obtained from the conditional simulation on the observed data of 200 realizations, the empirical distributions of various structural characteristics of threshold exceedance sets are analyzed and compared in terms of related VaR and AVaR risk measures. As in the spatial case, logarithms of the mean-centered precipitation data are use for model parameter estimation and for the conditional simulation. Risk analysis is carried out with the true values of the magnitude.

Table 4.2 displays the parameter estimates for the model considered.

As in the spatial analysis performed in Section 4.1.1, the window size considered yo assess local variations is 9 pixels with a sliding step of 3 units, so that 1.295 square windows are used

for the spatiotamporal scenario. The choosen threshold and the confidence level, as well as the indicators to evaluate the VaR and AVaR risk measures are the same that in the previous spatial case.

Parameter	Estimate
α $(Cauchy)$	1.04
β $(Cauchy)$	0.68
γ $(Powered\ Exponential)$	0.35
σ^2 $(Cauchy)$	1.24

Table 4.2: Estimated parameter values for the Gneiting model (Rainfall).

Fig. 4.7 shows the precipitation measurement network considered at the province of Cádiz, first the UTM coordinates on a map of this province and then in the grid of pixels at 1 km scale. Fig. 4.8 displays a temporal dynamic obtained by the effect of conditioning on spatial and spatiotemporal dependence structure. In addition, in Fig. 4.9 it is observed how the degree of long-range spatial dependence given by the Cauchy model β parameter produces little local variability around the conditioning points in the first three stages. This does not happen in the same way for the last two times corresponding to May and June 2015 since there are no observed values in the stations for these future times; in fact, looking at the map globally, in these times there is, as expected, a greater variability. Here again, as in the spatial scenario, Fig. 4.10 shows how the AVaR maps are above those of the VaR for both, April and May. In this case it is clearly seen how the effect of conditioning is more clearly reflected in the risk map of the indicator for April than for May, because in April there are still available observations at the fixed stations. In addition, as expected, increasing the time horizon provides greater values of the risk measure considered. This is supported by Fig. 4.11 with respect to the VaR of the relative excess volume indicator.

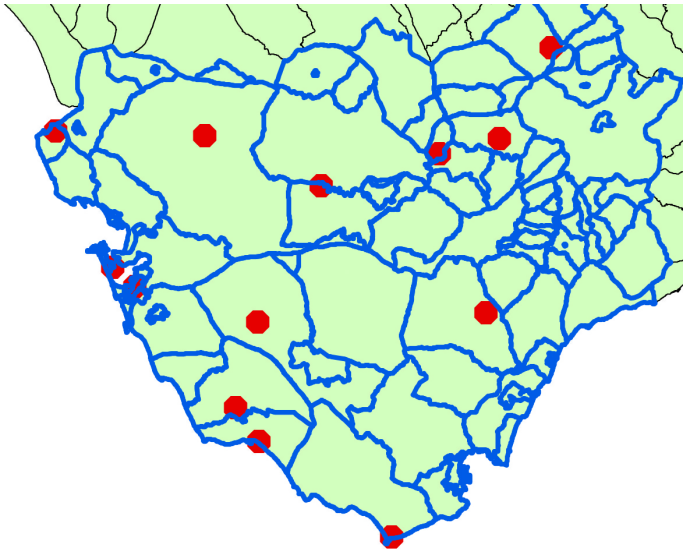

(a) UTM Network.

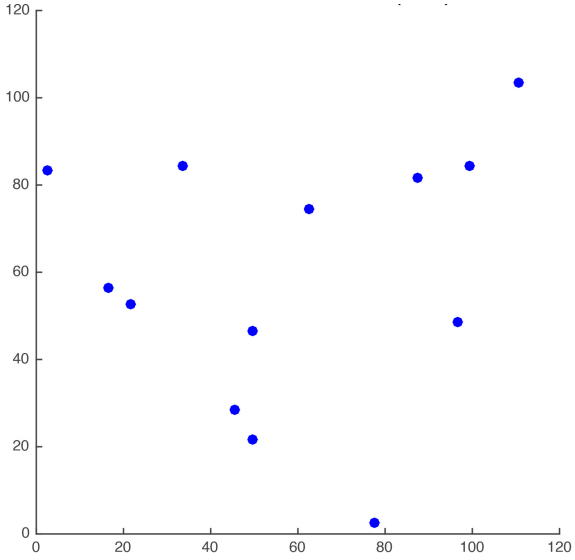

(b) Network within grid of pixels.

Figure 4.7: Rainfall measurement network in Cádiz province.

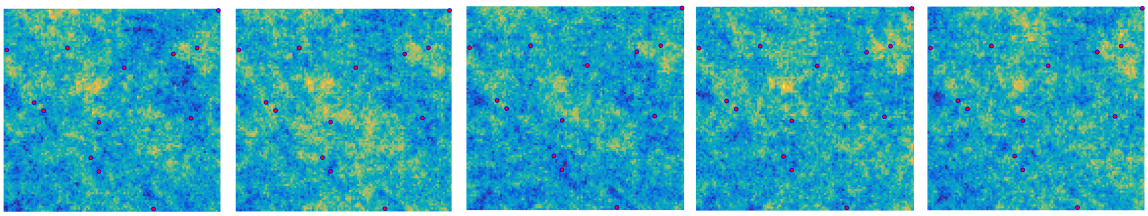

(a) February 2015. (b) March 2015. (c) April 2015. (d) May 2015. (e) June 2015.

Figure 4.8: Simulated realizations on the square $[0, 111] \times [0, 104]$ conditional to observed data.

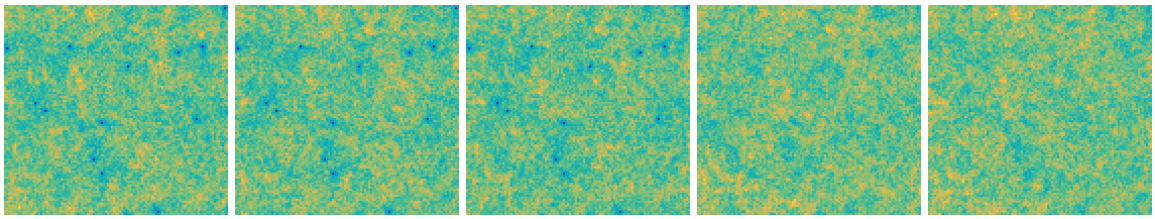

(a) February 2015. (b) March 2015. (c) April 2015. (d) May 2015. (e) June 2015.

Figure 4.9: Level plots for the map of variances (February to June 2015).

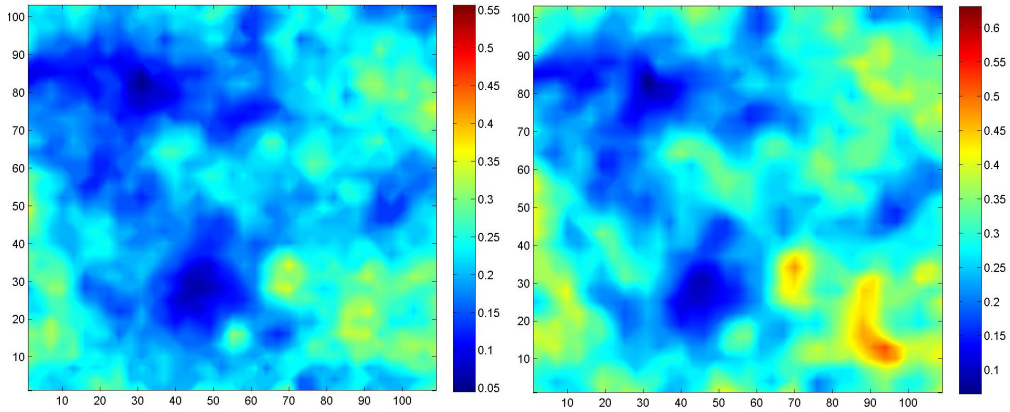

(a) April 2015.

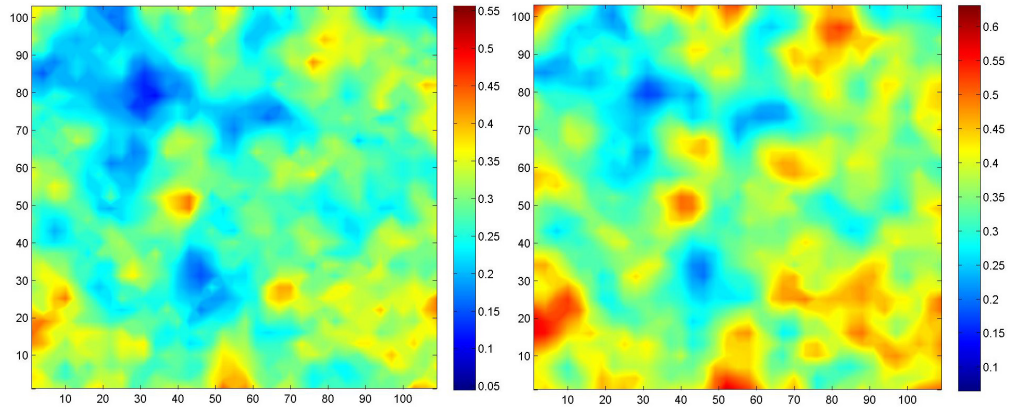

(b) May 2015.

Figure 4.10: Local measurements of VaR and AVaR for indicator $\lambda^{A'_u}$: $VaR_{0.95}(\lambda^{D'}(A_{0.9}(X,D')))$ (left) and $AVaR_{0.95}(\lambda^{D'}(A_{0.9}(X,D')))$ (right).

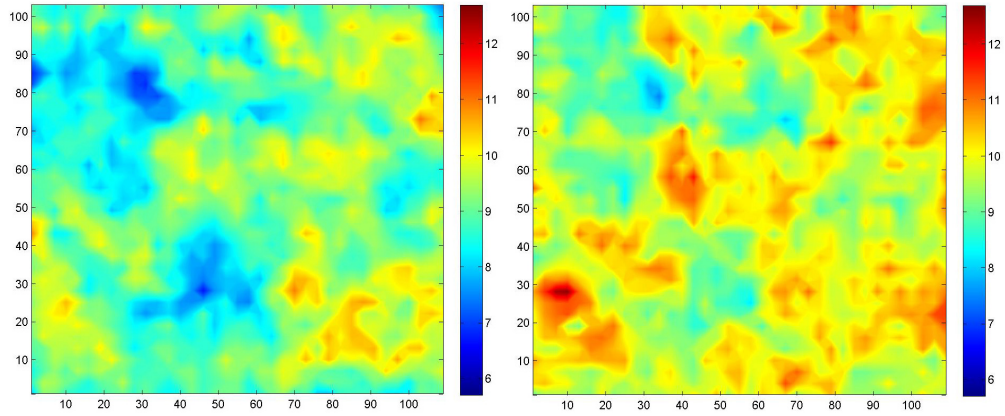

(a) April 2015. (b) May 2015.

Figure 4.11: Local measurements of VaR for indicator $V^{A'_u}$: $VaR_{0.95}(V^{D'}(A_{0.9}(X,D')))$.

4.2 Ambient PM10 Concentration Data

According to the glossary of the European Environment Agency (EEA), the particulate matter PM10 is: *an air pollutant consisting of small particles with an aerodynamic diameter less than or equal to a nominal 10 micrometer (about 1/7 the diameter of a single human hair). Their small size allows them to make their way to the air passages deep within the lungs where they may be deposited and result in adverse health effects. PM10 also causes visibility reduction.* While this thesis work was written, an extreme episode of pollution was taking place at Canary Islands (Spain). But this is only one more of the wide number of episodes around the world due to this stage of climate change and human development. The consequences for population of these high concentration levels of PM are, among others, almost unbreathable air, airports and other public institutions and services closed, people evacuated from their homes,etc. Methodologies like the specific one proposed in this thesis in Section 3.3 become relevant since they provide suitable tools for risk mapping to future horizons that may allow the authorities to provide a more effective management, from a predictive-risk point of view, in order to avoid adverse effects on population. Here the pollution issue of the *Carboneras* industrial area in the province of Almería is illustrated with this methodology as an example. The relevance of this problem is reflected in the Almería Air Quality Improvement Plan of the Andalusia Goverment (BOJA 46, pag. 6-197, https://www.juntadeandalucia.es/boja/2014/46/BOJA14-046-02582.pdf.)

For this illustration, daily averages of PM10 concentrations measured at 9 stations (within the network of Andalusia's zoning for assessing air quality) in the *Carboneras* area, along six consecutive days, are considered. As in Section 4.1.2, here the Gneiting model is also adopted as the best one that explains the dynamics of this phenomenon (see Table 4.3 for parameter estimates). The study area is defined to be the rectangular grid $[0,377] \times [0,175]$ of 65.975 pixels at 250m scale, where each pixel is identified, once more, with its physical centroid. Logarithms of the mean-centered PM10 data are used for model fitting and for conditional simulation. Using the last three days data at the fixed locations, 200 conditional realizations are simulated in the whole grid for the same three days and for the two days after.

Percentiles are fixed from the compound CDF on the 200 conditional realizations of the model. Results for areas, volumes, and volumes relative to areas, globally and locally per connected components, are derived and compared. The study is performed locally, based on sliding windows, for assessment of regional variations of risk. The scale of analysis and degree of interpolation are determined by the size of the window and the sliding step. Here we use 5.415 square windows of size 25, and step equal to 4 units (pixels). Risk maps are drawn for different indicators and percentiles.

Parameter	Estimate
α $(Cauchy)$	0.315
β $(Cauchy)$	0.706
γ $(Powered\ Exponential)$	0.346
σ^2 $(Cauchy)$	0.21

Table 4.3: Estimated parameter values for the Gneiting model (PM10).

Fig. 4.12 shows the zoning for assessing air quality in Andalusia and the data measurement network at *Carboneras* area. The temporal dynamics (along the five days considered) obtained by the effect of the fitted model is displayed in Fig. 4.13. Finally, Fig. 4.14 displays, for two consecutive days, the temporal dynamics of relative area at risk above a pre-fixed threshold level of critical concentration of PM10. As mentioned at the beginning of this section, risk maps of this type provide information concerning future areas at risk that authorities may use to prevent damages or adverse effects on population.

The spatial and spatiotemporal risk analysis performed in this chapter does not take into account that risk of extremal situations is relevant not necessarily in the whole domain but where adverse effects are of a real concern. For example, going back to the last real data application of PM10 pollution, risk assessment becomes more important where the population is living. Chapter 5 deals with formal extensions to generalized scenarios as, for instance, the effect of population covariates in spatiotemporal risk assessment (See Section 5.3.2 for risk assessment in relation to Ambient PM10 Pollution Population Exposure.)

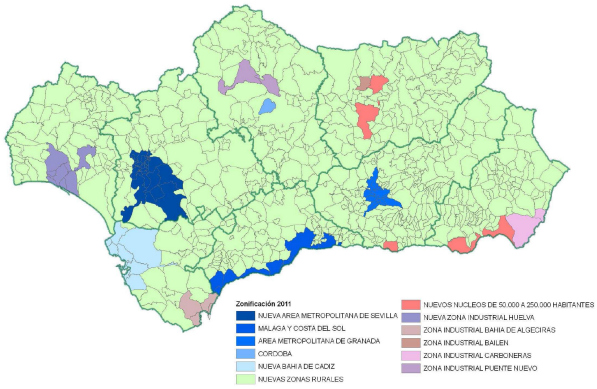

(a) UTM network in Andalusia.

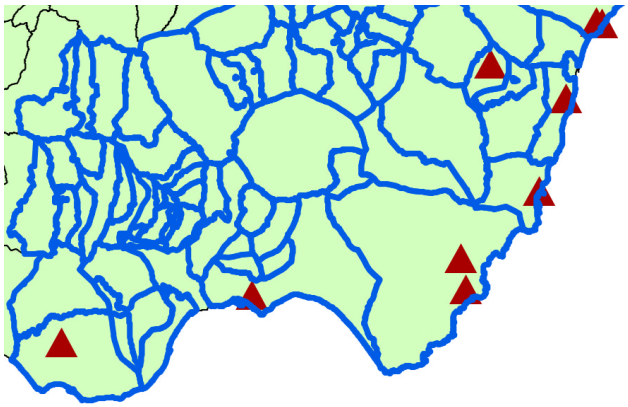

(b) UTM network in *Carboneras* area.

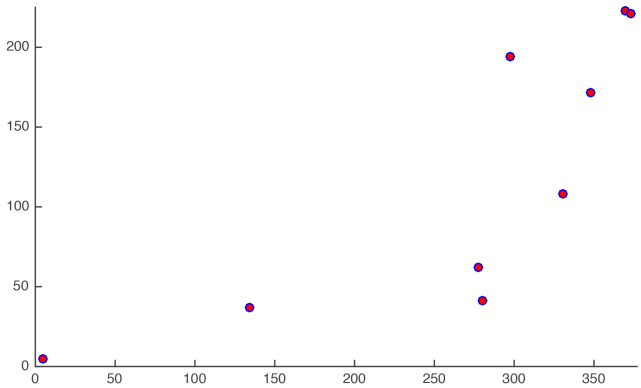

(c) Network within grid of pixels.

Figure 4.12: PM10 measurement network.

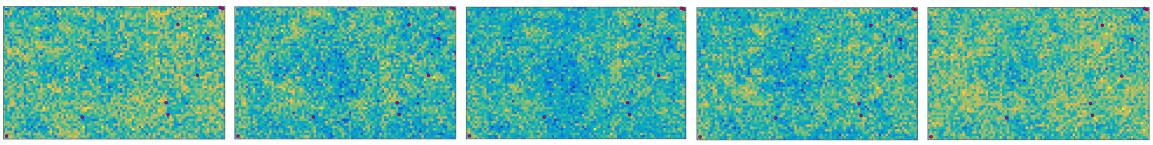

(a) $T = 1$. (b) $T = 2$. (c) $T = 3$. (d) $T = 4$. (e) $T = 5$.

Figure 4.13: Simulated realizations on the square $[0,377] \times [0,175]$ conditional to observed data.

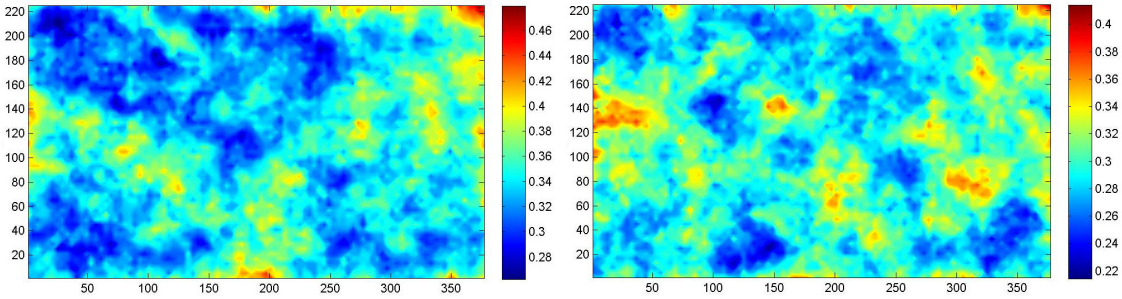

(a) $T = 3$. (b) $T = 4$.

Figure 4.14: Local measurements of VaR for indicator $\lambda^{A'_u}$, $VaR_{0.95}(\lambda^{D'}(A_{0.9}(X,D')))$.

Chapter 5

Analytical Aspects and Formal Extension to Generalized Scenarios

In this chapter, formal extensions to scenarios such as the effect under spatial deformation and population density covariate are addressed. A generalization covering these and others potential cases is formulated.

5.1 A Spatial Relationship Between Quantile-Based Risk Measures and Random Field Threshold Exceedances

This section is focused, firstly, on analytical aspects related to the relationship between VAR and AVaR measures with respect to structural characteristics of random field exceedances and, secondly, on the asymptotic behaviour and interpretation of this relationship for increasing threshold.

5.1.1 The Expected Volume vs. Expected Area Ratio in Terms of the Compound CDF AVaR-VaR Increment

The proposition below shows a reciprocal VaR-related interpretation of two of the structural random indicators considered in Chapter 3, the expected relative exceedance area and the expected relative excess volume with respect to the domain D, when the threshold level for the excursion set is the VaR of the compound r.v. X^D at a fixed confidence level.

Proposition 5.1.1. *If $u = VaR_{1-\alpha}(X^D)$, such that $F_X^D(u) = 1-\alpha$, then*

(i) $E\left[\lambda^D(A_{VaR_{1-\alpha}(X^D)}(X,D))\right] = \alpha$

(ii) $E\left[V^D(A_{VaR_{1-\alpha}(X^D)}(X,D))\right] = E\left[X^D_{VaR_{1-\alpha}(X^D)}\right] = UPM_{(1,VaR_{1-\alpha}(X^D))}(X^D)$ *where,*

$UPM_{(h,a)}(X) := E[\max\{0,(X-a)^h\}]$*, for* $h \geq 0$*, and* $a \in \mathbb{R}$ *(with* $UPM_{(0,a)}(X) := P[X \geq a]$*), is the upper partial moment of* X *of order* h *with respect to level* a*.*

Proof

(i) Prop. 3.2.1(iii), $E\left[\lambda^D(A_{VaR_{1-\alpha}(X^D)}(X,D))\right] = S^D_X(VaR_{1-\alpha}(X^D)) = 1 - F^D_X(VaR_{1-\alpha}(X^D))$, and $VaR_{1-\alpha}(X^D) = (F^D_X)^{-1}(1-\alpha)$, then $E\left[\lambda^D(A_{VaR_{1-\alpha}(X^D)}(X,D))\right] = 1-(1-\alpha) = \alpha$.

(ii) Prop. 3.2.1(vi) and definition of upper partial moment (see Kriele and Wolf 2014).

□

In terms of VaR and AVaR, the ratio of the expected relative excess volume with respect to the expected relative exceedance area can be directly interpreted as the difference between the AVaR and VaR of X^D.

Proposition 5.1.2. *For* $\alpha \in (0,1]$*,*

$$\frac{E\left[V^D(A_{VaR_{1-\alpha}(X^D)}(X,D))\right]}{E\left[\lambda^D(A_{VaR_{1-\alpha}(X^D)}(X,D))\right]} = AVaR_{1-\alpha}(X^D) - VaR_{1-\alpha}(X^D), \quad with \tag{5.1}$$

$$E\left[\lambda^D(A_{VaR_{1-\alpha}(X^D)}(X,D))\right] = \alpha \tag{5.2}$$

Proof

$$
\begin{aligned}
AVaR_{1-\alpha}(X^D) &= \frac{1}{\alpha}\int_{1-\alpha}^{1} VaR_p(X^D)dp = \frac{1}{\alpha}\int_{1-\alpha}^{1}(F_X^D)^{-1}(p)dp = \frac{1}{\alpha}\int_{VaR_{1-\alpha}(X^D)}^{+\infty} xf_X^D(x)dx \\
&\quad \big(\text{ch. of v. } (F_X^D)^{-1}(p) = x \to F_X^D)(x) = p, dp = f_X^D(x)dx\big) \\
&\quad \big(x = x - VaR_{1-\alpha}(X^D) + VaR_{1-\alpha}(X^D)\big) \\
&= \frac{1}{\alpha}[\int_{VaR_{1-\alpha}(X^D)}^{+\infty}(x - VaR_{1-\alpha}(X^D))f_X^D(x)dx + \\
&+ \int_{VaR_{1-\alpha}(X^D)}^{+\infty} VaR_{1-\alpha}(X^D)f_X^D(x)dx] \\
&= \frac{1}{\alpha}[\int_{0}^{+\infty}\max\{0, x - VaR_{1-\alpha}(X^D)\}f_X^D(x)dx + \\
&+ VaR_{1-\alpha}(X^D)\int_{VaR_{1-\alpha}(X^D)}^{+\infty} f_X^D(x)dx] \\
&= \frac{1}{\alpha}\left[E\left[X^D_{VaR_{1-\alpha}(X^D)}\right] + VaR_{1-\alpha}(X^D)\left(1 - F_X^D(VaR_{1-\alpha}(X^D))\right)\right] \\
&= \frac{1}{\alpha}\left[E\left[X^D_{VaR_{1-\alpha}(X^D)}\right] + VaR_{1-\alpha}(X^D)\left(1 - (1-\alpha)\right)\right] \\
&= \frac{1}{\alpha}E\left[X^D_{VaR_{1-\alpha}(X^D)}\right] + VaR_{1-\alpha}(X^D) \\
&= \frac{E\left[V^D(A_{VaR_{1-\alpha}(X^D)}(X,D))\right]}{E\left[\lambda^D(A_{VaR_{1-\alpha}(X^D)}(X,D))\right]} + VaR_{1-\alpha}(X^D)(\text{Prop. 5.1.1}).
\end{aligned}
$$

Then, $\frac{E\left[V^D(A_{VaR_{1-\alpha}(X^D)}(X,D))\right]}{E\left[\lambda^D(A_{VaR_{1-\alpha}(X^D)}(X,D))\right]} = AVaR_{1-\alpha}(X^D) - VaR_{1-\alpha}(X^D)$.

□

5.1.2 Asymptotics in Relation to the Shape Parameter of the Generalized Pareto Distribution

Here, the asymptotic behaviour of (5.1), as $\alpha \to 0$, is analyzed in relation to the the shape parameter of the Generalized Pareto Distribution (GPD).

Let X be a (loss) r.v. with CDF F. For a given threshold u, let F_u be the *excess* CDF, defined by

$$F_u(x) = P[X - u \le x | X > u] = \frac{F(x+u) - F(u)}{1 - F(u)},$$

for $0 \leq x < x_F - u$, where $x_F \leq \infty$ is the right endpoint of F. Furthermore, considering S as the decumulative distribution function (DDF) of X, the excess DDF is

$$S_u(x) = 1 - F_u(x) = 1 - \frac{F(x+u) - F(u)}{1 - F(u)} = 1 - \frac{S(u) - S(x+u)}{S(u)} = \frac{S(x+u)}{S(u)}.$$

According to Pickand-Balkema-de Haan's theorem (see, McNeil et al. 2005, p. 277), there exist a positive measurable function $\beta(u)$ such that

$$\lim_{u \to x_F} \sup_{0 \leq x < x_F - u} |F_u(x) - G_{\xi,\beta(u)}(x)| = 0,$$

where $G_{\xi,\beta(.)}$ represents the CDF of the GPD(ξ,β) with shape and scale parameters $\xi \in \mathbb{R}$ and $\beta > 0$, respectively, if and only if $F \in MDA(H_\xi)$, the Maximum Domain of Attraction of the Generalized Extreme Value Distribution (GEVD) class H_ξ with shape parameter $\xi \in \mathbb{R}$.

Proposition 5.1.3. *Under the assumption that the previous approximation holds for X with* $\xi \in \mathbb{R}$,

(i) $\lim_{\alpha \to 0} \frac{AVaR_{1-\alpha}(X)}{VaR_{1-\alpha}(X)} = \max\{1, (1-\xi)^{-1}\}$.

(ii) $AVaR_{1-\alpha}(X) - VaR_{1-\alpha}(X) \sim \max\{0, \xi(1-\xi)^{-1}\} VaR_{1-\alpha}(X), \quad as\ \alpha \to 0.$

Proof

(i) See McNeil et al. (2005), p. 283.

(ii) Trivial from (i).

□

Table 5.1 summarizes the asymptotics for the relationship introduced in the previous section in terms of the GPD shape parameter ξ as $\alpha \to 0$.

	$\xi < 0$	$\xi = 0$	$0 < \xi < 1$
$\frac{E\left[V^D(A_{\mathrm{VaR}_{1-\alpha}(X^D)}(X,D))\right]}{E\left[\lambda^D(A_{\mathrm{VaR}_{1-\alpha}(X^D)}(X,D))\right]}$	$0\ [\sim \alpha^{-\xi}]$	β [indep. of u]	$\infty\ [\sim \alpha^{-\xi}]$
$\frac{E\left[V^D(A_{\mathrm{VaR}_{1-\alpha}(X^D)}(X,D))\right]}{E\left[\lambda^D(A_{\mathrm{VaR}_{1-\alpha}(X^D)}(X,D))\right]\mathrm{VaR}_{1-\alpha}(X^D)}$	$0\ [\sim \alpha^{-\xi}]$	$0\ [\sim (-\ln\alpha)^{-1}]$	$\xi(1-\xi)^{-1}$

Table 5.1: Relationship between $E\left[V^D(A_{\mathrm{VaR}_{1-\alpha}(X^D)}(X,D))\right]$ and $E\left[\lambda^D(A_{\mathrm{VaR}_{1-\alpha}(X^D)}(X,D))\right]$ as $\alpha \to 0$.

5.2 Effect of Deformation in Spatiotemporal Risk Analysis

Spatial deformation has been used in different areas of application, such as image analysis or environmental studies, to represent certain forms of heterogeneity which can be explained by transformation of a reference stationary random field. See, for example, Sampson and Guttorp (1992) in the context of sampling network design, Anderes and Stein (2008), Clerc and Mallat (2003), Perrin and Senoussi (2000) concerning the estimation of deformed stationary or stationary-isotropic random fields, Mardia et al. (2006) on image warping and the evaluation of distortion induced by deformation, Goitía et al. (Goitía et al (2004)) regarding the joint estimation of spatial deformation and blurring under a generalized random field approach, with application to environmental data, Angulo and Madrid (2014) for the implementation of dynamic deformation in a spatio-temporal model, etc. Angulo and Madrid (2010) study through simulation the effect of deformation on the asymptotic behaviour of the Euler-Poincaré characteristic of threshold exceedance sets, considering different scenarios depending on local variability and long-range dependence properties of the underlying random field (see also Angulo and Madrid 2014 in the spatio-temporal case).

In this section, formal extensions of previous definitions and results are developed in generalized scenarios. Specifically, 'level' and 'flow' type deformation effects and population covariate effect are formalized. A generalized formulation in terms of non-constant thresholds an non-Lebesgue measures is established.

In the following definition, the concepts of spatially deformed random field for 'level' and 'flow' type magnitudes are introduced (see Angulo and Madrid 2010,2014.)

Definition 11. *Let X be a spatial random field on $D \subseteq \mathbb{R}^d$, and let $\Phi : D \to D' \subseteq \mathbb{R}$ be a spatial deformation (Φ is assumed to be a C^1-diffeomorphism with $|J_\Phi| > 0$). Then:*

(i) If X represents a 'level'-type magnitude, the deformed random field X_Φ on D' is defined by

$$X_\Phi(s') = X(\Phi^{-1}(s')), \quad \forall s' \in D' \tag{5.3}$$

(ii) If X represents a 'flow'-type magnitude, the deformed random field $X_{\tilde{\Phi}}$ on D' is defined by

$$X_{\tilde{\Phi}}(s') = X(\Phi^{-1}(s'))|J_\Phi(\Phi^{-1}(s'))|^{-1} = X(\Phi^{-1}(s'))|J_{\Phi^{-1}}(s')|, \quad \forall s' \in D' \tag{5.4}$$

□

In the 'level'-type case, the effect is to reallocate in the spatial domain the random field variables, with state values remaining as originally. In the 'flow'-type case, the transformation also involves a local change of measure. In both cases, stationarity and isotropy are not preserved in a deformed random field.

Next, formal aspects related to the effect on the compound CDF, as well as on the relationships obtained in the previous section are formalized.

5.2.1 'Level' Type Deformation Effects

Assume that X represents a 'level'-type magnitude. The deformed random field X_Φ on D', defined by Equation (5.3), induces a reinterpretation of the compound CDF that can be formalized as follows. First, for a local CDF,

$$F_{X_\Phi(s')}(x) = P[X_\Phi(s') \leq x] = P[X(\Phi^{-1}(s')) \leq x] = F_{X(\Phi^{-1}(s'))}(x).$$

Then,

$$\begin{aligned} F^{D'}_{X_\Phi}(x) &= \int_{D'} F_{X_\Phi(s')}(x)\lambda^{D'}(ds') \qquad \text{(ch. of v. } s' = \Phi(s)) \\ &= \int_D F_{X(s)}(x)\lambda^D_\Phi(ds) \;=:\; F^{D;\Phi}_X(x), \end{aligned}$$

where λ^D_Φ is the normalized measure on D defined by

$$\lambda^D_\Phi(ds) \;:=\; [\lambda_\Phi(D)]^{-1}\,\lambda_\Phi(ds), \quad \text{with} \quad \lambda_\Phi(ds) := |J_\Phi(s)|ds.$$

In this case, the compound distribution is constructed on the $\Phi-$deformed Lebesgue measure, which means that areas in D subject to 'dilation' are sampled more densely, and reciprocally.

As a consequence, the relationships derived in the previous section are similarly obtained, replacing the normalized Lebesgue measure λ^D with λ^D_Φ on D:

$$\frac{E\left[V^D_\Phi(A_{\mathrm{VaR}_{1-\alpha}(X^{D;\Phi})}(X,D))\right]}{E\left[\lambda^D_\Phi(A_{\mathrm{VaR}_{1-\alpha}(X^{D;\Phi})}(X,D))\right]} = \mathrm{ES}_{1-\alpha}(X^{D;\Phi}) - \mathrm{VaR}_{1-\alpha}(X^{D;\Phi}), \quad \text{with} \tag{5.5}$$

$$E\left[\lambda^D_\Phi(A_{\mathrm{VaR}_{-\alpha}(X^{D;\Phi})}(X,D))\right] = \alpha \tag{5.6}$$

Intuitively, these results can be generalized on the basis of any normalized measure on D (under suitable regularity conditions), as shown in Section 5.4.

An illustration

Here, Figs. 5.1 and 5.2 show the effect of a 'level'-type deformation, respectively a contraction and a dilation, on one particular realization of the Cauchy random field, (see Angulo and Madrid 2010 for details). Figs. 5.3 and 5.4 display the effect induced on local measurements of the AVaR for the random indicator defined as the average relative excess volume with respect to area per connected component, in both before and after deformation.

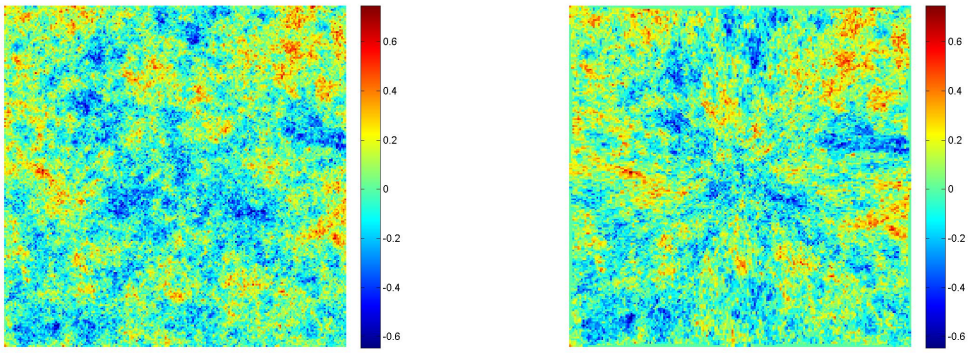

(a) (b)

Figure 5.1: Simulated realization on the square $[0,200]^2$ of RF of Cauchy class with $\alpha = 0.5$ and $\beta = 0.1$, with variance $\sigma^2 = 0.1$, conditional to given values at 50 fixed points: Original (left) and deformed towards origin (right).

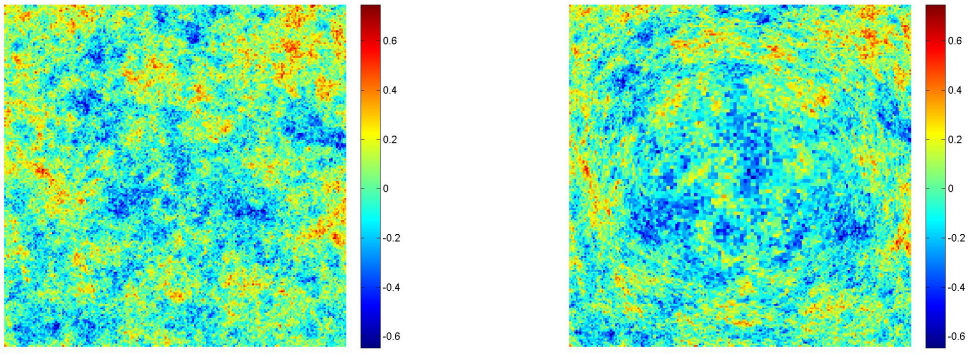

(a) (b)

Figure 5.2: Simulated realization on the square $[0,200]^2$ of RF of Cauchy class with $\alpha = 0.5$ and $\beta = 0.1$, with variance $\sigma^2 = 0.1$, conditional to given values at 50 fixed points: Original (left) and deformed towards edges (right).

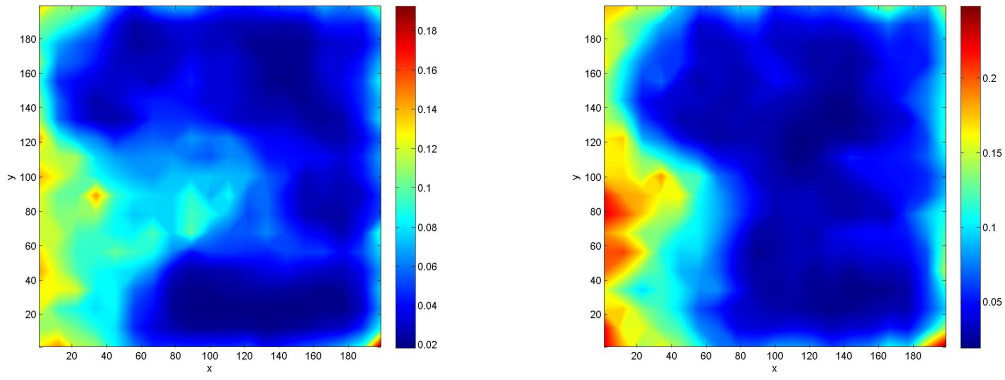

(a) (b)

Figure 5.3: Local measurements of AVaR ($1-\alpha_2 = 0.95$) of VOLUME/AREA PER CC, from Cauchy class model with $(\alpha,\beta) = (0.5, 0.1)$, $\sigma^2 = 0.1$, for excursion set at percentile level $1-\alpha_1 = 0.90$: Original (left) and deformed towards center (right).

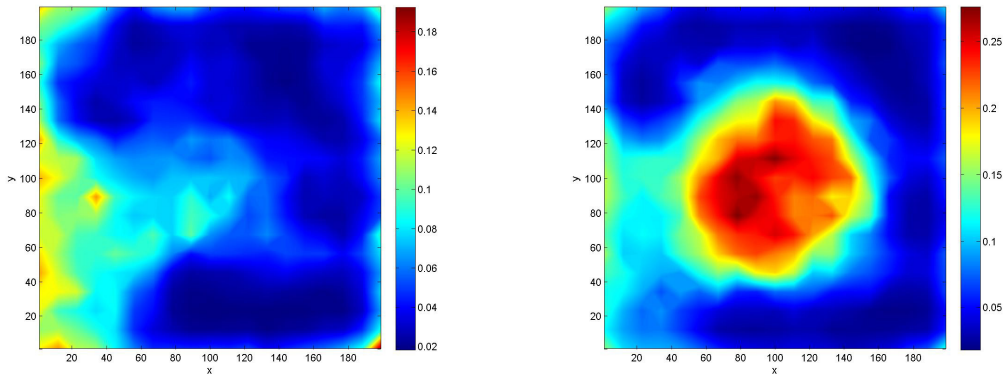

(a) (b)

Figure 5.4: Local measurements of AVaR ($1-\alpha_2 = 0.95$) of VOLUME/AREA PER CC, from Cauchy class model with $(\alpha,\beta) = (0.5, 0.1)$, $\sigma^2 = 0.1$, for excursion set at percentile level $1-\alpha_1 = 0.90$: Original (left) and deformed towards edges (right).

5.2.2 'Flow' Type Deformation Effects

Assuming now that X represents a 'flow'-type magnitude, the compound CDF of the $X_{\tilde{\Phi}}$ on D', defined by Equation (5.4), is also reinterpreted as follows.

First, for a local CDF,

$$\begin{aligned} F_{X_{\tilde{\Phi}}(s')}(x) &= P[X_{\tilde{\Phi}}(s') \leq x] = P[X(\Phi^{-1}(s'))|J_{\Phi}(\Phi^{-1}(s'))|^{-1} \leq x] \\ &= P[X(\Phi^{-1}(s')) \leq |J_{\Phi}(\Phi^{-1}(s'))|x] = F_{X(\Phi^{-1}(s'))}(|J_{\Phi}(\Phi^{-1}(s'))|x) \\ &= F_{X_{\Phi}(s')}(|J_{\Phi}(\Phi^{-1}(s'))|x). \end{aligned}$$

Then,

$$\begin{aligned} F^{D'}_{X_{\tilde{\Phi}}}(x) &= \int_{D'} F_{X_{\tilde{\Phi}}(s')}(x)\lambda^{D'}(ds') = \int_{D'} F_{X_{\Phi}(s')}(|J_{\Phi}(\Phi^{-1}(s'))|x)\lambda^{D'}(ds')(\text{ch. of v. } s' = \Phi(s)) \\ &= \int_{D} F_{X(s)}(|J_{\Phi}(s)|x)\lambda^{D}_{\Phi}(ds) \;=:\; F^{D;\tilde{\Phi}}_{X}(x), \end{aligned}$$

where, as before, λ^{D}_{Φ} is the normalized measure on D defined by $\lambda^{D}_{\Phi}(ds) := [\lambda_{\Phi}(D)]^{-1}\lambda_{\Phi}(ds)$, with $\lambda_{\Phi}(ds) := |J_{\Phi}(s)|ds$.

It can be interpreted as the consideration for X of a 'functional threshold', which varies locally according to the Jacobian determinant, $|J_{\Phi}(s)|$. Areas subject to spatial dilation led more densely in the $D-$space, with an increase in the argument of the original local CDF.

The relationships obtained in Section 5.1.1 are rewritten, replacing the normalized Lebesgue measure λ^{D} with λ^{D}_{Φ} on D, and using the intermediate rescaled random field

$$X_{[\tilde{\Phi}]}(s) = X(s)|J_{\Phi}(s)|^{-1}, \quad \forall s \in D.$$

That is, $X_{\tilde{\Phi}}$ can be viewed as a 'level'-type deformed random field with respect to $X_{[\tilde{\Phi}]}$. Indeed, noting that

$$\begin{aligned} F_{[\tilde{\Phi}]}(s)(x) &= P[X_{[\tilde{\Phi}]}(s) \leq x] = P[X(s)|J_{\Phi}(s)|^{-1} \leq x] = P[X(s) \leq |J_{\Phi}(s)|x] \\ &= P[X(s) \leq x_{\Phi}(s)] = F_{X(s)}(X_{\Phi}(s)), \end{aligned}$$

and, consequently,

$$F^{D;\tilde{\Phi}}_{X}(x) = \int_{D} F_{X(s)}(X_{\Phi}(s))\lambda^{D}_{\Phi}(ds) = \int_{D} F_{X_{[\tilde{\Phi}](s)}}(x)\lambda^{D}_{\Phi}(ds),$$

it is observed that, $F^{D;\tilde{\Phi}}_{X}(x) := F^{D;\Phi}_{X_{[\tilde{\Phi}]}}$, i.e., the compound CDF of the intermediate random field $X_{[\tilde{\Phi}]}$ with respect to the measure λ^{D}_{Φ}.

This allows to establish the Equation 5.5 applied to the 'flow'-type case, as follows. Denoting by $X^{D;\tilde{\Phi}}$ the r.v. with CDF $F^{D;\tilde{\Phi}}_{X} \equiv F^{D;\Phi}_{X_{[\tilde{\Phi}]}}$, (i.e. $X^{D;\tilde{\Phi}} \equiv X^{D;\Phi}_{[\tilde{\Phi}]}$ a.s., in the sense $\left(X_{[\tilde{\Phi}]}\right)^{D;\Phi}$ from the

intermediate random field $\{X_{[\tilde{\Phi}]}(s) : s \in D\}$),

$$\frac{E\left[V_{\Phi}^{D}(A_{VaR_{1-\alpha}(X^{D;\tilde{\Phi}})}(X_{[\tilde{\Phi}]},D))\right]}{E\left[\lambda_{\Phi}^{D}(A_{VaR_{1-\alpha}(X^{D;\tilde{\Phi}})}(X_{[\tilde{\Phi}]},D))\right]} = AVaR_{1-\alpha}(X^{D;\tilde{\Phi}}) - VaR_{1-\alpha}(X^{D;\tilde{\Phi}}), \quad \text{with} \tag{5.7}$$

$$E\left[\lambda_{\Phi}^{D}(A_{VaR_{1-\alpha}(X^{D;\tilde{\Phi}})}(X_{[\tilde{\Phi}]},D))\right] = \alpha \tag{5.8}$$

The intermediate random field $X_{[\tilde{\Phi}]}$ also provides a case of non-constant thresholds. Since, by definition in Chapter 2, $A_u(X,D) = \{s \in D : X(s) \geq u\}$ is the *excursion set* of X in D over level $u \in \mathbb{R}$, then $A_u(X_{[\tilde{\Phi}]},D) = \{s \in D : X_{[\tilde{\Phi}]}(s) \geq u\} = \{s \in D : X(s)|J_{\Phi}(s)|^{-1} \geq u\} = \{s \in D : X(s) \geq |J_{\Phi}(s)|u\} = \{s \in D : X(s) \geq u_{\Phi}(s)\} = A_{u_{\Phi}}(X,D)$. Hence, the 'constant-threshold exceedance set' $A_u(X_{[\tilde{\Phi}]},D)$ can now be seen as a 'non-constant-threshold exceedance set' $A_{u_{\Phi}}(X,D)$, with respect to the 'functional' threshold u_{Φ} defined as

$$u \to u_{\Phi} \equiv \{u_{\Phi}(s) = |J_{\Phi}(s)|u : s \in D\}.$$

Accordingly,

$$\frac{E\left[V_{\Phi}^{D}(A_{(VaR_{1-\alpha}(X^{D;\tilde{\Phi}}))_{\Phi}}(X_{[\tilde{\Phi}]},D))\right]}{E\left[\lambda_{\Phi}^{D}(A_{(VaR_{1-\alpha}(X^{D;\tilde{\Phi}}))_{\Phi}}(X_{[\tilde{\Phi}]},D))\right]} = AVaR_{1-\alpha}(X^{D;\tilde{\Phi}}) - VaR_{1-\alpha}(X^{D;\tilde{\Phi}}), \quad \text{with} \tag{5.9}$$

$$E\left[\lambda_{\Phi}^{D}(A_{(VaR_{1-\alpha}(X^{D;\tilde{\Phi}}))_{\Phi}}(X_{[\tilde{\Phi}]},D))\right] = \alpha \tag{5.10}$$

Or, in fact, given $u \in \mathbb{R}$ and calling (in this case) α_u the value in $(0,1]$ such that $F_X^{D;\tilde{\Phi}}(u) = 1 - \alpha_u$ ($\alpha_u = S_X^{D;\tilde{\Phi}}$), then

$$\frac{E\left[V_{\Phi}^{D}(A_{u_{\Phi}}(X,D))\right]}{E\left[\lambda_{\Phi}^{D}(A_{u_{\Phi}}(X,D))\right]} = AVaR_{1-\alpha_u}(X^{D;\tilde{\Phi}}) - u. \tag{5.11}$$

(since, in that case, $VaR_{1-\alpha_u}(X^{D;\tilde{\Phi}}) = (F_X^{D;\tilde{\Phi}})^{-1}(1-\alpha_u) = u$.)

Finally, it is important to remind that, although the set $A_{u_{\Phi}}(X,D)$ projects on the u_{Φ} non-linear surface, is must be clear that it is properly a subset of D, then the area $\lambda_{\Phi}^{D}(A_{u_{\Phi}}(X,D))$ is interpreted in the usual sense of the Lebesgue measures on D. As for the volume, it must be understood that it integrates the area (on D) of the layers of the intermediate rescaled random field $X_{[\tilde{\Phi}]}$ (with these layers as subsets of $D_u := D \times \{u\}$, for each u), with respect to the Lebesgue measure on the real line segment $[u_{\alpha}, +\infty)$.

These considerations suggest that a (more) general formulation can be established for non-constant thresholds, in an appropriate sense, as shown in Section 5.4.

An illustration

For this illustration, the Cauchy random field is also used. Here, Fig. 5.5 shows the effect of a 'flow'-type deformation on one particular realization of the random field. Fig. 5.6 illustrates the effect induced on local measurements of the AVaR for the random indicator defined as the average relative excess volume with respect to area per connected component, before and after deformation.

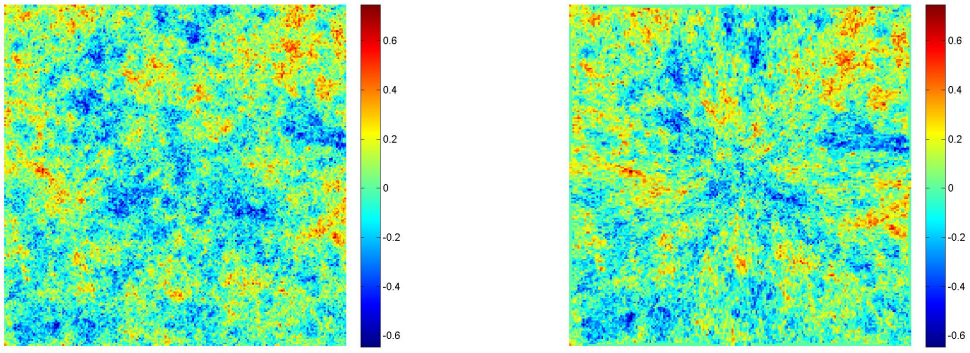

(a) (b)

Figure 5.5: Simulated realization on the square $[0,200]^2$ of RF of Cauchy class with $\alpha = 0.5$ and $\beta = 0.1$, with variance $\sigma^2 = 0.1$, conditional to given values at 50 fixed points: Original (left) and deformed towards origin (right).

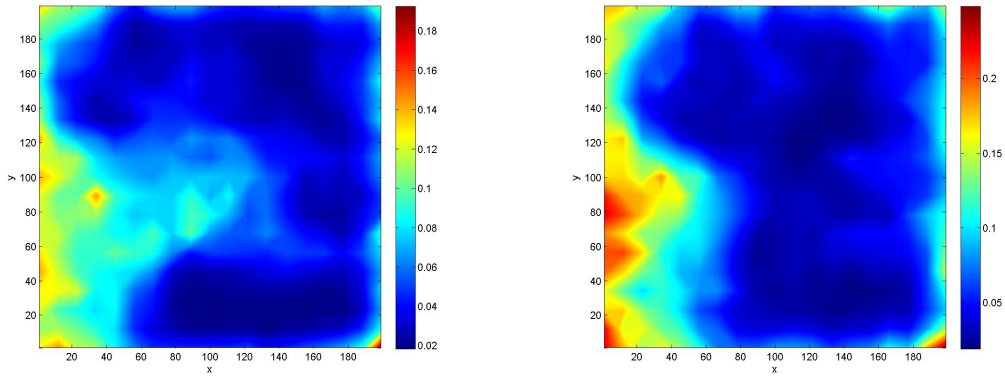

(a) (b)

Figure 5.6: Local measurements of AVaR ($1-\alpha_2 = 0.95$) of VOLUME/AREA PER CC, from Cauchy class model with $(\alpha,\beta) = (0.5,0.1)$, $\sigma^2 = 0.1$, for excursion set at percentile level $1-\alpha_1 = 0.90$: Original (left) and deformed towards center (right).

5.3 Effect of Covariates in Spatiotemporal Risk Assessment

As mentioned before, spatial and spatiotemporal risk assessment is not always strictly focused on the physical magnitude representing the underline phenomenon. For instance, risk related to population exposure should take into account covariates such as population density over the spatial domain. Recalling the example case of PM10 pollution analyzed in Chapter 4, a population based risk analysis may be more relevant. In this section, the effect of the population density covariate is illustrated. Population, as well as population proportion, exposed due to exceedance are relevant random indicators in this context.

5.3.1 Population Covariate

Let $\{H(s) : s \in D\}$ be the population density function on domain D. For $W \subseteq D$,

$$\begin{aligned} H(W) &= \int_W H(s)ds, \quad \text{and} \\ H^{\lambda(W)}(W) &= \frac{H(W)}{\lambda(W)} = \int_W H(s)\lambda^W(ds) \to H^{\lambda(W)}(s) = \frac{H(s)}{\lambda(W)} = \int_W H^{\lambda(W)}(s)ds \end{aligned}$$

represents, respectively, the population within W, and the average population density on W. Let $A_u(X,W)$ the excursion set of X on W above the threshold u. Random indicators of area, $\lambda(A_u(X,W))$, and area proportion, $\lambda^W(A_u(X,W)) = \frac{\lambda(A_u(X,W))}{\lambda(W)}$, were considered in Chapter 3. Now, the random indicator *population exposed* due to exceedance is considered. This indicator is given (for each realization) by

$$H(A_u(X,W)) = \int_{A_u(X,W)} H(s)ds = \int_W I_u^X(s)H(s)ds,$$

Proposition 5.3.1. *The expected population exposed due to exceedance is:*

$$E\left[H(A_u(X,W))\right] = H(W)\left[1 - F_X^{W,H}(u)\right] \tag{5.12}$$

with $F_X^{W,H}(u) = \int_W F_{X(s)}(u)\lambda^{W,H}(ds)$, *where* $\lambda^{W,H}(ds) = \frac{H(s)}{H^{\lambda(W)}(W)}\lambda^W(ds)$.

Proof Denoting $H^W(s)ds = \frac{H(s)}{H(W)}ds$ with $\left(\int_W H^W(s)ds = 1\right)$, and noting that

$H^{\lambda(W)}(s) = \frac{H(s)}{\lambda(W)} = \frac{H(s)}{H(W)}\frac{H(W)}{\lambda(W)} = H^W(s)H^{\lambda(W)}(W)$, by Fubini's Theorem,

$$\begin{aligned}
E\left[H(A_u(X,W))\right] &= E\left[\int_W I_u^X(s)H(s)ds\right] = \int_\Omega \left(\int_W I_u^X(s)H(s)ds\right)P(dw) \\
&= \int_W H(s)\left(\int_\Omega I_u^X(s)P(dw)\right)ds = \int_W H(s)P\left[X(s)\geq u\right]ds \\
&= \int_W H(s)S_{X(s)}(u)ds = \int_W H(s)\left[1-F_{X(s)}(u)\right]ds \\
&= H(W)\int_W \left[1-F_{X(s)}(u)\right]\frac{H(s)}{H(W)}ds = H(W)\left[1-\int_W F_{X(s)}(u)H^W(s)ds\right] \\
&= H(W)\left[1-\int_W F_{X(s)}(u)\frac{H(s)}{H^{\lambda(W)}(W)}\lambda^W(ds)\right] = H(W)\left[1-F_X^{W,H}(u)\right]
\end{aligned}$$

□

Then, the *weighted compound* CDF (population-density-based) is defined by

$$F_X^{W,H}(u) = \int_W F_{X(s)}(u)\lambda^{W,H}(ds),$$

where $\lambda^{W,H}(ds) = \frac{H(s)}{H^{\lambda(w)}(W)}\lambda^W(ds)$. Hence, $\lambda^{W,H}(ds)$ is obtained by a change of measure from $\lambda^W(ds)$, the weights in this change of measure being

$$\frac{H(s)}{H^{\lambda(W)}(W)} = \frac{\text{True local population density at } s}{\text{Average local population density on } W}$$

This is a density function on W (non-negative, integrates 1), which is the Radon-Nykodyn derivative of $\lambda^{W,H}$ with respect to λ^W.

Correspondingly, the indicator *proportion of population exposed* due to exceedance can be considered. This is given (for each realization) by

$$H^W(A_u(X,W)) = \frac{H(A_u(X,W))}{H(W)},$$

whose expected value is $E\left[H^W(A_u(X,W))\right] = 1 - F_X^{W,H}(u)$.

As before (see Section 5.2), this case also suggest considering a more general formulation involving non-Lebesgue measures for the compound CDF, as shown in Section 5.4.

5.3.2 Ambient PM10 Pollution Population Exposure

For this illustration, as in Section 4.2, daily averages of PM10 concentrations measured at 9 stations (within the network of Andalusia's zoning for assessing air quality) in the *Carboneras* area, along six consecutive days, are considered. Now, risk assessment takes into account the effect on population, i.e. the population density is considered as a the relevant covariate. Specifications for the model, parameter estimates, grid of pixels, threshold, confidence level, global an local analysis description, etc., remain as before. Population density distribution at 250m scale in the *Carboneras* area is considered (Institute of Statistic an Cartography of Andalusia's Goverment - http://www.juntadeandalucia.es/institutodeestadisticaycartografia/temas/index-car.htm).

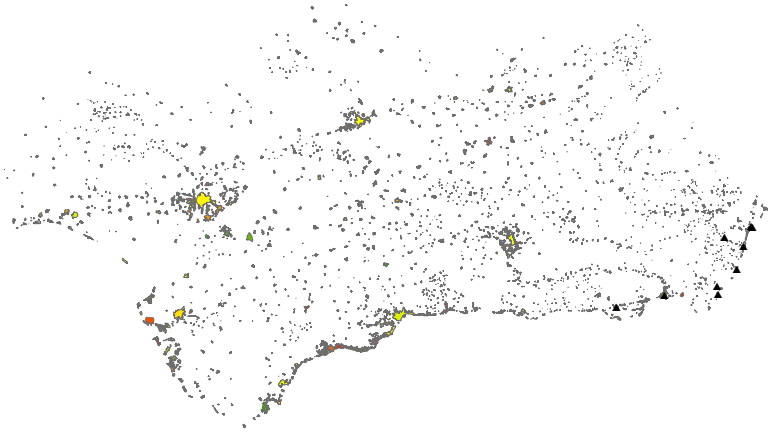

(a) Andalusia.

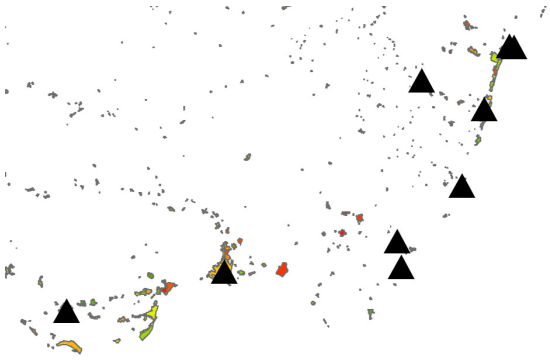

(b) *Carboneras* area in Almería province.

Figure 5.7: PM10 measurement network and population density distribution at 250m scale.

Fig. 5.7 shows the zoning for assessing air quality in Andalusia and the data measurement network at *Carboneras* area. Figs. 5.8 and 5.9 display, for two consecutive days, the temporal dynamics of absolute population density (first) and relative population density (second) at risk above a pre-fixed threshold level of critical concentration of PM10.

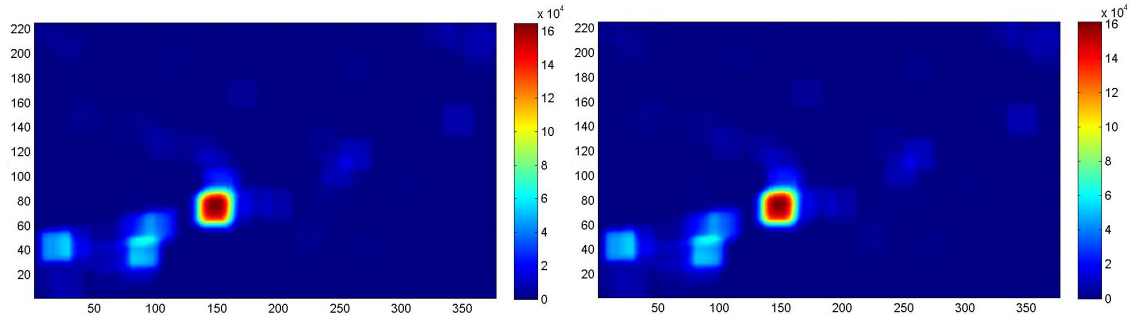

(a) $T = 3$. (b) May $T = 4$.

Figure 5.8: Local measurements of VaR for indicator population exposed.

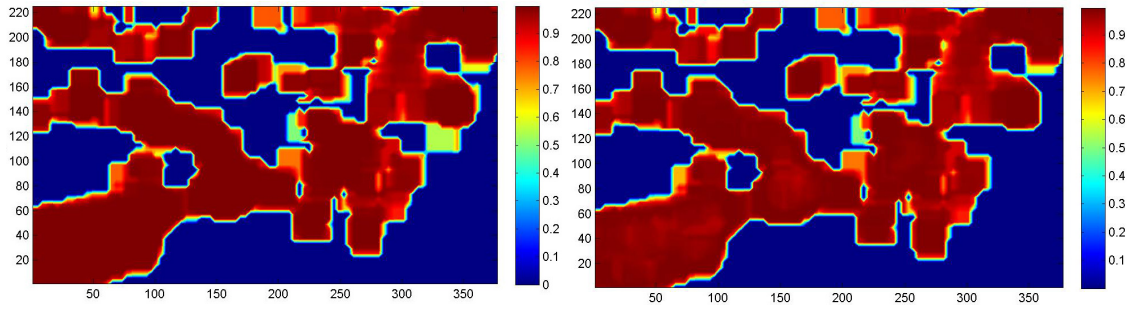

(a) $T = 3$. (b) $T = 4$.

Figure 5.9: Local measurements of VaR for indicator proportion of population exposed.

This illustration shows the relevance of risk assessment considering the population density covariate, since it provides a dynamic risk mapping focused on true areas at risk (inhabited areas) and focussed on the effects regarding population exposure.

5.4 Generalized Scenarios

Let X be a spatial random field on $D \subseteq \mathbb{R}^d$. Now a parametric family of surfaces (or 'parametric surface') $\xi = \{\xi_u(s) : s \in D, u \in \mathbb{R}\}$ is considered. In principle, ξ should satisfy:

(i) For fixed $s \in D$, $\xi_\cdot(s) : \mathbb{R} \to \mathbb{R}$ is a continuous (strictly) monotonically increasing function of u, with $\xi_\cdot(\mathbb{R}) \equiv \mathbb{R}$, i.e. $\xi_{-\infty}(s) = -\infty$ and $\xi_{+\infty}(s) = +\infty$ (as limits).

(ii) For fixed $u \in \mathbb{R}$, $\xi_u(\cdot) : D \to \mathbb{R}$ is a 'smooth' surface (e.g., with a bounded gradient on D.)

Note that, in general, $\xi_\cdot(s)$ (for fixed $s \in D$) does not need to be linear on u, that is, it represents a certain 'distortion' on $\mathbb{R}$. Let $\tilde{\lambda}$ be a (finite) measure on D, and $\tilde{\lambda}^D$ its normalization on D,

$$\tilde{\lambda}^D(ds) = \frac{\tilde{\lambda}(ds)}{\tilde{\lambda}(D)},$$

where it is implicitly assumed that $\tilde{\lambda}$ is absolutely continuous with respect to the Lebesgue measure, $\tilde{\lambda} << \lambda$. Special cases of this measure are:

(i) Φ- deformation ('level'-type) scenario:

- $\tilde{\lambda}(ds) = |J_\Phi(s)|\lambda(ds)$
- $\xi_u(s) \equiv u$, for each $u \in \mathbb{R}$

(ii) $\tilde{\Phi}$- deformation ('flow'-type) scenario:

- $\tilde{\lambda}(ds) = |J_\Phi(s)|\lambda(ds)$
- $\xi_u(s) = |J_\Phi(s)|u$, for each $u \in \mathbb{R}$

In the special case of a 'flow' type deformation, as seen in Section 5.4, a threshold u for $F_{X(s)}$ is transformed into a threshold $|J_\Phi(s)|u$ for $F_{X_\Phi(s')}$, with $s' = \Phi(s)$. Hence, in that particular case, the transformation is linear at each s, although with a different positive derivative $|J_\Phi(s)|$ for each s (or $|J_\Phi(\Phi^{-1}(s'))|$ for each s'). 'Smoothness' is guaranteed by the condition that Φ is a C^1-diffeomorphism, with positive Jacobian bounded for both Φ and Φ^{-1}.

A general definition of a compound CDF based on a functional threshold ξ, and a change of measure $\tilde{\lambda}$ on D, is introduced as follows:

$$F^D_{X;\tilde{\lambda},\xi}(u) = \int_D F_{X(s)}(\xi_u(s))\tilde{\lambda}^D(ds)$$

For a proper formalization, the definition of a ξ_u-level excursion set is derived as:

$$A_{\xi_u}(X,D) = \{s \in D : X(s) \geq \xi_u(s)\} \subseteq D$$

for a given functional threshold $\{\xi_u(s)\} \equiv \xi$ and a given value $u \in \mathbb{R}$. This is the excursion set of X in D over the function level ξ_u. Since, for each fixed $s \in D$, $\xi_\cdot(s) \equiv \{\xi_u(s) : u \in \mathbb{R}\}$ is a continuous (monotonically) increasing function of u, with $\xi(\mathbb{R}) \equiv \mathbb{R}$, hence it is an order-preserving bijection, with $[\xi_\cdot(s)]^{-1}$ also being a continuous (monotonically) increasing function on $\mathbb{R}$. Then,

$$X(s) \geq \xi_u(s) \iff [\xi_\cdot(s)]^{-1}(X(s)) \geq [\xi_\cdot(s)]^{-1}(\xi_u(s)) = u$$

and

$$A_{\xi_u}(X,D) = \{s \in D : ([\xi_\cdot(s)]^{-1} \circ X)(s) \geq u\} = A_u(X_{[\xi]},D),$$

where the '$\xi-$rescaled' random field $X_{[\xi]}$ is defined as $X_{[\xi]} = ([\xi_\cdot(s)]^{-1} \circ X)(s)$, for each $s \in D$. In this respect, the 'non-constant-threshold exceedance set' $A_u(X_{[\xi]},D)$ can be viewed as a 'constant-threshold exceedance set', $A_u(X_{[\xi]},D)$, with respect to the (locally) '$\xi-$rescaled random field', $X_{[\xi]}$.

As for the compound CDF $F^D_{X;\tilde{\lambda},\xi}(u)$, $u \in \mathbb{R}$:

$$F_X(s)(\xi_u(s)) = P[X(s) \geq \xi_u(s)] = P\left[X_{[\xi]}(s) \geq u\right] = F_{X_{[\xi](s)}}(u)$$

and therefore,

$$F^D_{X;\tilde{\lambda},\xi}(u) = \int_D F_{X_{[\xi](s)}}(u)\tilde{\lambda}^D(ds) = F^D_{X_{[\xi]};\tilde{\lambda}}(u);$$

that is, $F^D_{X;\tilde{\lambda},\xi}$ can be viewed, properly, as a true compound CDF, of the random field $X_{[\xi]}$ with respect to the measure $\tilde{\lambda}$.

Similarly to the results obtained for the case of a spatially deformed ('level' and 'flow' types) random field, the following relationship is established:

$$\frac{E\left[V^D_{\tilde{\lambda}}(A_{\mathrm{VaR}_{1-\alpha}(X^D_{\tilde{\lambda},\xi})}(X_{[\xi]},D))\right]}{E\left[\tilde{\lambda}^D(A_{\mathrm{VaR}_{1-\alpha}(X^D_{\tilde{\lambda},\xi})}(X_{[\xi]},D))\right]} = \mathrm{AVaR}_{1-\alpha}(X^D_{\tilde{\lambda},\xi}) - \mathrm{VaR}_{1-\alpha}(X^D_{\tilde{\lambda},\xi}), \quad \text{with} \tag{5.13}$$

$$E\left[\tilde{\lambda}^D(A_{\mathrm{VaR}_{1-\alpha}(X^D_{\tilde{\lambda},\xi})}(X_{[\xi]},D))\right] = \alpha, \tag{5.14}$$

where $X_{[\xi]}(s) := ([\xi(s)]^{-1} \circ X)(s)$ on D, and $X^D_{\tilde{\lambda},\xi}$ is the r.v. corresponding to the compound CDF

$F^D_{X;\tilde{\lambda},\xi}(u)$. Since $A_u(X_{[\xi]},D) = A_{\xi_u}(X,D)$, with $\xi_u \equiv \xi(.)$, then

$$\frac{E\left[V^D_{\tilde{\lambda}}(A_{\xi_{\mathrm{VaR}_{1-\alpha}(X^D_{\tilde{\lambda},\xi})}(\cdot)}(X,D))\right]}{E\left[\tilde{\lambda}^D(A_{\xi_{\mathrm{VaR}_{1-\alpha}(X^D_{\tilde{\lambda},\xi})}(\cdot)}(X,D))\right]} = \mathrm{AVaR}_{1-\alpha}(X^D_{\tilde{\lambda},\xi}) - \mathrm{VaR}_{1-\alpha}(X^D_{\tilde{\lambda},\xi}), \quad \text{with} \tag{5.15}$$

$$E\left[\tilde{\lambda}^D(A_{\xi_{\mathrm{VaR}_{1-\alpha}(X^D_{\tilde{\lambda},\xi})}(\cdot)}(X,D))\right] = \alpha \tag{5.16}$$

As before, given $u \in \mathbb{R}$ and calling (in this case) α_u the value in $[0,1]$ such that $F^D_{X;\tilde{\lambda},\xi}(u) = 1-\alpha_u$ ($\alpha_u = S^D_{X;\tilde{\lambda},\xi}(u)$, hence $u = \mathrm{VaR}_{1-\alpha}(X^D_{\tilde{\lambda},\xi})$), then

$$\frac{E\left[V^D_{\tilde{\lambda}}(A_{\xi_u}(X,D))\right]}{E\left[\tilde{\lambda}^D(A_{\xi_u}(X,D))\right]} = \mathrm{AVaR}_{1-\alpha_u}(X^D_{\tilde{\lambda},\xi}) - u. \tag{5.17}$$

Part III

EXTENSIONS OF THRESHOLD EXCEEDANCE ASYMPTOTIC ERROR BOUNDS

Chapter 6

Non-stationary Extensions for Random Field Threshold Exceedance Asymptotic Error Bounds

In this chapter, first, an asymptotic approach based on the well-known mollifier regularizing sequence is proposed under non-suitable regularity conditions for the underlying random field model. Second, the asymptotics of (2.1) for large u in generalized scenarios such as spatial deformation and blurring transformation is discussed.

6.1 Asymptotic Approach Based on Regularizing Sequences: mollifier

As mentioned before, real phenomena of interest in Geophysics and Environmental Sciences, among other areas, are usually modelled by locally non-regular random fields. Kernel-based blurring transformations have been used in applications for image analysis, environmental modelling, etc., to generate smooth representations suitable for analysis at lower resolution scales. Under appropriate assumptions, regularizing kernel sequences provide sample-path convergence to the reference model. Different approaches address the asymptotics of (2.1) under suitable regularity assumptions on the underlying random field model representing the phenomenon under analysis. The approach based on the mollifier regularizing sequence allows working with random fields under the only hypothesis of sample-path continuity or even L^p sample paths. Relationships between the excursion sets of the reference random field and the transformed sequence, as well as the asymptotic behaviour of first-order indicators related to structural properties of excursion sets, useful for risk assessment, are discussed. Finally, since it is usual being interested in a specific level of resolution, the previous relationships are also of relevance for practice. Indeed, in this

chapter, the smoothing effect and order of approximation are studied in relation to exceedance probabilities for increasing thresholds, considering different regularizing kernel sequences, within different scenarios regarding the underlying random field.

Definition 12. *A family of functions* $\{\phi_\delta : \delta > 0\}$ *is said to be a 'mollifier' or regularizing sequence, if and only if, it satisfies:*

(i) $\phi_\delta \in C^\infty(\mathbb{R}^d)$

(ii) $\phi_\delta(s) \geqslant 0$ *over* $\mathbb{R}^d$

(iii) $supp(\phi_\delta) = \bar{B}(0,\delta)$

(iv) $\int_{\mathbb{R}^d} \phi_\delta = 1$

□

Considering $\phi(s) = \exp\left(\frac{1}{|s|^2-1}\right)$ if $|s| < 1$ and $\phi(s) = 0$ if $|s| \geqslant 1$, the family of functions $\phi_\delta(s) = C\delta^{-d}\phi(\frac{s}{\delta})$, with $C = \frac{1}{\int_{\mathbb{R}^d}\phi}$, is a *mollifier*.

This mathematical object, *mollifier*, is a classical tool in areas such as Distribution Theory or Functional Analysis, as smooth functions sequences approximating non-smooth functions. The name mollifier[1] was first introduced by Friedrichs (1944), although the first one who used this regularizing sequence approach, without this name, was Sergei Sobolev in the proof of his Embedding Theorem (see, Sobolev 1938).

The mollifiers have an useful asymptotic behaviour (see Brezis 2011), i.e., given a mollifier $\{\phi_\delta : \delta > 0\}$ and a sample path x of X,

(i) if $x \in L^1_{loc}(\mathbb{R}^d)$, then $\phi_\delta * x \in C^\infty(\mathbb{R}^d)$ and $D^i(\phi_\delta * x) = D^i(\phi_\delta) * x$

(ii) if $x \in C(\mathbb{R}^d)$, then $\phi_\delta * x \xrightarrow[\delta\to 0]{} x$ uniformly for compact sets on $\mathbb{R}^d$

(iii) if $x \in L^p(\mathbb{R}^d)$ with $1 \leq p \leq \infty$, then $\phi_\delta * x \xrightarrow[\delta\to 0]{} x$ in $L^p(\mathbb{R}^d)$

Although the support of a Gaussian density is not compact, the family $\{\phi_\delta : \delta > 0\}$ based on $\phi(s) = \frac{1}{(2\pi)^{\frac{d}{2}}}\exp\left(-\frac{|s|^2}{2}\right), \forall s \in \mathbb{R}^d$, also provides convergence.

[1]According to the commentary of Peter Lax, whose thesis advisor was K. O. Friedrichs, in Friedrichs and Morawetz (1986): *On English usage Friedrichs liked to consult his friend and colleague, Donald Flanders, a descendant of puritans and a puritan himself, with the highest standard of his own conduct, noncensorious towards others. In recognition of his moral qualities he was called Moll by his friends. When asked by Friedrichs what to name the smoothing operator, Flanders remarked that they could be named mollifier after himself; Friedrichs was delighted, as on other occasions, to carry this joke into print.*

An illustration

The smoothing effect is analyzed by simulation for different scenarios of Cauchy class in the square $[1,200]^2$, by means of the mollifier regularizing sequence obtained for $d = 2$ and $\delta = \frac{32}{n}$ with $n = 1,2,4,8,16,32$. This simulation study considers $k = 2$, $supp(\phi) = \bar{B}(0,r)$ for $r > 0$, so that,

$$\phi(x) = \begin{cases} \exp\left(\frac{1}{|\frac{x}{r}|^2-1}\right) & if \quad |x| < r \\ \\ 0 & if \quad |x| \geqslant r \end{cases}$$

and $\delta = \frac{1}{n}$.

The expression (6.1) is computed for $n = 1,2,4,8,16,32$ with $r = 32$, obtaining 6 kernels in disks of radii $32,16,8,4,2,1$, respectively, as shown in Figs. 6.1 and 6.2,

$$\phi_n(x) = \begin{cases} Cn^2 \exp\left(\frac{1}{|\frac{nx}{r}|^2-1}\right) & if \quad |x| < \frac{r}{n} \\ \\ 0 & if \quad |x| \geqslant \frac{r}{n} \end{cases} \tag{6.1}$$

Fig. 6.1 displays the first six mollifier kernels simulated, whilst Fig. 6.2 shows the smoothing effect for two Cauchy random fields with parameter $\alpha = 2$.

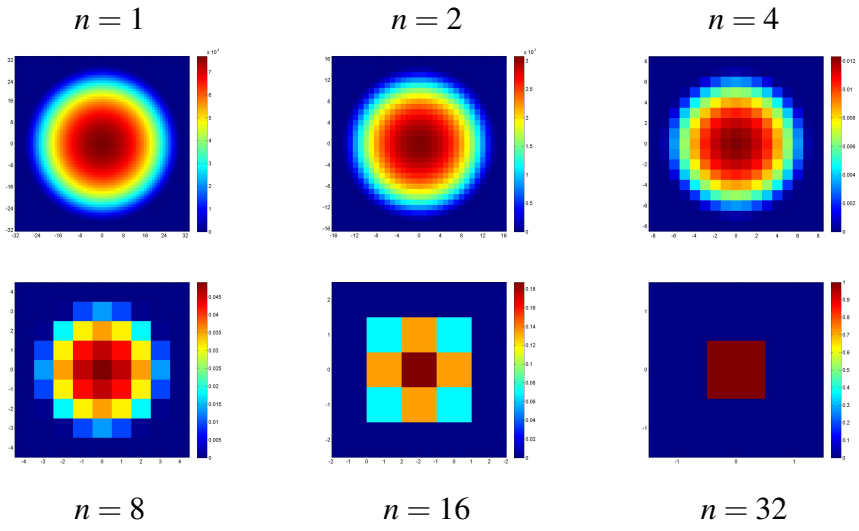

Figure 6.1: Mollifier kernels.

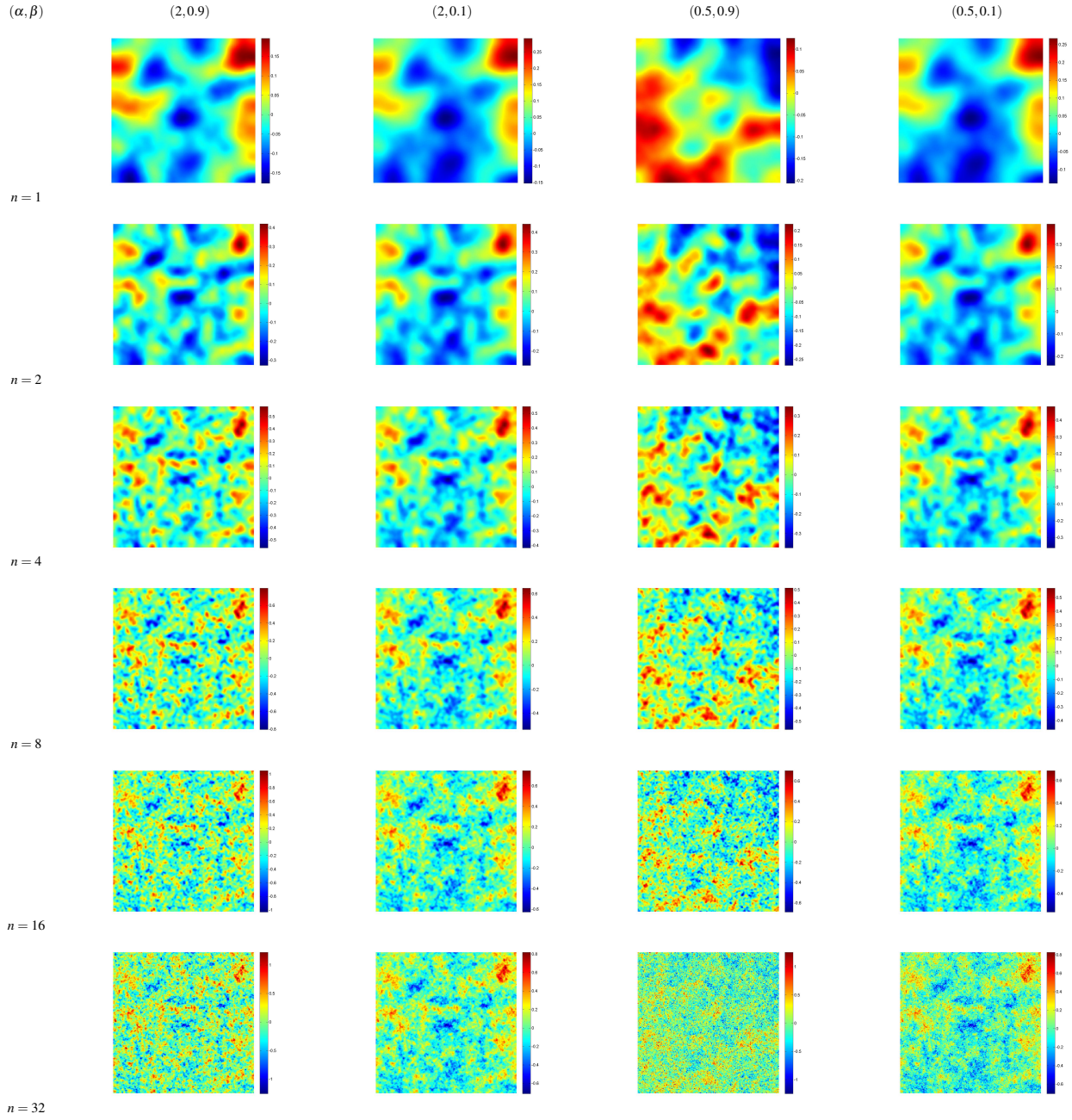

Figure 6.2: Mollifier smoothing effect.

As mentioned before, a relevant research issue is related to real cases for which the underlying random field model representing the phenomenon of interest has not suitable regularity conditions

(see, for example, Adler 1981). In this context, an asymptotic approach based on the mollifier regularizing sequence could be appropriate. From a methodological risk assessment point of view, some specific aspects should be analyzed. For instance:

(i) Relationships between the excursion sets of the reference random field model and the sequence of excursion sets under mollifier regularization.

(ii) Properties of $A_u(\phi_\delta * X, D) = \{s \in D : \phi_\delta * X(s) \geq u\}$.

(iii) Asymptotics of $A_u(\phi_\delta * X, D), \delta \to 0$.

(iv) Analysis of the sequence of first-order indicators (asymptotic behaviour):

- $\lambda(A_u(\phi_\delta * X, D)) = \int_{A_u(\phi_\delta * X, D)} \lambda(ds)$
- $\lambda^D(A_u(\phi_\delta * X, D)) = \frac{\lambda(A_u(\phi_\delta * X, D))}{\lambda(D)}$
- $V(A_u(\phi_\delta * X, D)) = \int_{\cup_{u' \geq u} A_{u'}(\phi_\delta * X, D)} \lambda(ds) du'$
- $V^D(A_u(\phi_\delta * X, D)) = \frac{V(A_u(\phi_\delta * X, D))}{\lambda(D)}$
- $V^{A_u}(A_u(\phi_\delta * X, D)) = \frac{V(A_u(\phi_\delta * X, D))}{\lambda(A_u(\phi_\delta * X, D))}$
- $\bar{V}^{cc}(A_u(\phi_\delta * X, D)) = \frac{1}{N_{cc}^D} \sum_{i=1}^{N_{cc}^D} \left\{ \frac{V(A_u(\phi_\delta * X, C_i))}{\lambda(A_u(\phi_\delta * X, C_i))} \right\}$

(v) Asymptotics of first-order indicator sequences, i.e., additional assumptions to get $\lim_{\delta \to 0} \lambda(A_u(\phi_\delta * X, D)) = \lambda(A_u(X, D))$ may be required.

(vi) For a specific level of resolution, i.e. if $\delta = \frac{1}{n}$, it might be possible to establish some relationships like:

- $A_u(\phi_\delta * X, D) \to A_u(X, D)$
- $\lambda(A_u(\phi_\delta * X, D)) = O\left(\frac{1}{n}\right) \lambda(A_u(X, D))$

This regularizing approach should provide: an improvement of the risk assessment methodology proposed in Chapter 3; sequential risk mapping allowing risk assessment for the reference random field models; extensions of asymptotic error-bound approximations between threshold exceedance probabilities at a specific resolution level and the expected value of Euler-Poincaré characteristic of the excursion set at this level, etc.

If X has C^2 sample paths, under appropriate assumptions, threshold exceedance probabilities are approximated, for large u-threshold, by the expectation of the Euler-Poincaré characteristic

of the excursion set at u-level. As mentioned in Chapter 2, general results by Adler and Taylor (2007) and Azaïs and Wschebor (2009) provide similar error bounds of the type

$$\left| P\left[\sup_{s\in D} X(s) \geq u\right] - E\left[\varphi(A_u(X,D))\right]\right| < O\left(e^{\frac{-u^2}{2}} f(s)\right),$$

where f depends on the random field and the geometry of the parameter set. Let X be a centered, isotropic and stationary random field with C^2 sample paths over a convex set D. Azaïs and Wschebor (2009) prove from (2.5) that in the expression above

$$f(s) = \left(1 + \frac{1}{12C''(0) - 1}\right). \tag{6.2}$$

Despite the restrictive assumptions on the domain and the underlying random field, this is a tractable expression for the error bound since the only needed calculation is related to the covariance function of the random field. Mollifier regularizing effect provides a sequence of C^∞ blurred sample paths. Under certain hypotheses on the non-regular random field this should provide an appropriate sequence of asymptotic error bounds in relation to the asymptotic error bound for threshold exceedance probabilities of the underlying random field.

6.2 Extension for Spatially Deformed Random Fields

In this section, the order of the error-bound approximation for threshold exceedance probabilities of random fields obtained by spatial deformation and blurring transformation is discussed.

Let X be a random field on D satisfying the suitable regularity conditions listed in Def. 10 and, in addition, assumptions in Azaïs and Wschebor (2009), Th. 8.12, Cor. 8.13 and Cor. 8.14, i.e., $E[X(s)] = 0$, $Var(X(s)) = 1$, $Var(X'(s)) = I_d$, $\forall s \in D$. Let Φ be a spatial deformation with both $|J_\Phi|$ and $|J_{\Phi^{-1}}|$ bounded.

An approach based on spatially deformed random fields will derive similar asymptotic error bounds for threshold exceedance probabilities under appropriate spatial deformations, since the needed computation from (2.5) is mainly relative to obtaining expressions for the first derivatives of the deformed random field. The assumptions on Φ, as a spatial deformation, jointly with the regularity conditions on X, provide regularity conditions for the deformed random field Y and for geometrical characteristics of $D' = \Phi(D)$.

In this context, the inequality (2.5) remains for the 'level'-type deformed random field $Y = X_\Phi$ on D' defined by Equation (5.3). Indeed, regularity assumptions for X provide a tractable expression for derivatives of the random field Y,

$$Y'(s') = (X_\Phi(s'))' = (X(\Phi^{-1}(s')))' = X'(\Phi^{-1}(s'))J_{\Phi^{-1}}(s') = X'_\Phi(s')J_{\Phi^{-1}}(s').$$

This expression is based on the composition between two differentiable functions.

Now, let $Y = X_{\tilde{\Phi}}$ be a 'flow'-type deformed random field. Expressions for the derivatives are not as direct as for the 'level'-type case. Recalling the expression for the first derivative of the determinant of a matrix function (see Harville 1997),

$$\frac{\partial}{\partial s_j}\left[|A(s)|\right] = tr\left[\text{adj}(A(s))\frac{\partial A}{\partial t_s}\right], \tag{6.3}$$

if in addition $A(t)$ is a nonsingular and differentiable matrix, then

$$\frac{\partial}{\partial s_j}\left[|A(s)|\right] = |A(s)|tr\left[A^{-1}(s)\frac{\partial A}{\partial s_j}\right]. \tag{6.4}$$

Regularity assumptions on the underlying random field and on the spatial deformation allow to apply the inverse function theorem and the chain rule:

$$\begin{aligned} Y^{'}(s) &= \left((X\circ\Phi^{-1})(s)|J_{\Phi^{-1}}(s)|\right)' \\ &= \left((X\circ\Phi^{-1})(s)\right)'|J_{\Phi^{-1}}(s)| + (X\circ\Phi^{-1})(s)\left(|J_{\Phi^{-1}}(s)|\right)' \\ &= X'_{\Phi}(s')J_{\Phi^{-1}}(s')|J_{\Phi^{-1}}(s)| + (X\circ\Phi^{-1})(s)|J_{\Phi^{-1}}(s)|\left(tr\left[\left(J_{\Phi^{-1}}(s)\right)^{-1}\frac{\partial J_{\Phi^{-1}}(s)}{\partial s_j}\right]\right)_{j=1,\ldots,d}. \end{aligned}$$

Therefore, $Y^{'}(s) = X^{'}_{\tilde{\Phi}}(s)J^{-1}_{\Phi}(s) + X_{\tilde{\Phi}}(s)B(s)$, with $B(s) = \left(tr\left[\left(J_{\Phi^{-1}}(s)\right)^{-1}\frac{\partial J_{\Phi^{-1}}(s)}{\partial s_j}\right]\right)_{j=1,\ldots,d}$.

For both, 'level' and 'flow' type deformed random fields, the error-bound approximation for the excursion probabilities is obtained relating the conditional variance and the covariance functions of the deformed random field.

Error-bound of approximation for excursion probabilities involve strong regularity assumptions on the random field. However, as mentioned in the previous section, real phenomena are modelled by random fields that do not always satisfy these regularity conditions. Extensions of (2.5) are possible for stationary random fields obtained by a convolution-based blurring transformation as (6.5) in which the underlying random field does not satisfies suitable regularity conditions. The 'blurred' random field is defined as (see Angulo and Madrid 2010; Angulo and Madrid 2014, Goitía et al. 2004, Mardia et al. 2006)

$$X[h](s) = h * X(s), \tag{6.5}$$

where h is a positive kernel integrating 1 over the whole space $\mathbb{R}^d$ and $*$ is the convolution operator. Let $Y = X[h]$, $h \in C_0^1(\mathbb{R}^d)$, with assumptions given in Azaïs and Wschebor (2009), Cor. 8.15 on the parameter set D. Then, expression (2.5) will be valid under appropriate blurring kernels, since, as before, the only needed calculation is related to the first derivative of the blurred random field. Here, suitable regularity conditions from Def. 10 remain for the spatial domain, whilst for the

blurred random field are supported by the regularity conditions of the kernel. The expression for the first derivative of the blurred random field is the derivative of the convolution operator between two functions, where at least one of them is differentiable (see, for example, Brezis 2011);

$$Y^{'}(s) = h^{'} * X(s).$$

As before, the error-bound approximation for the excursion probabilities is obtained relating the conditional variance and the covariance functions of the blurred random field.

An illustration

The rate of decrease of the error-bound for large u, considering the Cauchy class model with fixed parameter $\alpha = 2$ (because its regularity conditions), is analyzed with four different values of parameter β. Error-bound is computed from (6.2). Fig. 6.3 displays the Cauchy scenarios considered for this illustration. Fig. 6.4 shows the asymptotic behaviour of the error-bound for large u. It is remarkable that these four curves are confused in only two, one for the lower values of the parameter β and the other for higher values of this parameter. .

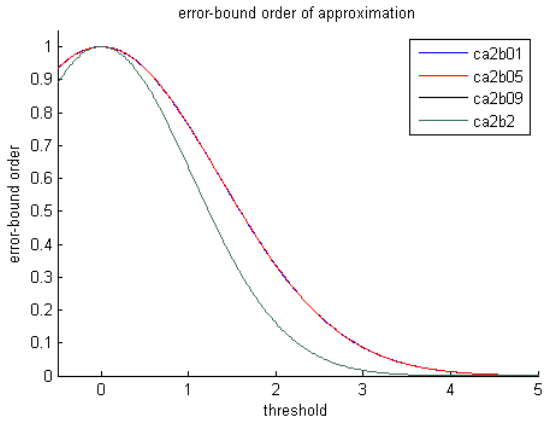

Figure 6.4: Error-bound order of approximation.

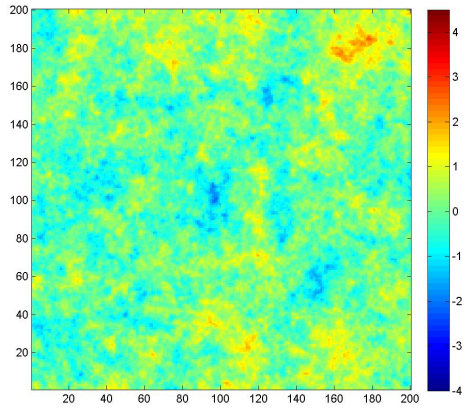

(a) Cauchy $(\alpha, \beta) = (2, 0.1)$.

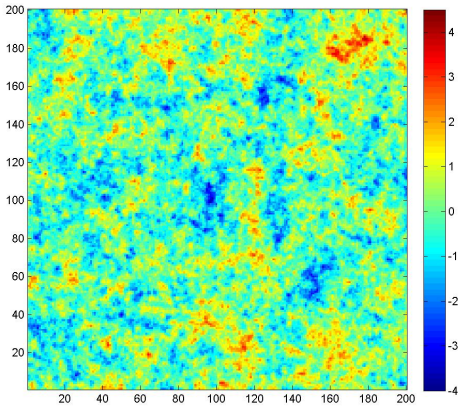

(b) Cauchy $(\alpha, \beta) = (2, 0.5)$.

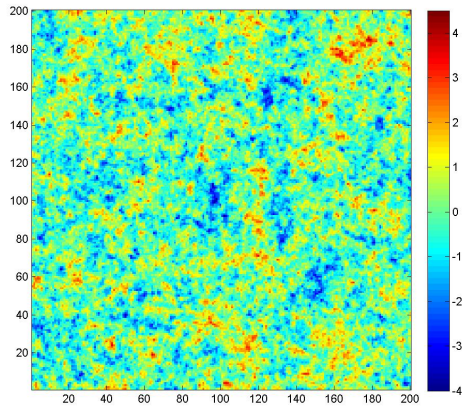

(c) Cauchy $(\alpha, \beta) = (2, 0.9)$.

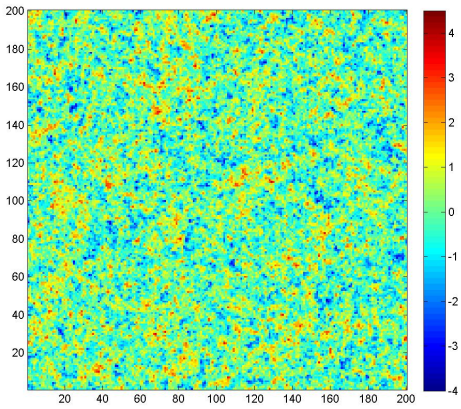

(d) Cauchy $(\alpha, \beta) = (2, 2)$.

Figure 6.3: Cauchy class sample paths.

Part IV

COMPLEMENTARY ASPECTS AND CONCLUSIONS

Chapter 7

Synthesis and Open Lines

7.1 Synthesis

In this thesis work, a flexible methodological approach for spatial and spatiotemporal risk assessment of threshold exceedances is introduced bringing together the theory of risk measures and the structural characteristics of threshold excursion sets of random fields. The methodology proposed can be applied in a wide variety of situations, with minimum requirements except for the ability to perform conditional simulation in the case under study. Indeed, in Chapter 3, using the empirical distribution, derived from conditional simulation on given observations, of selected indicators related to geometrical characteristics of the excursion sets, quantile-based risk measures such as Value-at-Risk and Average Value-at-Risk are evaluated at global or subregional scales. The latter allow the construction of (static or dynamic) risk maps at different resolution levels. In particular, first-order indicators such as absolute or relative versions of exceedance area and excess volume are formally shown to have a meaningful formalization in terms of the compound cumulative (and its reciprocal decumulative) distribution function, which further provides a global quantile correspondence and interpretation regarding the determination of the threshold exceedance level of interest for study. Computational aspects of the implementation of the procedure are described. Different issues related to the characteristics of the underlying random field, in the spatial case, are analyzed and discussed through simulated examples. These refer to the nature of the tails of the marginal distributions, as well as to the range of spatial dependence and local variability of realizations. In the spatiotemporal case, application to predictive risk for different horizons is illustrated based on a well-known autoregressive model involving blur-generated diffusivity. In Chapter 4 three applications of the methodology proposed in Chapter 3 are analyzed for spatial and spatiotemporal real scenarios (rainfall and ambient PM10 pollution). In Chapter 5 analytical aspects regarding VaR-related interpretation of the expected excess volume vs. expected excedance area ratio, in terms of the compound CDF AVaR-VaR increment are formalized. A detailed analysis for the asymptotics of this relationship is performed in relation to the shape parameter of the Gener-

alized Pareto Distribution. Effects in some special general scenarios of interest, such as spatially deformed random fields (with reference to both 'level' and 'flow' type deformation) and the consideration of population covariate, is also formalized in this context. A more general formulation involving non-constant thresholds and non-Lebesgue measures for the compound CDF is established. Finally, in Chapter 6, under the regularizing sequence approach, the asymptotics of error bound threshold exceedance probabilities is addressed for random fields without some restrictive regularity conditions.

7.2 Open Lines

Different directions for continuing research are open, some of them under development, among which the following ones are particularly stressed:

(i) Definitions of spatial risk measures and associated axiomatic, depending on the problem under study.

(ii) Distributional properties of the closed random sets obtained by exceedance thresholds and of the first-order random indicators introduced in this thesis based on the theory of closed random sets.

(iii) Analysis of structural characteristics of threshold exceedance sets under the regularizing sequence of mollifiers approach (to an established resolution scale, asymptotic behaviour, etc.)

(iv) Formal extensions of the results of this thesis for stochastic thresholds, test-function based thresholds, etc.

(v) Sensitivity analysis with respect to different sources of perturbation and model specifications.

(vi) Clustering and dynamics of 'hotspots'.

(vii) Analytical and methodological developments for second- and higher-order indicators.

(viii) Extension and application of state distortion and space deformation approaches in relation to model complexities.

7.3 Contributions

The research involved in this thesis work has derived in different contributions.

Publication:

- Romero J. L., Madrid A. E., Angulo J. M. (2018) Quantile-based spatiotemporal risk assessment of exceedances. *Stochastic Environmental Research and Risk Assessment*, Vol. 32 (8), August 2018, pp. 2275-2291.

Several papers related to contents of this thesis work are in process, involving:

- An applied analysis of the proposed methodology in Chapter 3 with real data according to Chapter 4.
- From Chapter 5, formal aspects of the effect of covariates as population density and an illustration with the relevant issue of ambient PM10 population exposure at the *Carboneras* industrial area.
- A formalization of the generalized approach for non-constant thresholds and non-Lebesgue measures, also from Chapter 5.
- Asymptotics for error bound approximations of threshold exceedance probabilities under non-regularity assumptions by means of the regularizing sequence approach introduced in Chapter 6.

Invited talks in national and international meetings:

- Romero J. L., Angulo J. M., Regularizing asymptotic approach for structural characteristics of random field excursion sets. Workshop on *Can Stochastic Geometry handle Dynamics of Risk Management?* School of Economics and Managment, Lund University, Sweeden. 18-20 April 2018.
- Angulo J. M, Romero J. L., A conditional approach for spatiotemporal risk assessment of random field threshold exceedances. Workshop on *Can Stochastic Geometry handle Dynamics of Risk Management?* School of Economics and Managment, Lund University, Sweeden. 18-20 April 2018.
- Angulo J. M., Madrid A. E., Romero J. L., Spatiotemporal risk assessment of exceedances. *8th International Workshop on Spatio-Temporal Modelling (METMA VIII)*, Valencia, Spain, 2016. ISBN: 978-84-608-8468-2, University of Valencia, 1, 2016.
- Romero J.L., Risk measures in spatial and spatio-temporal frameworks. *Seminar of Young Researchers in Mathematics*, IEMath-Granada, Granada, Spain, 2016.
- Angulo J. M., Madrid A. E., Romero J. L., Threshold exceedance risk assessment in complex space-time systems. *European Geosciences Union General Assembly (EGU2015)*, Vienna, Austria, 2015.

- Angulo J. M., Madrid A. E., Romero J. L., Measuring risk for space-time environmental processes. *The International Environmetrics Society Conference (TIES2014)*. Guangzhou, China, 2014.

- Angulo J. M., Madrid A. E., Romero J. L., Spatiotemporal risk assessment of random field exceedance indicators. *International Conference on Quantification of Uncertainty in Engineering (QUEST2015)*, Science & Technology, Beijing, China, 2015.

Contributed talks in national and international meetings:

- Romero J. L., Angulo J. M., Non-stationary extensions for random field threshold exceedance asymptotic error bounds. *XXXVII Congreso Nacional de Estadística e Investigación Operativa*. Oviedo, Spain, 2018.

- Romero J. L., Angulo J. M., Asymptotic error bound approximation of threshold exceedance probabilities for non-stationary random fields. *10th International Conference of the ERCIM WG on Computational and Methodological Statistics. 11th International Conference on Computational and Financial Econometrics*. Senate House, University of London, UK, 2017.

- Romero J. L., Madrid A. E., Angulo J. M., Risk measures on threshold exceedance structural indicators in spatiotemporal processes. *1st Spanish Young Statisticians and Operational Researchers Meeting (SYSORM 2017)*. Granada, Spain, 2017.

- Romero J. L., Madrid A. E., Angulo J. M., Effect of transformations in space-time risk assessment. *XXXVI Congreso Nacional de Estadística e Investigación Operativa*. Toledo, Spain, 2016. Doi: http://dx.doi.org/10.18239/jor07.2016, University of Castilla La Mancha (Toledo-Spain), 151, 2016.

- Angulo J. M., Madrid A. E., Romero J. L., Space-time risk assessment of threshold exceedances. *XXXV Congreso Nacional de Estadística e Investigación Operativa*, Pamplona, Spain, 2015. ISBN 978-84-606-7906-6, Department of Statistic and OR of University of Pamplona (Spain), 135, 2015.

- Romero J. L., Madrid A. E., Angulo J. M., Conditional risk assessment in spatial and spatiotemporal settings: effect of covariates. *International Conference of the ERCIM WG on Computational and Methodological Statistics*. London, United Kingdom, 2015.

- Angulo J. M., Madrid A. E., Romero J. L. , Quantile-based risk assessment of spatial threshold exceedances. *International Conference on Advances in Extreme Value Analysis and Application to Natural Hazards (EVAN2015)*. Santander, Spain, 2015.

- Romero J. L., Angulo J. M., Asymptotic extremal behavior of spatially deformed stationary random fields. *International Workshop on Proximity Data, Multivariate Analysis and Classification*. Granada, Spain, 2014.

- Romero J. L., Angulo J. M., On excursion probabilities for a class of non-stationary random fields. *METMA VII and GRASPA14 Conference*. Torino, Italy, 2014. GRASPA WORKING PAPERS, 2015-01-31T08:43:23Z, http://hdl.handle.net/10446/31676.

Poster in national meeting:

- Romero J. L., Madrid A. E., Angulo J. M., Smoothing asymptotic approximation for non-regular random fields. *XXXV Congreso Nacional de Estadística e Investigación Operativa*, Pamplona, Spain, 2015. ISBN 978-84-606-7906-6, Department of Statistic and OR of the University of Pamplona (Spain), 132, 2015.

Part IV

ASPECTOS COMPLEMENTARIOS Y DISCUSIÓN

Chapter 7

Síntesis y Líneas Abiertas

7.1 Síntesis

En este trabajo de tesis se ha introducido un enfoque metodológico flexible para la valoración de riesgos de excedencia de umbrales en entornos espaciales y espacio-temporales, haciendo interactuar la teoría de medidas de riesgo junto con el análisis de características estructurales de conjuntos de excursión de campos aleatorios. La metodología propuesta se puede aplicar en una amplia variedad de situaciones, con requerimientos mínimos excepto la capacidad de realizar simulación condicionada en el caso bajo estudio. En efecto, en el Cap. 3 el uso de la distribución empírica, obtenida a partir de la simulación condicionada sobre observaciones dadas, de indicadores relacionados con características geométricas de conjuntos de excursión, permite la evaluación de medidas de riesgo basadas en cuantiles como el Valor en Riesgo (VaR) y el Valor en Riesgo Promedio (AVaR) a escalas globales o regionales. Esto último posibilita la construcción de mapas de riesgo (estáticos o dinámicos) a diferentes niveles de resolución. En particular, se justifica que indicadores de primer orden tales como versiones absolutas o relativas de áreas de excedencia y volúmenes en exceso tienen una formalización significativa en términos de la función de distribución acumulativa (y su recíproca decumulativa) compuesta, lo que además ha proporcionado una correspondencia e interpretación de los cuantiles con respecto a la determinación del nivel de excedencia o umbral de interés para el estudio. Se han descrito los aspectos computacionales de la implementación de esta metodología. Se han analizado y discutido diferentes aspectos relacionados con las características del campo aleatorio subyacente, en el caso espacial, por medio de ejemplos de simulación. Estos se refieren a la naturaleza de las colas de las distribuciones marginales, así como al rango de dependencia espacial y variabilidad local de las realizaciones. En el caso espacio-temporal, se ha ilustrado una aplicación de riesgo predictivo para diferentes horizontes temporales basada en un modelo autoregresivo bien conocido que implica difusividad generada mediante borrosidad. En el Cap. 4 se han analizado tres aplicaciones para escenarios espaciales y espacio-temporales con datos reales de precipitación y contaminación ambiental por PM10. En

el Cap. 5 se han formalizado aspectos analíticos que relacionan la tasa de volumen esperado en exceso frente al área de excedencia esperada en términos del incremento AVaR-VaR de la variable aleatoria asociada a la función de distribución acumulativa compuesta. Se ha realizado un análisis detallado del comportamiento asintótico de esta relación en función del parámetro de forma de la distribución de Pareto generalizada. También se han formalizado los efectos sobre estas relaciones en escenarios de especial interés, tales como campos aleatorios deformados espacialmente (deformación de tipo 'nivel' y 'flujo') y el efecto de la covariable población. Se ha desarrollado una formulación más general que involucra umbrales no constantes y medidas no Lebesgue para la distribución compuesta. Finalmente, en el Cap. 6, bajo el enfoque de sucesiones regularizantes, se ha abordado el orden asíntotico del error de aproximación de las probabilidades de excedencia de umbrales para campos aleatorios sin algunas condiciones restrictivas de regularidad.

7.2 Líneas abiertas

Existen diferentes líneas investigación abiertas, entre las que destacan las siguientes:

1. Definiciones de medida de riesgo espacial y axiomática asociada, en función del problema bajo estudio.

2. Propiedades distribucionales de los conjuntos aleatorios cerrados obtenidos por excedencia de umbrales y de los indicadores aleatorios de primer orden introducidos en esta tesis, en base de la teoría de conjuntos aleatorios cerrados.

3. Análisis de características estructurales de los conjuntos de excedencia de umbrales bajo el enfoque sucesiones regularizantes tipo mollifiers (a una escala de resolución establecida, comportamiento asintótico, etc).

4. Extensiones formales de los resultados de esta tesis para umbrales generalizados estocásticos, umbrales basados en funciones test, etc.

5. Análisis de la sensibilidad con respecto a diferentes fuentes de perturbación y especificaciones del modelo.

6. Clustering y dinámicas de 'hotspots'.

7. Desarrollos analíticos y metodológicos para indicadores de segundo orden y superior.

8. Extensión y aplicación de enfoques de distorsión de estados y deformación espacial en relación con complejidades del modelo.

7.3 Contribuciones

La investigación realizada en este trabajo de tesis ha derivado en varias contribuciones.

Publicación:

- Romero J. L., Madrid A. E., Angulo J. M. (2018) Quantile-based spatiotemporal risk assessment of exceedances. *Stochastic Environmental Research and Risk Assessment*, Vol. 32 (8), August 2018, pp. 2275-2291.

Artículos en proceso relacionados con el contenido de este trabajo de tesis:

- Un análisis aplicado de la metodología propuesta en el Cap. 3 con datos reales en relación al Cap. 4.
- Con respecto al Cap. 5, una formalización del efecto de la covariable densidad de población y una ilustración del mismo en el problema de exposición de la población a contaminación por partículas PM10 en el área industrial de *Carboneras*.
- También, desde el Cap. 5, una formalización del enfoque generalizado para umbrales no constantes y medidas no Lebesgue.
- Desarrollo del enfoque basado en sucesiones regularizantes tipo mollifiers para el error de aproximación de probabilidades de excedencias de umbrales en condiciones adecuadas de regularidad, según el enfoque introducido en el desde Cap. 6.

Charlas invitadas en congresos nacionales e internacionales:

- Romero J. L., Angulo J. M., Regularizing asymptotic approach for structural characteristics of random field excursion sets. Workshop on *Can Stochastic Geometry handle Dynamics of Risk Management?* School of Economics and Managment, Lund University, Sweeden. 18-20 April 2018.
- Angulo J. M, Romero J. L., A conditional approach for spatiotemporal risk assessment of random field threshold exceedances. Workshop on *Can Stochastic Geometry handle Dynamics of Risk Management?* School of Economics and Managment, Lund University, Sweeden. 18-20 April 2018.
- Angulo J. M., Madrid A. E., Romero J. L., Spatiotemporal risk assessment of exceedances. *8th International Workshop on Spatio-Temporal Modelling (METMA VIII)*, Valencia, Spain, 2016. ISBN: 978-84-608-8468-2, University of Valencia, 1, 2016.

- Romero J.L., Risk measures in spatial and spatio-temporal frameworks. *Seminar of Young Researchers in Mathematics*, IEMath-Granada, Granada, Spain, 2016.

- Angulo J. M., Madrid A. E., Romero J. L., Threshold exceedance risk assessment in complex space-time systems. *European Geosciences Union General Assembly (EGU2015)*, Vienna, Austria, 2015.

- Angulo J. M., Madrid A. E., Romero J. L., Measuring risk for space-time environmental processes. *The International Environmetrics Society Conference (TIES2014)*. Guangzhou, China, 2014.

- Angulo J. M., Madrid A. E., Romero J. L., Spatiotemporal risk assessment of random field exceedance indicators. *International Conference on Quantification of Uncertainty in Engineering (QUEST2015)*, Science & Technology, Beijing, China, 2015.

Contribuciones orales en congresos nacionales e internacionales:

- Romero J. L., Angulo J. M., Non-stationary extensions for random field threshold exceedance asymptotic error bounds. *XXXVII Congreso Nacional de Estadística e Investigación Operativa*. Oviedo, Spain, 2018.

- Romero J. L., Angulo J. M., Asymptotic error bound approximation of threshold exceedance probabilities for non-stationary random fields. *10th International Conference of the ERCIM WG on Computational and Methodological Statistics. 11th International Conference on Computational and Financial Econometrics*. Senate House, University of London, UK, 2017.

- Romero J. L., Madrid A. E., Angulo J. M., Risk measures on threshold exceedance structural indicators in spatiotemporal processes. *1st Spanish Young Statisticians and Operational Researchers Meeting (SYSORM 2017)*. Granada, Spain, 2017.

- Romero J. L., Madrid A. E., Angulo J. M., Effect of transformations in space-time risk assessment. *XXXVI Congreso Nacional de Estadística e Investigación Operativa*. Toledo, Spain, 2016. Doi: http://dx.doi.org/10.18239/jor07.2016, University of Castilla La Mancha (Toledo-Spain), 151, 2016.

- Angulo J. M., Madrid A. E., Romero J. L., Space-time risk assessment of threshold exceedances. *XXXV Congreso Nacional de Estadística e Investigación Operativa*, Pamplona, Spain, 2015. ISBN 978-84-606-7906-6, Department of Statistic and OR of University of Pamplona (Spain), 135, 2015.

- Romero J. L., Madrid A. E., Angulo J. M., Conditional risk assessment in spatial and spatio-temporal settings: effect of covariates. *International Conference of the ERCIM WG on Computational and Methodological Statistics*. London, United Kingdom, 2015.

- Angulo J. M., Madrid A. E., Romero J. L. , Quantile-based risk assessment of spatial threshold exceedances. *International Conference on Advances in Extreme Value Analysis and Application to Natural Hazards (EVAN2015)*. Santander, Spain, 2015.

- Romero J. L., Angulo J. M., Asymptotic extremal behavior of spatially deformed stationary random fields. *International Workshop on Proximity Data, Multivariate Analysis and Classification*. Granada, Spain, 2014.

- Romero J. L., Angulo J. M., On excursion probabilities for a class of non-stationary random fields. *METMA VII and GRASPA14 Conference*. Torino, Italy, 2014. GRASPA WORKING PAPERS, 2015-01-31T08:43:23Z, http://hdl.handle.net/10446/31676.

Póster en congreso nacional:

- Romero J. L., Madrid A. E., Angulo J. M., Smoothing asymptotic approximation for non-regular random fields. *XXXV Congreso Nacional de Estadística e Investigación Operativa*, Pamplona, Spain, 2015. ISBN 978-84-606-7906-6, Department of Statistic and OR of the University of Pamplona (Spain), 132, 2015.

Bibliography

Adler RJ (1981) The Geometry of Random Fields. Wiley, Chichester

Adler RJ (2008) Some new random field tools for spatial analysis. Stochastic Environmental Research and Risk Assessment 22:809–822

Adler RJ, Taylor JE (2007) Random Fields and Geometry. Springer, New York

Adler RJ, Samorodnitsky G, Taylor JE (2010) Excursion sets of three classes of stable random fields. Advances in Applied Probability 42:293–318

Adler RJ, Samorodnitsky G, Taylor JE (2013) High-level excursion set geometry for non-Gaussian infinitely divisible random fields. The Annals of Probability 41:134–169

Ahmadi-Javid A (2012) Entropic Value-at-Risk: a new coherent risk measure. Journal of Optimization Theory and Applications 155:1105–1123

Ahmed M, Maume-Deschamps V, Ribereau P (2019) Spatial risk measures for max-stable and max-mixture processes. Stochastic - An International Journal of Probability and Stochastic Processes DOI 10.1080/17442508.2019.1687703

Amit Y, Grenander U, Piccioni M (1991) Structural image restoration through deformable templates. Journal of the American Statistical Association 86:376–387

Anderes EB, Chatterjee EB (2009) Consistent estimates of deformed isotropic Gaussian random fields on the plane. The Annals of Statistics 37:2324–2350

Anderes EB, Stein ML (2008) Estimating deformations of isotropic Gaussian random fields on the plane. Annals of Statistics 36:719–741

Angulo JM, Madrid AE (2010) Structural analysis of spatiotemporal threshold exceedances. Environmetrics 21:415–438

Angulo JM, Madrid AE (2014) A deformation/blurring-based spatiotemporal model. Stochastic Environmental Research and Risk Assessment 28:1061–1073

Angulo JM, Madrid AE, Romero JL (2016a) Spatiotemporal risk assessment of exceedances. In: Proceedings 8th International Workshop on Spatio-Temporal Modelling (METMAVIII), University of Valencia, Valencia, Spain, Universtiy of Valencia, ISBN: 978-84-608-8468-2, University of Valencia, 1

Angulo JM, Madrid AE, Romero JL (2016b) Effect of transformations in space-time risk assessment. In: XXXVI Congreso Nacional de Estadística e Investigación Operativa, Universidad de Castilla la Mancha, Toledo, Spain, ISBN: 978-84-608-8468-2, University of Valencia, 1, 151, DOI http://dx.doi.org/10.18239/jor07.2016

Artzner P (1998) Application of coherent risk measures to capital requierements in insurance. North American Actuarial Journal 3:1–15

Artzner P, Delbaen F, Eber JM, Heath D (1999) Coherent measures of risk. Mathematical Finance 9:203–228

Azaïs JM, Wschebor M (2009) Level Sets and Extrema of Random Processes and Fields. Wiley, New Jersey

Bellini F, Klar B, Muller A, Gianin ER (2014) Generalized quantiles as risk measures. Insurance: Mathematics and Economics 54:41–48

Berg C, Mateu J, Porcu E (2008) The Dagum family of isotropic correlation functions. Bernoulli 14:1134–1149

Bernardi M, Durante F, Jaworski P, Petrella L, Salvadori G (2018) Conditional risk based on multivariate hazard scenarios. Stochastic Environmental Research and Risk Assessment 32:203–211

Bohm S, Schmidt V (2003) Palm representation and approximation of the covariance of random closed sets. Advances in Applied Probability 35:295–302

Brezis H (2011) Functional Analysis, Sobolev Spaces and Partial Differential Equations. Springer, New York

Brown PE, Karesen KF, Roberts GO, Tonellato S (2000) Blur-generated non-separable space-time models. Journal of the Royal Statistical Society, Series B 62:847–860

Castaing C, Ezzaki F, Hess C (1997) Convergence of conditional expectations for unbounded closed convex random sets. Studia Mathematica 124:133–148

Chiles JP, Delfiner P (1999) Geostatistics. Modelling Spatial Uncertainty. Wiley, New York

Chiu SN, Stoyan D, Kendall WS, Mecke J (2013) Stochastic Geometry and its Applications. Wiley, Chichester

Christakos G (1992) Random Field Models in Earth Sciences. Academic Press, San Diego

Christakos G (2000) Modern Spatiotemporal Geostatistics. Oxford University Press, New York

Christakos G (2017) Spatiotemporal Random Fields, 2nd ed. Elsevier, Cambridge

Christakos G, Hristopulos DT (1996) Stochastic indicators for waste site characterization. Water Resources Research 32:2563–2578

Christakos G, Hristopulos DT (1997) Stochastic indicator analisys of contaminated sites. Journal of Applied Probability 34:988–1008

Christensen GE, Rabbitt RD, Miller MI (1996) Deformable templates using large deformation kinematics. IEEE Transactions on Image Proccessing 5:1435–1447

Clerc M, Mallat S (2003) Estimating deformations of statrionary processes. The Annals of Statistics 31:1772–1821

Craigmile PF, Cressie N, Santner TJ, Rao Y (2005) A loss function approach to identifying environmental exceedances. Extremes 8:143–159

Diggle PJ, Tawn JA, Moyeed RA (1998) Model-based geostatistics (with discussion). Applied Statistics 47:299–350

Filipović D, Kupper M (2008) Optimal capital and risk transfers for group divesification. Mathematical Finance 18:55–76

Föllmer H, Schied A (2002) Convex measures of risk and trading constraints. Finance and Stochastic 6:429–447

Föllmer H, Schied A (2016) Stochastic Finance. An Introduction in Discrete Time. Walter de Gruyter GmbH & Co. KG, Berlin/New York

Fölmer H, Knispel T (2011) Entropic risk measures: coherences vs. convexity, model ambiguity, and robust large deviations. Stochastics and Dynamics 11:333–351

Fouedjio F, Desassis N, Romary T (2015) Estimation of space deformation model for non-stationary random functions. Spatial Statistics 13:45–61

French JP, Sain SR (2013) Spatio-temporal exceedance locations and confidence regions. Annals of Applied Statistics 7:1421–1449

Friedrichs KO (1944) The identity of weak and strong extensions of differential operators. Transactions of the American Mathematical Society 55:132–151

Friedrichs KO, Morawetz CS (1986) Selecta. Contemporary Mathematicians. Birkhauser Verlag, Stuttgart

Frittelli M, Gianin E (2002) Putting order in risk measures. Journal of Banking and Finance 26:1473–1486

Gelfand AE, Diggle PJ, Fuentes M, Guttorp P (2010) Handbook of Spatial Statistics. CRC Press

Glasbey CA, Mardia KV (1998) A review of image-warping methods. Journal of Applied Statistics 25:155–171

Glasbey CA, Mardia KV (2001) A penalized likelihood approach to image warping. Journal of the Royal Statistical Society, Series B 63:465–485

Gneiting T, Schlather M (2004) Stochastic models that separate fractal dimension and the Hurst effect. SIAM Review 46:269–282

Goitía A, Ruiz-Medina MD, Angulo JM (2004) Joint estimation of spatial deformation and blurring in environmental data. Stochastic Environmental Research and Risk Assessment 19:1–7

Goovaerts MJ, Kaas R, Dhaene J, Tang Q (2004) Some new classes of consistent risk measures. Insurance: Mathematics and Insurances 34:505–5016

Guttorp P, Gneiting T (2006) Miscellanea. Studies in the history of probability and statistics XLIX. On the Matérn correlation family. Biometrika 93:989–995

Haier A, Molchanov I, Schmutz M (2016) Intragroup transfers, intragroup divesification and their risk assessment. Annals of Finance 12:363–392

Haimes YY (2004) Risk Modeling, Assessment, and Management. Wiley, New Jersey

Handcock MS, Wallis JR (1994) An approach to statistical spatial-temporal modeling of meteorological fields. Journal of the American Statistical Association 89:368–378

Harville DA (1997) Matrix Algebra From a Statistician's Perspective. Springer, New York

Kleinow J, Moreira F, Strobl S, Vähämaa S (2017) Measuring systemic risk: a comparison of alternative market-based approaches. Finance Research Letters 21:40–46

Klüppelberg C, Straub D, Welpe IM (eds) (2014) Risk - A Multidisciplinary Introduction. Springer, Berlin

Koch E (2017) Spatial risk measures and applications to max-stable processes. Extremes 20:635–670

Koch E (2019) Spatial risk measures and rate of spatial diversification. Risks 52:1–26

Kriele M, Wolf J (2014) Value-Oriented Risk Management of Insurance Companies. Springer, Berlin

Lahiri S, Kaiser MS, Cressie N, Hsu NJ (1999) Prediction of spatial cumulative distribution functions using subsampling. Journal of the American Statistical Association 94:86–97

Leonenko N, Olenko A (2014) Sojourn measures of Student and Fisher-Snedecor random fields. Bernoulli 20:1454–1483

Li QQ, Li YP, Huang GH, Wang CX (2018) Risk aversion based interval stochastic programming approach for agricultural water management under uncertainty. Stochastic Environmental Research and Risk Assessment 32:715–732

Madrid AE, Angulo JM, Mateu J (2012) Spatial threshold exceedance analysis through marked point processes. Environmetrics 23:108–118

Madrid AE, Angulo JM, Mateu J (2016) Point pattern analysis of spatial deformation and blurring effects on exceedances. Journal of Agricultural, Biological, and Environmental Statistics 21:512–530

Mardia KV, Angulo JM, Goitía A (2006) Synthesis of image deformation strategies. Image and Vision Computing 24:1–12

Matheron G (1975) Random Sets and Integral Geometry. Wiley, New York

McNeil AJ, Frey R, Embrechts P (2005) Quantitative Risk Management: Concepts, Techniques and Tools. Princeton University Press, Oxford

Molchanov I (2005) Theory of Random Sets. Springer, London

Molchanov I (2017) Random Closed Sets and Capacity Functionals. Springer, Switzerland

Perrin O, Senoussi R (2000) Reducing non-stationary random fields to stationary and isotropy using a space deformation. Statistics & Probability Letters 48:23–32

Piterbarg VI (1996) Asymptotic Methods in the Theory of Gaussian Processes and Fields. American Mathematical Society, Providence

Romero JL, Angulo JM (2014) On excursion probabilities for a class of non-stationary random fields. In: Proceedings of the METMA VII and GRASPA14 Conference, Torino, Italy, GRASPA WORKING PAPERS, 2015-01-31T08:43:23Z, http://hdl.handle.net/10446/31676

Romero JL, Madrid AE, Angulo JM (2015a) Conditional risk assessment in spatial and spatio-temporal settings: Effect of covariates. In: Proceeding 8th International Conference on the ERCIM Working Group and 9th International Conference on Computational and Methodological Statistics, London, ISBN 978-9963-2227-0-4, CMStatistics and CFEnetwork. (Ed.), 224

Romero JL, Madrid A, Angulo JM (2015b) Smoothing asymptotic approximation for non-regular random fields. In: Proceedings XXXV Congreso Nacional de Estadítica e Investigación Operativa, Pamplona, Spain, ISBN 978-84-606-7906-6, Department of Statistic and OR of the University of Pamplona (Spain), 132

Romero JL, Madrid AE, Angulo JM (2018) Quantile-based spatiotemporal risk assessment of exceedances. Stochastic Environmental Research and Risk Assessment 32:2275–2291

Sampson PD, Guttorp P (1992) Nonparametric estimation of nonstationary spatial covariance structure. Journal of the American Statistical Association 87:108–119

Schneider R, Weil W (2008) Stochastic and Integral Geometry. Wiley, New York

Sobolev SL (1938) Sur un théoreme d'analyse fonctionnelle. Recueil Mathématique 46:471–497

Souza SRSD, Silva TC, Tabak BM, Guerra SM (2016) Evaluating systemic risk using bank default probabilities in financial networks. Journal of Economic Dynamics & Control 66:54–75

Stein ML (1999) Interpolation of Spatial Data. Springer, New York

Stein ML (2002) Fast and exact simulation of fractional Brownian surfaces. Journal of Computational and Graphical Statistics 11:587–599

Strokorb K, Ballani F, Schalther M (2015) Tail correlation functions of max-stable processes. Construction principles, recovery and diversity of some mixing max-stable processes with identical TCF. Extremes 18:241–271

Szego G (2002) Measures of risk. Jounal of Banking and Finance 26:1253–1272

Teran P (2008) On the equivalence of Aumann and Herer expectations of random sets. Test 17:505–514

Vanmarcke E (2010) Random Fields. Analysis and Synthesis. World Scientific, Singapore

Vera F, Angulo JM, Roldán JA (2017) Stability analysis in nonstationary spatial covariance estimation. Stochastic Environmental Research and Risk Assessment 31:815–828

Vila E (2014) On the local approximation of mean densities of random closed sets. Bernoulli 20:1–27

Wang R, Ziegel JF (2015) Elicitable distortion risk measures: a concise proof. Statistics and Probability Letters 100:172–175

Wang S (2000) A class of distortion operators for pricing financial and insurance risks. The Journal of Risk and Insurance 67:15–36

Wang S, Dhaene J (1998) Comonotonicity, correlation order and premium principles. Insurance: Mathematics and Economics 22:235–242

Wright DL, Stern HS, Cressie N (2003) Loss functions for estimation of extrema with an application to disease mapping. Canadian Journal of Statistics 31:251–266

Yaglom AM (1987a) Correlation Theory of Stationary and Related Random Functions I - Basic Results. Springer, New York

Yaglom AM (1987b) Correlation Theory of Stationary and Related Random Functions II - Supplementary Notes and References. Springer, New York

Yakir B (2013) Extremes in Random Fields. A Theory and its Applications. Wiley, Chichester

Yang Y, Christakos G (2015) Spatiotemporal characterization of ambient PM2.5 concentrations in shandong province (China). Environmental Science & Technology 49:13.431–13.438

Zhang J, Craigmile PF, Cressie N (2008) Loss function approaches to predict a spatial quantile and its exceedance region. Technometrics 50:216–227

Appendix

This appendix collects a selection of **MATLAB** and **R** source codes developed for the elaboration of this thesis.

Matlab Source Code

1. **Mollifier and Gaussian kernels:**

```
%%%%%%%%%%%%%%%%%%%%%%%%%%%%%%%%%%%%%%%%%%%%%%%%%%%%%%%%%%%%%%%%%%%%%%%%%
%            Case 1: Mollifier (6 blurring kernels)                    %
%%%%%%%%%%%%%%%%%%%%%%%%%%%%%%%%%%%%%%%%%%%%%%%%%%%%%%%%%%%%%%%%%%%%%%%%%
% Kernel base function:                                                %
% n=1; f(x)=C*exp(1/(|x/r|^2-1)) if |x|<r ; 0 if x|>=r                 %
% n>1; f_n(x)=n^2*exp(1/(|nx/r|^2-1)) if |x|<r/n ; 0 otherwise         %
% Radius=r/n (Diameter=2*r/n)                                          %
% Center is in one pixel of the grid                                   %
%%%%%%%%%%%%%%%%%%%%%%%%%%%%%%%%%%%%%%%%%%%%%%%%%%%%%%%%%%%%%%%%%%%%%%%%%


clear all;
clc;
nucleo_1=zeros(65,65);
nucleo_2=zeros(33,33);
nucleo_3=zeros(17,17);
nucleo_4=zeros(9,9);
nucleo_5=zeros(5,5);
nucleo_6=zeros(3,3);

n=[1,2,4,8,16,32];
```

```
r=32;

for k=1:size(n,2)
for i=1:2*r/n(k)+1
for j=1:2*r/n(k)+1
    % Module is the distance to center
    % Center is in (r/n+1,r/n+1)
    module=sqrt((i-r/n(k)-1)^2+(j-r/n(k)-1)^2);
    if module<r/n(k)
        % There are six variables, one for each kernel
        if k==1
            nucleo_1(i,j)=n(k)^2*exp(1/((module*n(k)/r)^2-1));
        end
        if k==2
            nucleo_2(i,j)=n(k)^2*exp(1/((module*n(k)/r)^2-1));
        end
        if k==3
            nucleo_3(i,j)=n(k)^2*exp(1/((module*n(k)/r)^2-1));
        end
        if k==4
            nucleo_4(i,j)=n(k)^2*exp(1/((module*n(k)/r)^2-1));
        end
        if k==5
            nucleo_5(i,j)=n(k)^2*exp(1/((module*n(k)/r)^2-1));
        end
        if k==6
            nucleo_6(i,j)=n(k)^2*exp(1/((module*n(k)/r)^2-1));
        end
    else
        if k==1
            nucleo_1(i,j)=0;
        end
        if k==2
            nucleo_2(i,j)=0;
        end
        if k==3
            nucleo_3(i,j)=0;
        end
        if k==4
            nucleo_4(i,j)=0;
        end
```

```
            if k==5
                nucleo_5(i,j)=0;
            end
            if k==6
                nucleo_6(i,j)=0;
            end
        end
    end
    end
    end

    % This is the constant so that they integrate one
    S1=sum(sum(nucleo_1));
    S2=sum(sum(nucleo_2));
    S3=sum(sum(nucleo_3));
    S4=sum(sum(nucleo_4));
    S5=sum(sum(nucleo_5));
    S6=sum(sum(nucleo_6));

    nucleo_1=nucleo_1./S1;
    nucleo_2=nucleo_2./S2;
    nucleo_3=nucleo_3./S3;
    nucleo_4=nucleo_4./S4;
    nucleo_5=nucleo_5./S5;
    nucleo_6=nucleo_6./S6;

    % They integrate one: only checking
    S1=sum(sum(nucleo_1));
    S2=sum(sum(nucleo_2));
    S3=sum(sum(nucleo_3));
    S4=sum(sum(nucleo_4));
    S5=sum(sum(nucleo_5));
    S6=sum(sum(nucleo_6));

    % Drawing and saving the picture of the six blurring kernels

    for k=1:size(n,2)
            figure();
            if k==1
                imagesc(nucleo_1);
            end
```

```
        if k==2
            imagesc(nucleo_2);
        end
        if k==3
            imagesc(nucleo_3);
        end
        if k==4
            imagesc(nucleo_4);
        end
        if k==5
            imagesc(nucleo_5);
        end
        if k==6
            imagesc(nucleo_6);
        end
        xlim([1.0 2.0*r/n(k)+1]);
        ylim([1.0 2.0*r/n(k)+1]);
        set(gca,'YDir','normal');
        set(gca,'XDir','normal');
        set(gca,'dataAspectRatio',[1 1 1])
        number = num2str(n(k));
        name=['Mollifier kernel n = ',number];
        X=eval('name');
        title(X);
        saveas(gcf,X,'jpg');
end


%%%%%%%%%%%%%%%%%%%%%%%%%%%%%%%%%%%%%%%%%%%%%%%%%%%%%%%%%%%%%%%%%%%%%
%            Case 2: Gaussian (6 blurring kernels)                  %
%%%%%%%%%%%%%%%%%%%%%%%%%%%%%%%%%%%%%%%%%%%%%%%%%%%%%%%%%%%%%%%%%%%%%
% Kernel base function (it's not a mollifier but it has the        %
% same properties of convergence)                                   %
% n=1; f(x)=1/sqrt(2Pi)*exp(-|x|^2/2) if |x|<r ; 0 if x|>=r         %
% n>1; f_n(x)=n^2*1/sqrt(2Pi)*exp(-|x/n|^2/2) if |x|<r/n            %
% Radius=r/n (Diameter=2*r/n)                                       %
% Center is in one pixel of the grid                                %
%%%%%%%%%%%%%%%%%%%%%%%%%%%%%%%%%%%%%%%%%%%%%%%%%%%%%%%%%%%%%%%%%%%%%


clear all;
```

```
clc;
nucleo_1=zeros(65,65);
nucleo_2=zeros(33,33);
nucleo_3=zeros(17,17);
nucleo_4=zeros(9,9);
nucleo_5=zeros(5,5);
nucleo_6=zeros(3,3);

n=[1,2,4,8,16,32];
r=32;

for k=1:size(n,2)
for i=1:2*r/n(k)+1
for j=1:2*r/n(k)+1
    % Module is the distance to center
    % Center is in (r/n+1,r/n+1)
    module=sqrt((i-r/n(k)-1)^2+(j-r/n(k)-1)^2);
    if module<=r
      if k==1
        nucleo_1(i,j)=n(k)^2*1/(2*pi)*exp(-(module*n(k)/r)^2/2);
      end
      if k==2
        nucleo_2(i,j)=n(k)^2*1/(2*pi)*exp(-(module*n(k)/r)^2/2);
      end
      if k==3
        nucleo_3(i,j)=n(k)^2*1/(2*pi)*exp(-(module*n(k)/r)^2/2);
      end
      if k==4
        nucleo_4(i,j)=n(k)^2*1/(2*pi)*exp(-(module*n(k)/r)^2/2);
      end
      if k==5
        nucleo_5(i,j)=n(k)^2*1/(2*pi)*exp(-(module*n(k)/r)^2/2);
      end
      if k==6
        nucleo_6(i,j)=n(k)^2*1/(2*pi)*exp(-(module*n(k)/r)^2/2);
      end
    else
      if k==1
          nucleo_1(i,j)=0;
      end
      if k==2
```

```
            nucleo_2(i,j)=0;
        end
        if k==3
            nucleo_3(i,j)=0;
        end
        if k==4
            nucleo_4(i,j)=0;
        end
        if k==5
            nucleo_5(i,j)=0;
        end
        if k==6
            nucleo_6(i,j)=0;
        end
    end
end
end
end

% This is the constant so that they integrate one
S1=sum(sum(nucleo_1));
S2=sum(sum(nucleo_2));
S3=sum(sum(nucleo_3));
S4=sum(sum(nucleo_4));
S5=sum(sum(nucleo_5));
S6=sum(sum(nucleo_6));

nucleo_1=nucleo_1./S1;
nucleo_2=nucleo_2./S2;
nucleo_3=nucleo_3./S3;
nucleo_4=nucleo_4./S4;
nucleo_5=nucleo_5./S5;
nucleo_6=nucleo_6./S6;


% They integrate one: only checking
S1=sum(sum(nucleo_1));
S2=sum(sum(nucleo_2));
S3=sum(sum(nucleo_3));
S4=sum(sum(nucleo_4));
S5=sum(sum(nucleo_5));
```

```
S6=sum(sum(nucleo_6));

% Drawing and saving the picture of the six blurring kernels

for k=1:size(n,2)
        figure();
        if k==1
            imagesc(nucleo_1);
        end
        if k==2
            imagesc(nucleo_2);
        end
        if k==3
            imagesc(nucleo_3);
        end
        if k==4
            imagesc(nucleo_4);
        end
        if k==5
            imagesc(nucleo_5);
        end
        if k==6
            imagesc(nucleo_6);
        end
        colorbar();
        xlim([1.0  2.0*r/n(k)+1]);
        ylim([1.0  2.0*r/n(k)+1]);
        set(gca,'YDir','normal');
        set(gca,'XDir','normal');
        set(gca,'dataAspectRatio',[1  1  1])
        number = num2str(n(k));
        name=['Gaussian kernel n = ',number];
        X=eval('name');
        title(X);
        saveas(gcf,X,'jpg');
end
```

2. **Sliding windows:**

```
%%%%%%%%%%%%%%%%%%%%%%%%%%%%%%%%%%%%%%%%%%%%%%%%%%%%%%%%%%%%%%%%%%%%%%%%%
%                        Sliding windows                                %
%%%%%%%%%%%%%%%%%%%%%%%%%%%%%%%%%%%%%%%%%%%%%%%%%%%%%%%%%%%%%%%%%%%%%%%%%
% This code allows running the same source code in a grid               %
% of sliding windows defined dynamically and covering the               %
% domain.                                                               %
%%%%%%%%%%%%%%%%%%%%%%%%%%%%%%%%%%%%%%%%%%%%%%%%%%%%%%%%%%%%%%%%%%%%%%%%%

% Window size. Odd number to avoid a sliding of the center
size=21;

% Definition of the sliding step
% floor function avoids decimal jumps (movement is pixel to pixel)
% Plus 1 to avoid steps less than one
incremento=floor(size/4)+1;

% x and y coordinates of the first center to consider
x_0=(size+1)/2;
y_0=(size+1)/2;

% How many centers are there?
% Counter of centers = number of windows
num_centro=0;
x_aux=x_0;
y_aux=y_0;

% Auxiliar centers counter
i=1;

while x_aux<=200

    while y_aux<=200
        x_centro(i)=x_aux;
        y_centro(i)=y_aux;

        % Controlling the edge effect
        if x_aux>200-(size-1)/2
            % This is to weird cases where the edge effect
            % produces rectangles instead of squares
```

```
            if y_aux>200-(size-1)/2
                area_ventana(i)=2*(200-y_aux)*2*(200-x_aux);
            else
                tamano_ventana=2*(200-x_aux);
                area_ventana(i)=tamano_ventana*tamano_ventana;
            end
        else
            if y_aux>200-(size-1)/2
                tamano_ventana=2*(200-y_aux);
                area_ventana(i)=tamano_ventana*tamano_ventana;
            else
                area_ventana(i)=size*size;
            end
        end
        % Next center
        i=i+1;
        num_centro=num_centro+1;
        % Next center to the right with the same x coordinate
        y_aux=y_aux+incremento;

    end
    y_aux=y_0;
    x_aux=x_aux+incremento;

end

% Saving the centers in a 2x2 variable
centros=[x_centro;y_centro;area_ventana];
% Only for presentation
centros=centros';



% Dynamic sliding windows definition
for i=1:num_centro
    area_ventana=size*size
    if centros(i,3)== area_ventana
        % Vertices for the square windows with maximum area

        % Top left vertix
        x_supizq=centros(i,1)-(size+1)/2+1;
```

```
        y_supizq=centros(i,2)-(size+1)/2+1;
        centros(i,4)=x_supizq;
        centros(i,5)=y_supizq;

        % Top right vertix
        x_supdcho=centros(i,1)-(size+1)/2+1;
        y_supdcho=centros(i,2)+(size+1)/2-1;
        centros(i,6)=x_supdcho;
        centros(i,7)=y_supdcho;

        % Down left vertix
        x_infizq=centros(i,1)+(size+1)/2-1;
        y_infizq=centros(i,2)-(size+1)/2+1;
        centros(i,8)=x_infizq;
        centros(i,9)=y_infizq;

        % Down right vertix
        x_infdcho=centros(i,1)+(size+1)/2-1;
        y_infdcho=centros(i,2)+(size+1)/2-1;
        centros(i,10)=x_infdcho;
        centros(i,11)=y_infdcho;
    else
        % Vertices for windows with non pre-fixed area
        sizex=200-centros(i,1);
        sizey=200-centros(i,2);

        %Top left vertix
        x_supizq=centros(i,1)-sizex;
        y_supizq=centros(i,2)-sizey;
        centros(i,4)=x_supizq;
        centros(i,5)=y_supizq;

        % Top right vertix
        x_supdcho=centros(i,1)-sizex;
        y_supdcho=centros(i,2)+sizey;
        centros(i,6)=x_supdcho;
        centros(i,7)=y_supdcho;

        % Down left vertix
        x_infizq=centros(i,1)+sizex;
        y_infizq=centros(i,2)-sizey;
```

```
            centros(i,8)=x_infizq;
            centros(i,9)=y_infizq;

            % Down rigth vertix
            x_infdcho=centros(i,1)+sizex;
            y_infdcho=centros(i,2)+sizey;
            centros(i,10)=x_infdcho;
            centros(i,11)=y_infdcho;
        end

        for j=x_supizq:x_infizq

            for k=y_supizq:y_supdcho
                % Here the common source code to run
                % for every sliding window
            end
        end
    end
```

3. **Error bounds:**

```
%%%%%%%%%%%%%%%%%%%%%%%%%%%%%%%%%%%%%%%%%%%%%%%%%%%%%%%%%%%%%%%%%%%%%%%%%%%
%                         Error-bound                                     %
%%%%%%%%%%%%%%%%%%%%%%%%%%%%%%%%%%%%%%%%%%%%%%%%%%%%%%%%%%%%%%%%%%%%%%%%%%%
% This code computes the error bound for the first order                  %
% approximation for threshold exceedance probabilities. Here              %
% two suitable regular Cauchy models are considered.                      %
%%%%%%%%%%%%%%%%%%%%%%%%%%%%%%%%%%%%%%%%%%%%%%%%%%%%%%%%%%%%%%%%%%%%%%%%%%%

% Loading Cauchy models sample paths
load C:\Simulaciones\Cauchy_a2b01.txt;
load C:\Simulaciones\Cauchy_a2b09.txt;

% Proccesing and drawing data
mat=Cauchy_a2b01;
mat=vec2mat(mat,200);
figure();
imagesc(mat); colorbar(); caxis([-4 4.5]);
set(gca,'YDir','normal');
set(gca,'dataAspectRatio',[1 1 1]);
saveas(gcf,'Cauchy_a2b01','jpg');

mat3=Cauchy_a2b09;
mat3=vec2mat(mat3,200);
figure();
imagesc(mat3); colorbar(); caxis([-4 4.5]);
set(gca,'YDir','normal');
set(gca,'dataAspectRatio',[1 1 1]);
grid off;
saveas(gcf,'Cauchy_a2b09','jpg');

% This is the error bound computation for every model
% considered. With these parameters the models are suitably
% regular. The error bound is obtained evaluating by 0 the
% second derivative. The bound only depends on beta

% First model
b=0.1;
max_umbral=max(max(mat));
min_umbral=min(min(mat));
u=max_umbral;
```

```
v=min_umbral;

i=1;
umbral=min_umbral;
while(umbral<100)
    cota=exp(-0.5*umbral^2*(1-1/(12*b+1)));
    error(i,1)=umbral;
    error(i,2)=cota;
    umbral=umbral+0.02;
    i=i+1;
end

% Second model
b=0.9;
max_umbral=max(max(mat3));
min_umbral=min(min(mat3));
u=max_umbral;
v=min_umbral;

i=1;
umbral=min_umbral;
while(umbral<100)
    cota=exp(-0.5*umbral^2*(1-1/(12*b+1)));
    error3(i,1)=umbral;
    error3(i,2)=cota;
    umbral=umbral+0.02;
    i=i+1;
end


% Plotting the error bounds
figure();
hold on
    plot(error(:,2),error(:,1));
    plot(error3(:,2),error3(:,1));

    title('Analytical order of approximation');
    legend('ca2b01','ca2b09');
hold off
```

4. **3D samples (Spatial):**

```
%%%%%%%%%%%%%%%%%%%%%%%%%%%%%%%%%%%%%%%%%%%%%%%%%%%%%%%%%%%%%%%%%%%%%%%%%%%%%%%%
%                          Spatial analysis                                    %
%%%%%%%%%%%%%%%%%%%%%%%%%%%%%%%%%%%%%%%%%%%%%%%%%%%%%%%%%%%%%%%%%%%%%%%%%%%%%%%%
% Sample paths of the same month in different years                            %
% Their maps of variances and standard desviations                             %
%%%%%%%%%%%%%%%%%%%%%%%%%%%%%%%%%%%%%%%%%%%%%%%%%%%%%%%%%%%%%%%%%%%%%%%%%%%%%%%%

clear all;
clc;
% Loading fixed locations
load /Volumes/Datos/Simulations/Spatial/Locations_matlab.txt;
locations=Locations_matlab;

hold on;
    scatter(locations(:,1),locations(:,2),'MarkerEdgeColor',...
        'b','MarkerFaceColor','b','LineWidth',0.25 )
    xlim([0.0 540.0]);
    ylim([0.0 280.0]);
    set(gca,'YDir','normal');
    set(gca,'XDir','normal');
    set(gca,'dataAspectRatio',[1 1 1]);
    title('Rainfall measurement locations');
hold off;

saveas(gcf,'Locations_grid_matlab','pdf');

% Loading data
load /Volumes/Datos/Simulations/Spatial/Cauchy_201404_all.txt;
load /Volumes/Datos/Simulations/Spatial/Cauchy_201504_all.txt;
Data_201404=Cauchy_201404_all;
Data_201504=Cauchy_201504_all;

% Matrix 93x175 because this is the grid size of the data
% Third dimension is 200 because there are 200 sample paths
Data_201404_3D=zeros(175,93,200);
Data_201504_3D=zeros(175,93,200);

for i=1:200
    Data_201404_3D(:,:,i)=vec2mat(Data_201404(:,i),93);
    Data_201504_3D(:,:,i)=vec2mat(Data_201504(:,i),93);
```

```
end

% Choosing the sample path to plot
m1=(Data_201504_3D(:,:,1))';
m2=(Data_201404_3D(:,:,1))';
max1=max(max(max(m1,m2)));
min1=min(min(min(m1,m2)));

% Fixed locations centroid of pixel identification
estacionesx=(locations(:,1)-1.5)/3;
estacionesy=(locations(:,2)-1.5)/3;

% April 2015 sample path
figure();
imagesc(m1);

hold on;
scatter(estacionesx,estacionesy,'MarkerEdgeColor','b',...
    'MarkerFaceColor','r','LineWidth',1);
colorbar('southoutside');
xlim([0.0 175.0]);
ylim([0.0 93.0]);
axis('off');
caxis([min1 max1]);
set(gca,'YDir','normal');
set(gca,'XDir','normal');
set(gca,'dataAspectRatio',[1 1 1]);
title('Sample path n = 1 (201504)');
hold off;
saveas(gcf,'Sample_201504','pdf');

% April 2014 sample path
figure();
imagesc(m2);
hold on;
    scatter(estacionesx,estacionesy,'MarkerEdgeColor','b',...
        'MarkerFaceColor','r','LineWidth',1);
    colorbar('southoutside');
    xlim([0.0 175.0]);
    ylim([0.0 93.0]);
```

```
    axis('off');
    caxis([min1 max1]);
    set(gca,'YDir','normal');
    set(gca,'XDir','normal');
    set(gca,'dataAspectRatio',[1 1 1]);
    title('Sample path n = 1 (201404)');
hold off;

saveas(gcf,'Sample_201404','pdf');


%%%%%%%%%%%%%%%%%%%%%%%%%%%%%%%%%%%%%%%%%%%%%%%%%%%%%%%%%%%%%%%%%%%%%%%%%
%       Map of variances plotted as surface and mesh                    %
%%%%%%%%%%%%%%%%%%%%%%%%%%%%%%%%%%%%%%%%%%%%%%%%%%%%%%%%%%%%%%%%%%%%%%%%%
var_T1=zeros(175,93);
var_T2=zeros(175,93);

for i=1:175
   for j=1:93
       var_T1(i,j)=var(Data_201504_3D(i,j,:));
       var_T2(i,j)=var(Data_201404_3D(i,j,:));
   end
end

var_T1=(var_T1)';
var_T2=(var_T2)';

max1=max(max(max(var_T1,var_T2)));
min1=min(min(min(var_T1,var_T2)));

figure();
mesh(var_T1);colorbar('southoutside');
grid off;
caxis([min1 max1]);
title('Map of variances (201504)');

saveas(gcf,'sup_201504_var_Cauchy','pdf');

figure();
imagesc(var_T1);
hold on;
```

```
    colorbar();
    xlim([0.0 175.0]);
    ylim([0.0 93.0]);
    axis('off');
    caxis([min1 max1]);
    set(gca,'YDir','normal');
    set(gca,'XDir','normal');
    set(gca,'dataAspectRatio',[1 1 1]);
    title('Map of variances (201504)')
hold off;
saveas(gcf,'var_Cauchy_201504','pdf');

figure();
mesh(var_T2);colorbar('southoutside');
grid off;
caxis([min1 max1]);
title('Map of variances (201404)');

saveas(gcf,'sup_201404_var_Cauchy','pdf');

figure();
imagesc(var_T2);
colorbar();
xlim([0.0 175.0]);
ylim([0.0 93.0]);
axis('off');
caxis([min1 max1]);
set(gca,'YDir','normal');
set(gca,'XDir','normal');
set(gca,'dataAspectRatio',[1 1 1]);
title('Map of variances (201404)')

saveas(gcf,'var_Cauchy_201404','pdf');


%%%%%%%%%%%%%%%%%%%%%%%%%%%%%%%%%%%%%%%%%%%%%%%%%%%%%%%%%%%%%%%%%%%%%%%%%%%%
%       Map of standard desviations plotted as contour                     %
%%%%%%%%%%%%%%%%%%%%%%%%%%%%%%%%%%%%%%%%%%%%%%%%%%%%%%%%%%%%%%%%%%%%%%%%%%%%

var_T1=zeros(175,93);
var_T2=zeros(175,93);
```

```
for i=1:175
    for j=1:93
        var_T1(i,j)=std(Data_201504_3D(i,j,:));
        var_T2(i,j)=std(Data_201404_3D(i,j,:));
    end
end
% Remark: 'std' for standard desviation and
% 'var' for variance

var_T1=(var_T1)';
var_T2=(var_T2)';

% This is for the colour scale
max1=max(max(max(var_T1,var_T2)));
min1=min(min(min(var_T1,var_T2)));

figure();
imagesc(var_T1);
hold on;
     colorbar();
     xlim([0.0 175.0]);
     ylim([0.0 93.0]);
     axis('off');
     caxis([min1 max1]);
     set(gca,'YDir','normal');
     set(gca,'XDir','normal');
     set(gca,'dataAspectRatio',[1 1 1]);

     title('Map of desviances (201504)')
hold off;
saveas(gcf,'desv_Cauchy_201504','pdf');

figure();
imagesc(var_T2);
hold on;
     colorbar();
     xlim([0.0 175.0]);
     ylim([0.0 93.0]);
     axis('off');
     caxis([min1 max1]);
```

```
        set(gca,'YDir','normal');
        set(gca,'XDir','normal');
        set(gca,'dataAspectRatio',[1 1 1]);

        title('Map of desviances (201404)')
    hold off;
    saveas(gcf,'desv_Cauchy_201404','pdf');
```

5. **3D samples (S-T):**

```
%%%%%%%%%%%%%%%%%%%%%%%%%%%%%%%%%%%%%%%%%%%%%%%%%%%%%%%%%%%%%%%%%%%%%%%%%%%%%%%%
%       Processing data simulated with R code into MATLAB      %
%%%%%%%%%%%%%%%%%%%%%%%%%%%%%%%%%%%%%%%%%%%%%%%%%%%%%%%%%%%%%%%%%%%%%%%%%%%%%%%%
% This source code imports data simulated with R code in a text%
% file into a 3D-matrix in MATLAB. Then first sample path at   %
% any time is plotted.                                         %
% Finally a map of variances is computed and plotted            %
%%%%%%%%%%%%%%%%%%%%%%%%%%%%%%%%%%%%%%%%%%%%%%%%%%%%%%%%%%%%%%%%%%%%%%%%%%%%%%%%

% Cadiz province data
clear all;
clc;
% Fix locations for conditioning
load /Volumes/Datos/Simulations/Spatio_Temporal/locations_...
    matlab_Cadiz.txt;
locations_Cadiz=locations_matlab_Cadiz;

figure();
hold on;

scatter(locations_Cadiz(:,1),locations_Cadiz(:,2),...
'MarkerEdgeColor','b','MarkerFaceColor','b','LineWidth',0.25 )
set(gca,'YDir','normal');
set(gca,'XDir','normal');
set(gca,'dataAspectRatio',[1 1 1]);
title('Rainfall measurement locations (Cadiz)');
hold off;

saveas(gcf,'Locations_Grid_Cadiz_matlab','pdf');

% Loading simulated spatiotemporal data
load /Volumes/Datos/Simulations/Spatio_Temporal/...
    Gneiting_all_Cadiz.txt;

% This is an auxiliary variable where loading all the data
% before saving them in a 3D-matrix por each time.
% The grid is a 111x104 pixels grid at 5 times, so that
% each column has 57.720 observations, being for each time
% as follow:
```

```
% T=1 from 1:11544
% T=2 from 11555:23088
% T=3 from 23089:34632
% T=4 from 34633:46176
% T=5 from 46177:57720
Cadiz=Gneiting_all_Cadiz;

% Saving the 200 sample paths in variables for each time
Cadiz_T_1=Cadiz(1:11544,1:200);
Cadiz_T_2=Cadiz(11545:23088,1:200);
Cadiz_T_3=Cadiz(23089:34632,1:200);
Cadiz_T_4=Cadiz(34633:46176,1:200);
Cadiz_T_5=Cadiz(46177:57720,1:200);

% This is the 3D-matrix mentioned above. Third dimension
% is 200 because there are 200 sample paths
Cadiz_T_1_3D=zeros(111,104,200);
Cadiz_T_2_3D=zeros(111,104,200);
Cadiz_T_3_3D=zeros(111,104,200);
Cadiz_T_4_3D=zeros(111,104,200);
Cadiz_T_5_3D=zeros(111,104,200);

for i=1:200
    Cadiz_T_1_3D(:,:,i)=vec2mat(Cadiz_T_1(:,i),104);
    Cadiz_T_2_3D(:,:,i)=vec2mat(Cadiz_T_2(:,i),104);
    Cadiz_T_3_3D(:,:,i)=vec2mat(Cadiz_T_3(:,i),104);
    Cadiz_T_4_3D(:,:,i)=vec2mat(Cadiz_T_4(:,i),104);
    Cadiz_T_5_3D(:,:,i)=vec2mat(Cadiz_T_5(:,i),104);
end

% First sample path at the five times
m1g=(Cadiz_T_1_3D(:,:,1))';
m2g=(Cadiz_T_2_3D(:,:,1))';
m3g=(Cadiz_T_3_3D(:,:,1))';
m4g=(Cadiz_T_4_3D(:,:,1))';
m5g=(Cadiz_T_5_3D(:,:,1))';


% This is for the colour scale
max1=max(max(max(max(Cadiz_T_1_3D,Cadiz_T_2_3D))));
max2=max(max(max(max(Cadiz_T_3_3D,Cadiz_T_4_3D))));
```

```
max3=max(max(max(Cadiz_T_5_3D)));
maxim=max(max1,max2);
maximo=max(maxim,max3);

min1=min(min(min(min(Cadiz_T_1_3D,Cadiz_T_2_3D))));
min2=min(min(min(min(Cadiz_T_3_3D,Cadiz_T_4_3D))));
min3=min(min(min(Cadiz_T_5_3D)));
minim=min(min1,min2);
minimo=min(minim,min3);

% Plotting the first sample path at any time
%highlighting the fixed locations
estacionesxg=(locations_Cadiz(:,1)-0.5)/1;
estacionesyg=(locations_Cadiz(:,2)-0.5)/1;

figure();
imagesc(m1g);
hold on;
scatter(estacionesxg,estacionesyg,'MarkerEdgeColor',...
    'b','MarkerFaceColor','r','LineWidth',1);
colorbar('southoutside');
xlim([0.0 111.0]);
ylim([0.0 104.0]);
axis('off');
caxis([minimo maximo]);
set(gca,'YDir','normal');
set(gca,'XDir','normal');
set(gca,'dataAspectRatio',[1 1 1]);
title('Sample path n = 1 (T = 1 Cadiz)');
hold off;
saveas(gcf,'T1_Cadiz','pdf');

figure();
imagesc(m2g);
hold on;
scatter(estacionesxg,estacionesyg,'MarkerEdgeColor',...
    'b','MarkerFaceColor','r','LineWidth',1);
colorbar('southoutside');
xlim([0.0 111.0]);
ylim([0.0 104.0]);
axis('off');
```

```
caxis([minimo maximo]);
set(gca,'YDir','normal');
set(gca,'XDir','normal');
set(gca,'dataAspectRatio',[1 1 1]);
title('Sample path n = 1 (T = 2 Cadiz)');
hold off;
saveas(gcf,'T2_Cadiz','pdf');

figure();
imagesc(m3g);

hold on;
scatter(estacionesxg,estacionesyg,'MarkerEdgeColor',...
    'b','MarkerFaceColor','r','LineWidth',1);
colorbar('southoutside');
xlim([0.0 111.0]);
ylim([0.0 104.0]);
axis('off');
caxis([minimo maximo]);
set(gca,'YDir','normal');
set(gca,'XDir','normal');
set(gca,'dataAspectRatio',[1 1 1]);
title('Sample path n = 1 (T = 3 Cadiz)');
hold off;
saveas(gcf,'T3_Cadiz','pdf');

figure();
imagesc(m4g);
hold on;
scatter(estacionesxg,estacionesyg,'MarkerEdgeColor',...
    'b','MarkerFaceColor','r','LineWidth',1);
colorbar('southoutside');
xlim([0.0 111.0]);
ylim([0.0 104.0]);
axis('off');
set(gca,'YDir','normal');
set(gca,'XDir','normal');
set(gca,'dataAspectRatio',[1 1 1]);
title('Sample path n = 1 (T = 4 Cadiz)');
hold off;
saveas(gcf,'T4_Cadiz','pdf');
```

```
figure();
imagesc(m5g);
axis('off');
hold on;
scatter(estacionesxg,estacionesyg,'MarkerEdgeColor',...
    'b','MarkerFaceColor','r','LineWidth',1);
colorbar('southoutside');
xlim([0.0 111.0]);
ylim([0.0 104.0]);
axis('off');
caxis([minimo maximo]);
set(gca,'YDir','normal');
set(gca,'XDir','normal');
set(gca,'dataAspectRatio',[1 1 1]);
title('Sample path n = 1 (T = 5 Cadiz)');
hold off;
saveas(gcf,'T5_Cadiz','pdf');

% Map of variances
var_T1g=zeros(111,104);
var_T2g=zeros(111,104);
var_T3g=zeros(111,104);
var_T4g=zeros(111,104);
var_T5g=zeros(111,104);

for i=1:111
    for j=1:104
        var_T1g(i,j)=var(Cadiz_T_1_3D(i,j,:));
        var_T2g(i,j)=var(Cadiz_T_2_3D(i,j,:));
        var_T3g(i,j)=var(Cadiz_T_3_3D(i,j,:));
        var_T4g(i,j)=var(Cadiz_T_4_3D(i,j,:));
        var_T5g(i,j)=var(Cadiz_T_5_3D(i,j,:));
    end
end
% Remark: 'std' for standard desviation and
% 'var' for variance

var_T1g=(var_T1g)';
var_T2g=(var_T2g)';
var_T3g=(var_T3g)';
```

```
var_T4g=(var_T4g)';
var_T5g=(var_T5g)';

% This is for the colour scale
max1=max(max(max(max(var_T1g,var_T2g))));
max2=max(max(max(max(var_T3g,var_T4g))));
max3=max(max(max(var_T5g)));
maxim=max(max1,max2);
maximo=max(maxim,max3);

min1=min(min(min(min(var_T1g,var_T2g))));
min2=min(min(min(min(var_T3g,var_T4g))));
min3=min(min(min(var_T5g)));
minim=min(min1,min2);
minimo=min(minim,min3);

figure();
imagesc(var_T1g);colorbar('southoutside');
axis('off');
caxis([minimo maximo]);
set(gca,'YDir','normal');
set(gca,'XDir','normal');
set(gca,'dataAspectRatio',[1 1 1]);
title('Map of variances T = 1 (Cadiz)');
saveas(gcf,'var_T1_Cadiz','pdf');

figure();
imagesc(var_T2g);colorbar('southoutside');
axis('off');
caxis([minimo maximo]);
set(gca,'YDir','normal');
set(gca,'XDir','normal');
set(gca,'dataAspectRatio',[1 1 1]);
title('Map of variances T = 2 (Cadiz)');
saveas(gcf,'var_T2_Cadiz','pdf');

figure();
imagesc(var_T3g);colorbar('southoutside');
axis('off');
caxis([minimo maximo]);
set(gca,'YDir','normal');
```

```
set(gca,'XDir','normal');
set(gca,'dataAspectRatio',[1 1 1]);
title('Map of variances T = 3 (Cadiz)');
saveas(gcf,'var_T3_Cadiz','pdf');

figure();
imagesc(var_T4g);colorbar('southoutside');
axis('off');
caxis([minimo maximo]);
set(gca,'YDir','normal');
set(gca,'XDir','normal');
set(gca,'dataAspectRatio',[1 1 1]);
title('Map of variances T = 4 (Cadiz)');
saveas(gcf,'var_T4_Cadiz','pdf');

figure();
imagesc(var_T5g);colorbar('southoutside');
axis('off');
caxis([minimo maximo]);
set(gca,'YDir','normal');
set(gca,'XDir','normal');
set(gca,'dataAspectRatio',[1 1 1]);
title('Map of variances T = 5 (Cadiz)');
saveas(gcf,'var_T5_Cadiz','pdf');


%%
%%%%%%%%%%%%%%%%%%%%%%%%%%%%%%%%%%%%%%%%%%%%%%%%%%%%%%%%%%%%%%%%%%%%%%%%%%%%%
%                        Map of variances                              %
%%%%%%%%%%%%%%%%%%%%%%%%%%%%%%%%%%%%%%%%%%%%%%%%%%%%%%%%%%%%%%%%%%%%%%%%%%%%%
% Contour and surface graphics for the map of variances of    %
% two Cauchy models fitted to rainfall data precipitation   %
%%%%%%%%%%%%%%%%%%%%%%%%%%%%%%%%%%%%%%%%%%%%%%%%%%%%%%%%%%%%%%%%%%%%%%%%%%%%%

% Loading data
load C:\Simulaciones\Varianzas_Cauchy_scm_a0.76b0.11.txt;
load C:\Simulaciones\Varianzas_Cauchy_scm_a0.81b0.15.txt;

% Graphics (contour and surface) for the first model
% Necessary for plotting
mat4=(Varianzas_Cauchy_scm_a0_76b0_11)';
```

```
% Surface
figure();
mesh(mat4);colorbar('southoutside');
zlim([0.0 800]);
grid off;
caxis([0.0 800.0]);
set(gca,'dataAspectRatio',[1 1 16]);
title('Variance map - Cauchy conditional simulation '...
    'alpha 0.76 - beta 0.11 (Rainfall 201403)');
saveas(gcf,'sup_variances_map_scm_201403','pdf');

% Contour
figure();
imagesc(mat4);
colorbar();
xlim([0.0 179.0]);
ylim([0.0 97.0]);
caxis([0.0 800.0]);
set(gca,'YDir','normal');
set(gca,'XDir','normal');
set(gca,'dataAspectRatio',[1 1 1]);
title('Variance map - Cauchy conditional simulation '...
    'alpha 0.76 - beta 0.11 (Rainfall 201403)')
saveas(gcf,'image_variances_map_scm_201403','pdf');

% Graphics (contour and surface) for the first model
% Necessary for plotting

mat5=(Varianzas_Cauchy_scm_a0_81b0_15)';

% Surface
figure();
mesh(mat5);
colorbar('southoutside');
zlim([0.0 800.0]);
grid off;
caxis([0.0 800.0]);
set(gca,'dataAspectRatio',[1 1 16]);shading interp;
title('Variance map - Cauchy conditional simulation '...
    'alpha 0.81 - beta 0.15 (Rainfall 201503)');
```

```
saveas(gcf,'sup_variances_map_scm_201503','pdf');

% Contour
figure();
imagesc(mat5);
colorbar();
xlim([0.0 179.0]);
ylim([0.0 97.0]);
caxis([0.0 800.0]);
set(gca,'YDir','normal');
set(gca,'XDir','normal');
set(gca,'dataAspectRatio',[1 1 1]);
title('Variance map - Cauchy conditional simulation '...
    'alpha 0.81 - beta 0.15 (Rainfall 201503)')
saveas(gcf,'image_variances_map_scm_201503','pdf');
```

6. **Empirical compound distributions:**

```
%%%%%%%%%%%%%%%%%%%%%%%%%%%%%%%%%%%%%%%%%%%%%%%%%%%%%%%%%%%%%%%%%%%%%%%%%%%%%%%%%%%%%%%%
%            Empirical compound distribution functions                    %
%%%%%%%%%%%%%%%%%%%%%%%%%%%%%%%%%%%%%%%%%%%%%%%%%%%%%%%%%%%%%%%%%%%%%%%%%%%%%%%%%%%%%%%%
% This source code plots the cdf of 4 Cauchy models.                     %
% Furthermore, threshold files are saved for each model.                 %
%%%%%%%%%%%%%%%%%%%%%%%%%%%%%%%%%%%%%%%%%%%%%%%%%%%%%%%%%%%%%%%%%%%%%%%%%%%%%%%%%%%%%%%%

clear all;
clc;

% Number of sample paths within the files
n=200;

% Loading data
load C:\Simulaciones\CAUCHY_COND_NOSEED\sc_todas_a2b01.txt;
load C:\Simulaciones\CAUCHY_COND_NOSEED\sc_todas_a2b09.txt;
load C:\Simulaciones\CAUCHY_COND_NOSEED\sc_todas_a1b01.txt;
load C:\Simulaciones\CAUCHY_COND_NOSEED\sc_todas_a1b09.txt;

% Matrix with 200 sample paths as only column vector
m1=sc_todas_a2b01(:,1);
for i=2:n
    m1=[m1;sc_todas_a2b01(:,i)];
end

m2=sc_todas_a2b09(:,1);
for i=2:n
    m2=[m2;sc_todas_a2b09(:,i)];
end

m3=sc_todas_a1b01(:,1);
for i=2:n
    m3=[m3;sc_todas_a1b01(:,i)];
end

m4=sc_todas_a1b09(:,1);
for i=2:n
    m4=[m4;sc_todas_a1b09(:,i)];
end
```

```
cd C:\Simulaciones\CAUCHY_COND_NOSEED

hold on
    cdfplot(m1);
    [g,y] = ecdf(m1);
    probabilidad=0.5:0.05:1;
    umbrales=probabilidad';
    for i=1:length(probabilidad)
        umbrales(i,2)=y(min(find(g>=probabilidad(i))));
    end
    save umbralesa2b01.txt umbrales -ascii

    cdfplot(m2);
    [g,y] = ecdf(m2);
    probabilidad=0.5:0.05:1;
    umbrales=probabilidad';
    for i=1:length(probabilidad)
        umbrales(i,2)=y(min(find(g>=probabilidad(i))));
    end
    save umbralesa2b09.txt umbrales -ascii

    cdfplot(m3);
    [g,y] = ecdf(m3);
    probabilidad=0.5:0.05:1;
    umbrales=probabilidad';
    for i=1:length(probabilidad)
        umbrales(i,2)=y(min(find(g>=probabilidad(i))));
    end
    save umbralesa05b01.txt umbrales -ascii

    cdfplot(m4);
    [g,y] = ecdf(m4);
    probabilidad=0.5:0.05:1;
    umbrales=probabilidad';
    for i=1:length(probabilidad)
        umbrales(i,2)=y(min(find(g>=probabilidad(i))));
    end
    save umbralesa05b09.txt umbrales -ascii

    title('ecdf cond NOSEED Localizaciones SEED');
```

```
    legend('ca2b01','ca2b09','ca1b01','ca1b09');
hold off

%%%%%%%%%%%%%%%%%%%%%%%%%%%%%%%%%%%%%%%%%%%%%%%%%%%%%%%%%%%%%%%%%%%%%%%%%%%%
% This source code plots the cdf of 4 heavy-tail models.                   %
% (Fisher and Student).                                                    %
%%%%%%%%%%%%%%%%%%%%%%%%%%%%%%%%%%%%%%%%%%%%%%%%%%%%%%%%%%%%%%%%%%%%%%%%%%%%

% Retrieving data
load C:\Simulaciones\Heavy_Tail\COND\Fisher_a2b01\...
    sc_todas_F_2_a2b01.txt;
load C:\Simulaciones\Heavy_Tail\COND\Fisher_a2b09\...
    sc_todas_F_2_a2b09.txt;
load C:\Simulaciones\Heavy_Tail\COND\Fisher_a05b01\...
    sc_todas_F_2_a05b01.txt;
load C:\Simulaciones\Heavy_Tail\COND\Fisher_a05b09\...
    sc_todas_F_2_a05b09.txt;

m1=sc_todas_F_2_a2b01(:,1);
for i=2:n
   m1=[m1;sc_todas_F_2_a2b01(:,i)];
end

m2=sc_todas_F_2_a2b09(:,1);
for i=2:n
   m2=[m2;sc_todas_F_2_a2b09(:,i)];
end

m3=sc_todas_F_2_a05b01(:,1);
for i=2:n
   m3=[m3;sc_todas_F_2_a05b01(:,i)];
end

m4=sc_todas_F_2_a05b09(:,1);
for i=2:n
   m4=[m4;sc_todas_F_2_a05b09(:,i)];
end

figure();
hold on
    cdfplot(m1);
```

```
    cdfplot(m2);
    cdfplot(m3);
    cdfplot(m4);

    title('ecdf cond (FISHER Heavy Tail)');
    legend('ca2b01','ca2b09','ca05b01','ca05b09');
hold off

% Student (conditional simulation)

load C:\Simulaciones\Heavy_Tail\COND\Student_a2b01 \...
    sc_todas_T_2_a2b01.txt;
load C:\Simulaciones\Heavy_Tail\COND\Student_a2b09 \...
    sc_todas_T_2_a2b09.txt;
load C:\Simulaciones\Heavy_Tail\COND\Student_a05b01 \...
    sc_todas_T_2_a05b01.txt;
load C:\Simulaciones\Heavy_Tail\COND\Student_a05b09 \...
    sc_todas_T_2_a05b09.txt;

m1=sc_todas_T_2_a2b01(:,1);
for i=2:n
   m1=[m1;sc_todas_T_2_a2b01(:,i)];
end

m2=sc_todas_T_2_a2b09(:,1);
for i=2:n
   m2=[m2;sc_todas_T_2_a2b09(:,i)];
end

m3=sc_todas_T_2_a05b01(:,1);
for i=2:n
   m3=[m3;sc_todas_T_2_a05b01(:,i)];
end

m4=sc_todas_T_2_a05b09(:,1);
for i=2:n
   m4=[m4;sc_todas_T_2_a05b09(:,i)];
end


figure();
```

```
hold on
    cdfplot(m1);
    cdfplot(m2);
    cdfplot(m3);
    cdfplot(m4);

    title('ecdf cond (Student Heavy Tail)');
    legend('ca2b01','ca2b09','ca05b01','ca05b09');
hold off
```

R Source Code

1. **Preparing data:**

```
#*************************************************************
#                          PROCESSING DATA                    *
#*************************************************************

setwd("/Volumes/Datos/Simulations/Spatio_Temporal")
datos <- read.table("Datos_utilizados.txt", header = TRUE,
                    sep = "\t")
datos<-subset(datos,datos$PROVINCIA=="Cadiz")

# Preparing spatial data
x_datos<-as.array(datos$UTM_X_30)
y_datos<-as.array(datos$UTM_Y)

# UTM_x & UTM_y meters to kilometers
x_datos<-round(x_datos/1000)
y_datos<-round(y_datos/1000)

# Grid +4km, so that locations are not at the edge
max_x<-max(x_datos)
min_x<-min(x_datos)
max_y<-max(y_datos)
min_y<-min(y_datos)

# Case S-T: grid 1km
x_malla<-(min_x-2):(max_x+2)
y_malla<-(min_y-2):(max_y+2)

# Change of coordinates so that center will be (0,0)
# These are the true locations in the grid [0,531]x[0,271]
x_datos<-x_datos-x_malla[1]
y_datos<-y_datos-y_malla[1]

# Locations are assigned to the centroid of the pixel
giv<-cbind(x_datos,y_datos)
giv<-giv-giv%%1+0.5

# Saving new coordinates within the grid
datos$UTM_X<-giv[,1]
```

```
datos$UTM_Y<-giv[,2]

# Plotting locations in the grid
plot(giv)


# Rainfall means and variances of every month
datos$X201410<-log(datos$X201410)
datos$X201411<-log(datos$X201411)
datos$X201412<-log(datos$X201412)
datos$X201501<-log(datos$X201501)
datos$X201502<-log(datos$X201502)
datos$X201503<-log(datos$X201503)
datos$X201504<-log(datos$X201504)
datos$X201404<-log(datos$X201404)

value_total<-c(datos$X201410,datos$X201411,datos$X201412,
               datos$X201501,datos$X201502,datos$X201503,
               datos$X201504,datos$X201404)
mean_total<-mean(value_total)

datos$X201410<-datos$X201410-mean_total
datos$X201411<-datos$X201411-mean_total
datos$X201412<-datos$X201412-mean_total
datos$X201501<-datos$X201501-mean_total
datos$X201502<-datos$X201502-mean_total
datos$X201503<-datos$X201503-mean_total
datos$X201504<-datos$X201504-mean_total
datos$X201404<-datos$X201404-mean_total

# Shapiro-Wilk normality test and QQ-plot
shap1<-shapiro.test(datos$X201410)
qqnorm(datos$X201410)
qqline(datos$X201410)
shap2<-shapiro.test(datos$X201411)
qqnorm(datos$X201411)
qqline(datos$X201411)
shap3<-shapiro.test(datos$X201412)
qqnorm(datos$X201412)
qqline(datos$X201412)
shap4<-shapiro.test(datos$X201501)
```

```
qqnorm(datos$X201501)
qqline(datos$X201501)
shap5<-shapiro.test(datos$X201502)
qqnorm(datos$X201502)
qqline(datos$X201502)
shap6<-shapiro.test(datos$X201503)
qqnorm(datos$X201503)
qqline(datos$X201503)
shap7<-shapiro.test(datos$X201504)
qqnorm(datos$X201504)
qqline(datos$X201504)
shap8<-shapiro.test(datos$X201404)
qqnorm(datos$X201404)
qqline(datos$X201404)
shaptotal<-shapiro.test(value_total)
qqnorm(value_total)
qqline(value_total)

# Initial average. Shapiro-Wilk normality test p-values
pvalues<-c(shap1$p.value,shap2$p.value,shap3$p.value,
           shap4$p.value,shap5$p.value,shap6$p.value,
           shap7$p.value,shap8$p.value)

namesrow<-c('201410','201411','201412','201501','201502',
            '201503','201504','201404')
mean_pvalue<-data.frame(mean_total,pvalues,row.names=namesrow)

# Saving the new work datafile
filename=paste('Output_locations_Cadiz','.txt',sep="")
write.table(datos,file=filename,row.names=F,col.names=TRUE,
            sep = "\t")

# Saving initial means and variances
filename=paste('mean_locations_Cadiz','.txt',sep="")
write.table(mean_pvalue,file=filename,row.names=T,
            col.names=TRUE,sep = "\t")

# Saving grid locations (only) for MATLAB
filename=paste('locations_matlab_Cadiz','.txt',sep="")
write.table(giv,file=filename,row.names=F,col.names=FALSE,
            sep = "\t")
```

2. **Conditional simulation (S-T):**

```
#*************************************************************
#*                  SPATIO-TEMPORAL FRAMEWORK                *
#*************************************************************
#* Example : RMiaco model for conditional simulation         *
#*************************************************************

# Covariance function: C(r,t)=(1.0 + r^v + t^lambda)^delta

# Definition and drawing the De Iaco model
model <- RMiaco(nu=1, lambda=1.5, delta=0.5)
plot(model, dim=2)

# First: fixed locations data simulation for conditioning
# Grid for simulation
x<-5:10
y<-5:10
T<-1:2

# Processing grid for RFsimulate function
giv<-cbind(rep(x,each=length(y)), rep(y,length(x)),
           rep(T,each=length(x)*length(y)))

# Simulation of 5 times of De Iaco model in the previous grid
fijas<-RFsimulate(model,x=giv)

# These are the fixed locations for conditional simulation
data<-data.frame(fijas)

# Grid for conditional simulation
x<-1:200
y<-1:200
T<-1:10

# Processing grid for RFsimulate function
giv<-cbind(rep(x,each=length(y)), rep(y,length(x)),
           rep(T,each=length(x)*length(y)))

# Conditional simulation
simul<-RFsimulate(model=model,x=giv,data=data)
simul
```

```
#*************************************************************
#*                  SPATIO-TEMPORAL FRAMEWORK                *
#*************************************************************
#* Example : Gneiting model conditional simulation           *
#*************************************************************

model <- RMnsst(phi=RMgencauchy(alpha=2,beta=0.2,var=0.1,
                  scale=1),psi=RMgencauchy(alpha=1,beta=0.1,
                  var=0.1,scale=1), delta=2)
plot(model, dim=2)

# Simulation grid definition for conditional simulation
x<-1:200
y<-1:200
T<-1:10

# Processing grid for RFsimulate function
giv<-cbind(rep(x,each=length(y)), rep(y,length(x)),
           rep(T,each=length(x)*length(y)))

# Conditional simulation
simul<-RFsimulate(model=model,x=giv,data=data,n=20)
simul
```

3. **Fixed allocations from generalized Cauchy class:**

```
#*************************************************************
#* Getting fixed allocations by simulation for different     *
#* models of the generalized Cauchy class                    *
#*************************************************************

library(RandomFields)

# ANY simulation will have the random seed -953631453
# (Set RFoptions(seed=NA) to make them all random again)
RFoptions(seed=-953631453)

# Number of sample paths
n=1

# Grid definition
x <- 1:200
y <- 1:200

# Cauchy models parameters
alpha <- 2
beta <- 0.1

alpha1<-2
beta1<-0.5

alpha2<-2
beta2<-0.9

alpha3<-2
beta3<-2

var <- 1
scale<-1

# RandomField package Cauchy model definitions
model <- RMgencauchy(alpha=alpha, beta=beta, var=var,
                     scale=scale)
model1 <- RMgencauchy(alpha=alpha1, beta=beta1, var=var,
                      scale=scale)
```

```
model2 <- RMgencauchy(alpha=alpha2, beta=beta2, var=var,
                      scale=scale)
model3 <- RMgencauchy(alpha=alpha3, beta=beta3, var=var,
                      scale=scale)

# One sample path for every Cauchy model
cond <- RFsimulate(model = model, x=x, y=y, grid=TRUE, n=1)
cond1 <- RFsimulate(model = model1, x=x, y=y, grid=TRUE, n=1)
cond2 <- RFsimulate(model = model2, x=x, y=y, grid=TRUE, n=1)
cond3 <- RFsimulate(model = model3, x=x, y=y, grid=TRUE, n=1)

# Saving data in a text file
filename=paste('Cauchy_a2b01.txt',sep="")
write.table(cond, file=filename, row.names=F, col.names=F)

filename=paste('Cauchy_a2b05.txt',sep="")
write.table(cond1, file=filename, row.names=F, col.names=F)

filename=paste('Cauchy_a2b09.txt',sep="")
write.table(cond2, file=filename, row.names=F, col.names=F)

filename=paste('Cauchy_a2b2.txt',sep="")
write.table(cond3, file=filename, row.names=F, col.names=F)
```

4. **Parameter estimation:**

```
#*************************************************************
#*                    Paramenter estimation                  *
#*************************************************************
#* Easy example of parameter estimation and uncondicional    *
#* simulation of a two-dimensional Gaussian random field     *
#* with exponential covariance function                      *
#*************************************************************

library(RandomFields)

# ANY simulation will have the random seed 0
# (Set RFoptions(seed=NA) to make them all random again)
RFoptions(seed=0)
RFoptions(modus_operandi="sloppy")

# Grid definition
x <- 1:30
y <- 1:30


# Covariance Cauchy model parameters
alpha <- 2
beta <- 0.1
var <- 0.1
scale<-1

# Cauchy model simulation
model <- RMgencauchy(alpha=alpha, beta=beta, var=var,
                     scale=scale)
data <- RFsimulate(model=model, x=x, y=y, grid=TRUE)


# Cauchy model parameter estimation
ajustar <- RMgencauchy(alpha=NA, beta=NA, var=var, scale=scale)

fitted<-RFfit(model=ajustar, data=data)
fitted
```

5. **Heavy-Tail Fisher and Student covariance random field models simulation (unconditional and condtional):**

```
#*************************************************************
#*      Heavy-tail Fisher and Student random fields          *
#*************************************************************
#* Unconditional and conditional simulation of Fisher and    *
#* and Student random fields                                 *
#*************************************************************

# Four scenarios are considered for each covariance model

# Loading RandomFields package

library(RandomFields)


# Number of sample paths (200)
n <- if (interactive()) 200 else 2

# Cauchy covariance models are previously generated and saved
# for the four scenarios. Here these simulations are loaded
# Depending on de previous simulations considered, conditional
# or unconditional, Fisher and Student simulations are
# conditional or unconditional. Here unconditional simulations
# are considered

setwd("C:\\Simulaciones\\Heavy_Tail\\UNCOND\\Input\\
      Cauchy_a2b01")
filename=paste('su1_todas_a2b01.txt',sep="")
muestra<-read.table(file=filename)
filename=paste('su2_todas_a2b01.txt',sep="")
muestra1<-read.table(file=filename)
filename=paste('su3_todas_a2b01.txt',sep="")
muestra2<-read.table(file=filename)
filename=paste('su4_todas_a2b01.txt',sep="")
muestra3<-read.table(file=filename)

setwd("C:\\Simulaciones\\Heavy_Tail\\UNCOND\\Input\\
      Cauchy_a2b09")
filename=paste('su1_todas_a2b09.txt',sep="")
```

```
muestra4<-read.table(file=filename)
filename=paste('su2_todas_a2b09.txt',sep="")
muestra5<-read.table(file=filename)
filename=paste('su3_todas_a2b09.txt',sep="")
muestra6<-read.table(file=filename)
filename=paste('su4_todas_a2b09.txt',sep="")
muestra7<-read.table(file=filename)

setwd("C:\\Simulaciones\\Heavy_Tail\\UNCOND\\Input\\
      Cauchy_a05b01")
filename=paste('su1_todas_a05b01.txt',sep="")
muestra8<-read.table(file=filename)
filename=paste('su2_todas_a05b01.txt',sep="")
muestra9<-read.table(file=filename)
filename=paste('su3_todas_a05b01.txt',sep="")
muestra10<-read.table(file=filename)
filename=paste('su4_todas_a05b01.txt',sep="")
muestra11<-read.table(file=filename)

setwd("C:\\Simulaciones\\Heavy_Tail\\UNCOND\\Input\\
      Cauchy_a05b09")
filename=paste('su1_todas_a05b09.txt',sep="")
muestra12<-read.table(file=filename)
filename=paste('su2_todas_a05b09.txt',sep="")
muestra13<-read.table(file=filename)
filename=paste('su3_todas_a05b09.txt',sep="")
muestra14<-read.table(file=filename)
filename=paste('su4_todas_a05b09.txt',sep="")
muestra15<-read.table(file=filename)

# Student random field simulations for each scenario
T_2_a2b01<-muestra/sqrt(0.5*(muestra1^2+muestra2^2))
T_2_a2b09<-muestra4/sqrt(0.5*(muestra5^2+muestra6^2))
T_2_a05b01<-muestra8/sqrt(0.5*(muestra9^2+muestra10^2))
T_2_a05b09<-muestra12/sqrt(0.5*(muestra13^2+muestra14^2))

# Fisher random field simulations for each scenario
F_2_a2b01<-(muestra^2+muestra1^2)/(muestra2^2+muestra3^2)
F_2_a2b09<-(muestra4^2+muestra5^2)/(muestra6^2+muestra7^2)
F_2_a05b01<-(muestra8^2+muestra9^2)/(muestra10^2+muestra11^2)
F_2_a05b09<-(muestra12^2+muestra13^2)/(muestra14^2+muestra15^2)
```

```
# Saving Student data
setwd("C:\\Simulaciones\\Heavy_Tail\\UNCOND\\Student_a2b01")
# Each column within the file is a sample path
filename=paste('su_todas','_T_2_a2b01','.txt',sep="")
write.table(T_2_a2b01,file=filename,row.names=F,col.names=F)

setwd("C:\\Simulaciones\\Heavy_Tail\\UNCOND\\Student_a2b09")
filename=paste('su_todas','_T_2_a2b09','.txt',sep="")
write.table(T_2_a2b09,file=filename,row.names=F,col.names=F)
for (i in 1:n)
{
filename=paste('su',as.character(i),'_a2b09','.txt',sep="")
write.table(as.matrix(T_2_a2b09[,i],nrow=n,ncol=n),
                      file=filename,row.names=F,col.names=F)
}

setwd("C:\\Simulaciones\\Heavy_Tail\\UNCOND\\Student_a05b01")
filename=paste('su_todas','_T_2_a05b01','.txt',sep="")
write.table(T_2_a05b01,file=filename,row.names=F,col.names=F)

setwd("C:\\Simulaciones\\Heavy_Tail\\UNCOND\\Student_a05b09")
filename=paste('su_todas','_T_2_a05b09','.txt',sep="")
write.table(T_2_a05b09,file=filename,row.names=F,col.names=F)


# Saving Fisher data
setwd("C:\\Simulaciones\\Heavy_Tail\\UNCOND\\Fisher_a2b01")
# Each column within the file is a samle path
filename=paste('su_todas','_F_2_a2b01','.txt',sep="")
write.table(F_2_a2b01,file=filename,row.names=F,col.names=F)

setwd("C:\\Simulaciones\\Heavy_Tail\\UNCOND\\Fisher_a2b09")
filename=paste('su_todas','_F_2_a2b09','.txt',sep="")
write.table(F_2_a2b09,file=filename,row.names=F,col.names=F)

setwd("C:\\Simulaciones\\Heavy_Tail\\UNCOND\\Fisher_a05b01")
filename=paste('su_todas','F_2_a05b01','.txt',sep="")
write.table(F_2_a05b01,file=filename,row.names=F,col.names=F)
```

```
setwd("C:\\Simulaciones\\Heavy_Tail\\UNCOND\\Fisher_a05b09")
filename=paste('su_todas','_F_2_a05b09','.txt',sep="")
write.table(F_2_a05b09,file=filename,row.names=F,col.names=F)
```